Response to the Re-review of:

"Recent dynamic changes on Fleming Glacier after the disintegration of Wordie Ice Shelf. Friedl et al., 2017 "

by Peter Friedl et al.

Anonymous Referee #1
Received and published: 23 January 2018

We would like to thank the reviewer for taking again the time to comment on our revised manuscript. Our responses are written in bold face type and changes in the manuscript are written in *blue*.

General comments:

I wish to thank the authors for their efforts in revising the manuscript and preparing the detailed response to the reviews. The revised version addresses adequately the main issues raised by the reviewers. Since submission of the first version of the manuscript two other papers on the dynamic behaviour of Wordie Ice Shelf glaciers were published (Walker and Gardner, 2017; Zhao et al., 2017). The paper of Walker and Gardner covers same topics as this manuscript, dealing with the acceleration and drawdown of the glaciers in connection with break-up of the ice shelf. Beyond that, Walker and Gardner present also a detailed analysis on oceanic and atmospheric conditions and a thorough discussion of driving mechanisms for the observed glacier changes. Friedl et al. present a detailed time series of flow velocities and spatial details on surface elevation change, of significant interest for characterization of glacier behaviour complementary to the material reported in the other publications. However, the discussion and conclusion sections lacks a clear message on the added value of these data for advancing the understanding of flow dynamics, mass balance and driving factors for the observed changes. Main conclusions refer to oceanic and atmospheric driving mechanisms that have been elaborated and reported in much more detail by Walker and Gardner. The relevance of the presented material for further advancing the knowledge on the dynamic response and mass budget of Fleming Glacier should be better worked out.

We have added some statements on the added value of our data and results to the discussion and conclusion sections. In particular our dense time series of surface velocities is the most detailed information on glacier velocity at Fleming Glacier available so far. It enabled us to precisely date and characterize two pronounced phases of glacier acceleration for the first time. This information is very important for the interpretation of the observed changes. Furthermore we are the first who estimate the recent position of the grounding line on the central part of the glacier, by combining new information on hydrostatic equilibrium with new data on elevation change (TSX/TDX, ICESat), ice velocity and modelled bedrock topography. Whereas earlier publications rely on the grounding line position of 1996, we show that the grounding line had substantially retreated and that this is a key factor for the explanation of recent glacier behaviour. We also see a positive trend of elevation change rates towards the glacier front between 2011 and 2014, which is a sign of floatation of the glacier tongue and which has not been reported before. By relating velocity change and elevation change to grounding line retreat and oceanic forcing we complement previously published data and add new information to the understanding of the pronounced changes at Fleming Glacier and their drivers.

Further comments:

P2, L18 to L21: Please specify the time periods for the different numbers on basal melt rates and the ratios basal melt/calving flux. This might possibly explain the different numbers.
Rignot et al. (2013) estimated the basal melt rates for the period 2003-2008 whereas Depoorter et al. (2013) corrected all input data to the year 2009. Differences may also result from different assumptions on ice thickness. We have added the time periods of the basal melt rates throughout the text.

P3, L3-L4 and P4, L15-L17: The statement " … feature tracking in 2014 and 2015 revealed that the glacier had sped up by ~400–500 m/a which is the largest acceleration in ice flow recorded across all of Antarctica" is incorrect, apparently based on an incomplete sample. This speed up reported by Walker and Gardner (2017) refers to the period 2008 to 2014. In the abstract (P1, L20) Friedl et al. report "a remarkable median speedup of ~1.3 m/d (~30 %) between 2007 and 2011. Much stronger acceleration events are not uncommon for tidewater calving glaciers. For example, the ice flow near the calving front of Hektoria Glacier (Larsen B embayment) accelerated between 2008 and 2011 from 1.4 m/d to 4.2 m/d (300%) (The Cryosphere Discuss., https://doi.org/10.5194/tc-2017-259.. I am sure, detailed analysis of ice motion time series would depict a considerable number of Antarctic glaciers with speed-up >30% during that period.
We thank the reviewer for pointing this out. We have removed the term "remarkable" in the abstract and in the discussion section. Moreover, we have removed the phrases stating the largest acceleration across Antarctica on P3, L3-L4 and P4, L15-L17

P9, L23: The term "median absolution deviation" is incorrect. Should rather be "absolute"?
We are sorry for this typo. We have changed it to "median absolute deviation".

P9, L25: Not sure if showing only the median velocity of the 16 km profile is the optimum choice. Would be of interest highlighting also velocity changes in subsections of the profile.
We have largely overhauled the velocity results section by now discussing velocity changes in subsections of the profile more intensively. For this purpose we have also changed Figures 3 a, b. With regard to the reviewer`s comment on P13, L14-15, we have added velocity changes between Jan. 2008–Apr. 2008 and 2010–2011 to the figure and discuss the changes in the text. In order to make the figure tidier, we have binned absolute and relative velocity change by 1 km intervals.

P13, L14-L15: "Rapidity of acceleration" is not evident in Fig. 2, showing a gradual overall acceleration of 30% between 2007 and 2011 (see also comment P2, L18).
We assume that the reviewer refers to comment P9, L25 instead of P2, L18. Apart from that, same answer as P9, L25.

P13, L25-26: There is no "contrast to Walker and Gardner (2017)" regarding the trend of elevation change. Differences are due to the different spatial filtering and the start of the profile further upstream. Besides, Fig. 5a (P27) shows negative dh/dt also in the lowest section, not a positive elevation change for the same ATM data set.
The reviewer is right that differences to Walker and Gardner (2017) mainly result from their approach of excluding all data up to 5.5 km landward of the 1996 grounding line. Of course for 2011-2014 the elevation change rates in the lowest section are still negative, but the trend in this subsection of the profile clearly goes towards lower ice thinning rates. This difference to

previous observations (2004 -2008) is important for the explanation of the glacier`s recent behaviour, since this signal now indicates floatation of the adjacent glacier tongue. The observation is in sharp contrast to the statement of Walker and Gardner, 2017 (Supplement, P1 L 37) that 'in all cases, the elevation change rates illustrate a clear trend towards increased surface lowering close to the glacier front'. For a detailed comparison between our data and the data published by Walker and Gardner (2017) we would like to refer the reviewer to our response to reviewer #3. We have changed the section into:

This has neither been observed by Zhao et al. (2017), who did not specifically analyse elevation change for this time period, nor by Walker and Gardner (2017), who calculated elevation change from the same OIB ATM dataset. The latter binned elevation change in 5 km intervals and excluded all data up to 5.5 km landward of the 1996 grounding line, which is the part of the profile where the trend towards lower ice thinning is most prominent.

P13, L28: Please specify the periods for the basal melt rates.

See answer P2, L18 to L21

P14, L19: In Fig. 8 a retrograde bedrock slope is not obvious for these glaciers. It shows a complex pattern of ridges and depressions.

If looking at Fig. S6 b (0-6 km) a retrograde bed slope is obvious for the central part of the trough. We have added a reference to Fig. S6 b to the text:

Furthermore, the bed topography reveals that the trough underneath the joint Airy-Rotz-Seller-Fleming glacier tongue has a retrograde slope on its central part (Fig. S6 b, 0–6 km).

References

Depoorter, M. A., Bamber, J. L., Griggs, J. A., Lenaerts, J T M, Ligtenberg, S R M, van den Broeke, M R and Moholdt, G.: Calving fluxes and basal melt rates of Antarctic ice shelves, Nature, 502, 89–92, doi: 10.1038/nature12567, 2013.

Rignot, E., Jacobs, S., Mouginot, J. and Scheuchl, B.: Ice-shelf melting around Antarctica, Science (New York, N.Y.), 341, 266–270, doi: 10.1126/science.1235798, 2013.

Walker, C. C. and Gardner, A. S.: Rapid drawdown of Antarctica's Wordie Ice Shelf glaciers in response to ENSO/Southern Annular Mode-driven warming in the Southern Ocean, Earth and Planetary Science Letters, 476, 100–110, doi: 10.1016/j.epsl.2017.08.005, 2017.

Zhao, C., King, M. A., Watson, C. S., Barletta, V. R., Bordoni, A., Dell, M. and Whitehouse, P. L.: Rapid ice unloading in the Fleming Glacier region, southern Antarctic Peninsula, and its effect on bedrock uplift rates, Earth and Planetary Science Letters, 473, 164–176, doi: 10.1016/j.epsl.2017.06.002, 2017.

Response to the Re-review of:

"Recent dynamic changes on Fleming Glacier after the disintegration of Wordie Ice Shelf. Friedl et al., 2017 "

by Peter Friedl et al.

Anonymous Referee #3
Received and published: 23 January 2018

We would like to thank the reviewer for taking again the time to comment on our revised manuscript. Our responses are written in bold face type and changes in the manuscript are written in *blue*.

This revised paper on Fleming Glacier is much improved from its original form. For example, vertically registering the TSX DEM's over sea ice has now been discarded in favor of using ground control points on stable mountains peaks. However, further information on the magnitude of this correction still needs to be provided. While many of the the methodological concerns have been addressed, the authors have not improved their approach to characterizing their measurement error. It is not unreasonable for a reviewer to request a spatially variable error estimate for the datasets presented, therefore the authors must calculate one before this paper is ready for publication, rather than to 'assume an error' as they have stated in their comments. As noted by the authors, the text throughout this paper, particularly in the discussion section, has been completely overhauled which has improved the clarity of the paper. Despite these significant improvements, and the quality of dense ice velocity time series, the authors have not convinced me that the ice thinning rates from the airborne data and DEM differencing are robust. The data has a huge noise range on it which is significantly greater than the stated error, and simply fitting a polynomial through it to get a plausible but unvalidated mean value, doesn't provide enough evidence to conclude with confidence that the magnitude of the thinning signal has been correctly characterized. Given that the authors acknowledge that their result contradicts the previously published estimate by Walker and Gardener (2017), the accuracy of the thinning estimate does need to be properly interrogated before this result is published.

Specific Edits

Original comment P5 L6 – The authors have responded to this comment. Although the coverage of ice velocity measurements is different for each image pair, it is possible to state % removed relative to the original pre-filtered result. The approach of only stating % removed on the fast flowing ice tongue is better than nothing, but this number will be biased low because as the authors acknowledge its harder to get good tracking results further inland. In my view, the fact that the measurements are poor in the interior, isn't a good reason for excluding this region from the filter removed stats.

We have added a column to Tab. S3 which contains the % of removed velocities for each complete velocity field. We have changed the caption of Tab. S3 accordingly.

Original comment P5 L16 – The authors have not responded to this important concern. The original comment was that the sensor accuracy is not an estimate of the measurement error on the ice thinning rates. As previously stated 0.2 m is the accuracy of the original point elevation measurements, not the elevation change measurement. The authors are also using the elevation data after re-gridding it so they need to state the accuracy of the gridded dataset instead of the accuracy of the raw point data. The

elevation change error is different for different sensors, so the authors should provide formal error statistics for each dataset.

We have calculated uncertainty statistics for the LiDAR elevation measurements after re-gridding and how this propagates into uncertainties in elevation change rates. We have added some sentences on this to the text:

The uncertainty of the gridded measurements can be attributed to both physical topographical features and measurement error. We approximated the uncertainty of each gridded median surface elevation similar as recommended in the IceBridge ATM L2 user guide (https://nsidc.org/data/ILATM2/versions/2/) by calculating the normalized median absolute deviation (NMAD) of all measurements in a 50 m grid cell. For each LiDAR dataset the median NMAD value of all grid cells was taken as the total uncertainty in surface elevation. Total uncertainties in surface elevation were 0.46 m (2004), 0.39 m (2008), 0.38 m (2011) and 0.43 m (2014). For each pair of overlapping gridded median surface elevations we derived the uncertainty in elevation change rate by calculating the root of the sum squares (RSS) of the corresponding NMAD values and dividing the result by the difference in acquisition time (years). The total uncertainty in elevation change rate for a complete dataset was calculated as the median of the elevation change rate uncertainties of all grid cells. The total uncertainties in elevation change rate were 0.32 m a^{-1} for 2004–2008 and 0.24 m a^{-1} for 2011–2014.

We have further estimated the uncertainties in ICESat elevation change rates and have added a note on this to the text:

By calculating the RSS of the ICESat elevation uncertainties and dividing the result by the time interval between the measurements (years), we estimated the uncertainty in ICESat elevation change rates to be 0.13 m a^{-1}.

Original comment P6 L2/3 – The authors have only partially addressed this comment. Although the method for vertical registration has been completely overhauled to use stable ground control points rather than variable sea ice, the size of the vertical correction has not been stated in the paper. This is important because if the authors are adjusting the DEM heights by 10's of meters, to then measure a few meters of elevation change, then this would indicate that the raw data may not be suitable for the task. Additionally, is the vertical co-registration spatially variable, or is the mean of all ground control points used, and again if it is spatially variable the range of values should be stated. The precise method employed must be stated more clearly.

We have adjusted each DEM according to the median of all ground control measurements over stable areas (n = 35452). Hence, the adjustment was not spatially variable. The vertical correction was 0.48 m for the 2014 DEM and -5.1 m for the 2011 DEM. We have added a sentence on this to the manuscript:

For this purpose the vertical offset between the DEMs and the TanDEM-X global DEM was measured over stable areas (i.e. tops of nunataks and rock outcrops, which were not affected by image distortions) at altitudes between 150 m and 1000 m (Fig. S1). Both DEMs were adjusted according to the median values of all ground control measurements (n= 35452), which were -5.1 m for the 2011 DEM and 0.48 m for the 2014 DEM.

However we also would like to note that the amount of vertical adjustment does not necessarily reflect the quality of the DEM. The amount of vertical adjustment strongly depends on the reference height value used for the phase to height conversion of the interferogram. At a single location in the interferogram usually a roughly estimated elevation value is assigned to the corresponding phase difference. The location of the reference point and the assigned height value may vary between different interferograms. According to the phase-to-height-sensitivity, the unwrapped phase differences in the interferogram are then converted to surface heights relative to this elevation value (e.g. 100 m). However, if the real height at the reference point is largely different (e.g. 60 m), all values in the DEM have a huge constant offset to reality (e.g. 60 m). Nonetheless, also in this case the DEM still contains the correct relative height values. After correcting for the offset during vertical registration (e.g. by subtracting 60 m from the DEM),

the raw data is leveled to the correct surface height and contains valid information of elevation. In this case it doesn`t matter for the quality of the result whether the vertical correction was 60 m or 0.60 m.

Original comment P6 L20 – The authors have not sufficiently addressed this comment. As other reviewers also pointed out, having a penetration bias account for 50% of the signal is a significant error therefore it can't be dismissed without a proper solution. The authors statement that they 'have to deal with the data they have in hand' is just not true. There are other available methods of measuring elevation change, such as using altimetry data. The TSX DEM differencing results could be inter-compared with altimetry elevation change from the same time period to establish the extent to which the dhdt numbers can be trusted.
We now compare the penetration bias corrected TSX/TDX elevation change rates with an independent dataset of 2011-2014 ATM elevation change rates that goes across Fleming Glacier. This dataset is a subsection of the complete OIB flight tracks in 2011 and 2014 and to our knowledge the only existing airborne altimetry data over Fleming Glacier for this time period. The elevation change in the TSX/TDX and the ATM datasets are in good agreement. The RMSE of the cubic fits of both datasets is 0.24 m a^{-1}. At least this gives us a rough estimate of the remaining uncertainties due to uncorrected penetration depth biases and we assume that 0.3 m a^{-1} is a reasonable value. The value is similar to what has been reported by Rott et al. (2017) for a comparison between TSX/TDX dh/dt and ATM dh/dt measurements over glaciers in the Larsen A and B embayments. We have added Figure S4 e to the supplement, showing the comparison of the TSX/TDX data with the independent ATM data. We have also added the ATM validation track to Figure 4. Furthermore we have added a note on this to the text:
Nevertheless, penetration depths of the radar signal may be spatially variable at the same altitude e.g. due to local differences in surface melt or ice properties. Hence we checked the validity of the applied penetration depth correction by comparing the corrected TSX/TDX elevation change rates with an independent validation track of 2011–2014 ATM dh/dt rates (see Fig. 4 for location). Figure S4 e shows that the elevation change rates of both datasets are in good agreement. The RMSE between the cubic fits of the data was 0.24 m a^{-1}. Hence we estimate the uncertainty due to remaining penetration depth differences to be 0.3 m a^{-1}.

Original comment P6 L27 – The authors have not addressed this comment. Just because the study area is small, it doesn't mean the error is also small. Mountain glaciers and ice caps are significantly smaller than this Antarctic ice sheet drainage basin, but spatially variable error measurements are still made. It is a completely reasonable reviewer request to ask for a spatially variable error estimate, therefore the authors response to just 'assume an error', rather than to calculate one, is not acceptable.
See previous answer.

Original comment P8 L14 – Wording still not correct English, suggest edit to: *Since 2008 the glacier tongue has not advanced seaward of the 1996 grounding line position.*
We have changed the sentence accordingly.

Original comment P8 L28 – yes fine.

P13, L26-27 – The authors state the following reason for the disagreement of their elevation change result compared with Walker and Gardener (2017), as: 'Their approach of averaging elevation change in 5 km intervals probably filtered out the positive trend that is most prominent on the lowest 3 km of

the profile.' It would be trivial for the authors to test this hypothesis, so I suggest they do this rather than postulate, as this new result conflicts with the published literature.

We have applied the approach of Walker and Gardner (2017) of averaging measurements in 5 km intervals to our re-gridded data (Figure 1), which allows us to fully reproduce their results for 2011–2014 (Figure 2 c, Walker and Gardner, 2017). It is obvious that excluding all data up to 5.5 km landward of the 1996 grounding line almost completely eliminates the trend towards decreasing ice thinning in the lower areas of the glacier tongue. However, if extending the 5 km averaging approach to the complete dataset, the trend is clearly visible. Hence, the statement of Walker and Gardner, 2017 (Supplement, P1 L 37) that 'in all cases, the elevation change rates illustrate a clear trend towards increased surface lowering close to the glacier front' is not true if considering all data.

We have changed the sentence by also taking into account the comment of reviewer #1 to:

This has neither been observed by Zhao et al. (2017), who did not specifically analyse elevation change for this time period, nor by Walker and Gardner (2017), who calculated elevation change from the same OIB ATM dataset. The latter binned elevation change in 5 km intervals and excluded all data up to 5.5 km landward of the 1996 grounding line, which is the part of the profile where the trend towards lower ice thinning is most prominent.

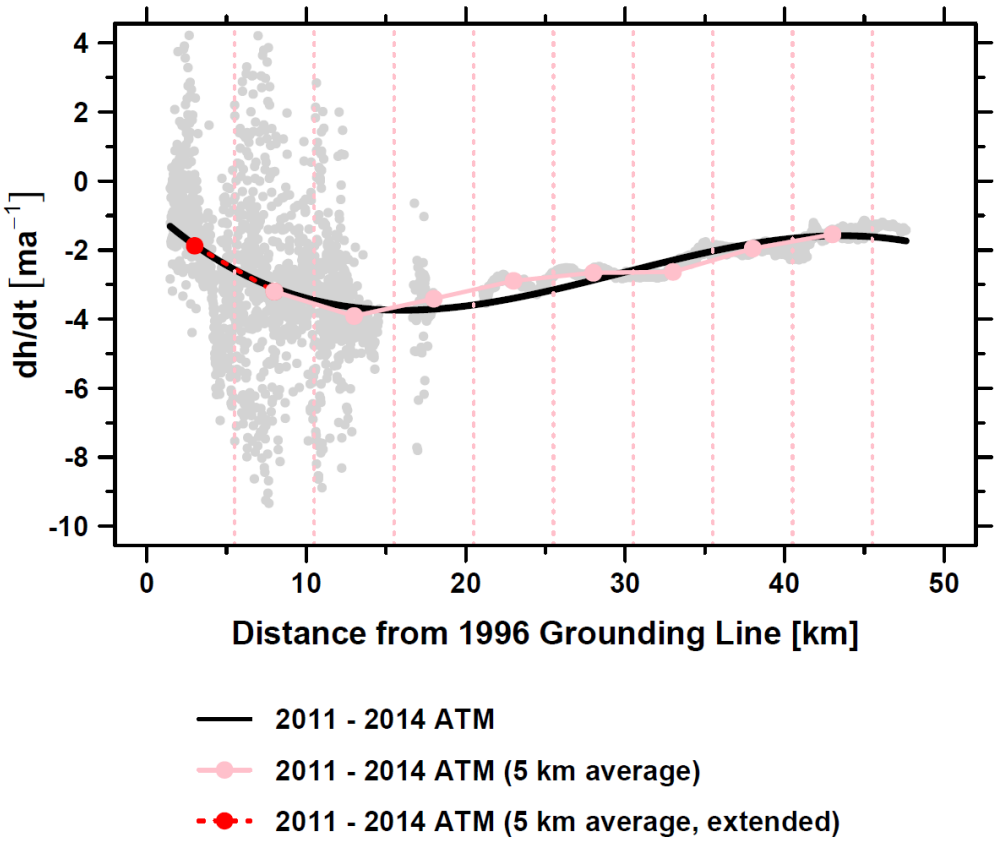

Figure 1: Elevation change rates on Fleming Glacier in 2011–2014 plotted against distance from the 1996 grounding line. Grey dots: re- gridded elevation change rates from OIB ATM LiDAR measurements in 2011 and 2014. Black line: Cubic function fitted to median filtered elevation change rates. Pink dots: Elevation change rates averaged in 5 km dots as shown by Walker and Gardner, 2017. Pink dotted lines: margins of the 5 km bins used by Walker and Gardner, 2017. Red dot with dotted line: Average elevation change rate in a 5 km interval, if applied to the data excluded by Walker and Gardner, 2017.

Figure 6 - The wording 'Likely recent grounding line', for the authors new grounding line is not good. It either is a measurement of the new grounding line position, or its not. A time stamp for the new line

should also be provided. This lack of commitment to the measurement limits usefulness of the information.

We have changed the wording in Figures 6 and S7 to 'Interpolated recent GL (2014)'.

Figure S8 - This figure is incorrect. In 1) there is no dynamic thinning yet because the ice shelf is still providing buttressing force, and the ice velocities are stable. If the ice was dynamically thinning, then the ice velocity would have accelerated. There should be dynamic thinning in 2). And there should also be dynamic thinning in 3) if the ice velocities have continued to accelerate. This schematic is incorrect as it stands, and doesn't really add anything to the discussion so I would just remove the figure.

We have removed the figure.

References

Rott, H., Abdel Jaber, W., Wuite, J., Scheiblauer, S., Floricioiu, D., van Wessem, J. Melchior, Nagler, T., Miranda, N. and Van Den Broeke, Michiel R.: Changing pattern of ice flow and mass balance for glaciers discharging into the Larsen A and B embayments, Antarctic Peninsula, 2011 to 2016, The Cryosphere Discuss., 1–34, doi: 10.5194/tc-2017-259, 2017.

Walker, C. C. and Gardner, A. S.: Rapid drawdown of Antarctica's Wordie Ice Shelf glaciers in response to ENSO/Southern Annular Mode-driven warming in the Southern Ocean, Earth and Planetary Science Letters, 476, 100–110, doi: 10.1016/j.epsl.2017.08.005, 2017.

Zhao, C., King, M. A., Watson, C. S., Barletta, V. R., Bordoni, A., Dell, M. and Whitehouse, P. L.: Rapid ice unloading in the Fleming Glacier region, southern Antarctic Peninsula, and its effect on bedrock uplift rates, Earth and Planetary Science Letters, 473, 164–176, doi: 10.1016/j.epsl.2017.06.002, 2017.

Recent dynamic changes on Fleming Glacier after the disintegration of Wordie Ice Shelf, Antarctic Peninsula

Peter Friedl[1], Thorsten C. Seehaus[2], Anja Wendt[3], Matthias H. Braun[2], Kathrin Höppner[1]

[1]German Remote Sensing Data Center (DFD), German Aerospace Center (DLR), Oberpfaffenhofen, 82234, Germany
[2]Institute of Geography, Friedrich-Alexander-University Erlangen-Nuremberg, Erlangen, 91058, Germany
[3]Bavarian Academy of Sciences and Humanities, Munich, 80539, Germany

Correspondence to: Peter Friedl (peter.friedl@dlr.de)

Abstract. The Antarctic Peninsula is one of the world`s regions most affected by climate change. Several ice shelves retreated, thinned or completely disintegrated during recent decades, leading to acceleration and increased calving of their tributary glaciers. Wordie Ice Shelf, located in Marguerite Bay at the south-western side of the Antarctic Peninsula, completely disintegrated in a series of events between the 1960s and the late 1990s. We investigate the long-term dynamics (1994–2016) of Fleming Glacier after the disintegration of Wordie Ice Shelf by analysing various multi-sensor remote sensing datasets. We present a dense time series of Synthetic Aperture Radar (SAR) surface velocities that reveals a rapid acceleration of Fleming Glacier in 2008 and a phase of further gradual acceleration and upstream propagation of high velocities in 2010–2011.The timing in acceleration correlates with strong upwelling events of warm Circumpolar Deep Water (CDW) into Wordie Bay, most likely leading to increased submarine melt. This, together with continuous dynamic thinning and a deep subglacial trough with a retrograde bed slope close to the terminus probably has induced unpinning of the glacier tongue in 2008 and gradual grounding line retreat between 2010 and 2011. Our data suggest that the glacier`s grounding line had retreated by ~6–9 km between 1996 and 2011, which caused ~56 km^2 of the glacier tongue to go afloat. The resulting reduction in buttressing explains a ~~remarkable~~ median speedup of ~1.3 m d^{-1} (~27~~30~~ %) between 2008~~2007~~ and 2011, which we observed along a centreline extending between the grounding line in 1996 and ~16 km upstream. Current median ice thinning rates (2011–2014) along profiles in areas below 1000 m altitude range between ~2.6 to 3.2 m a^{-1} and are ~70 % higher than between 2004 and 2008. Our study shows that Fleming Glacier is far away from approaching a new equilibrium and that the glacier dynamics are not primarily controlled by the loss of the former ice shelf anymore. Currently, the tongue of Fleming Glacier is grounded in a zone of bedrock elevation between ~-400 and -500 m. However, about 3–4 km upstream modelled bedrock topography indicates a retrograde bed which transitions into a deep trough of up to ~-1100 m at ~10 km upstream. Hence, this endangers upstream ice masses, which can significantly increase the contribution of Fleming Glacier to sea level rise in the future.

1 Introduction

Recent studies have shown that the Antarctic Peninsula ice masses are strong contributors to sea level rise. In a consolidated effort Shepherd et al. (2012) estimated the contribution between 2005 and 2010 to 36 ± 10 Gt a^{-1} corresponding to 0.1 ± 0.03 mm a^{-1} SLE (sea level equivalent). This is considerably higher than their reported ice mass loss for the period from 1992 to 2000 of 8 ± 17 Gt a^{-1} (Shepherd et al., 2012). Huss and Farinotti (2014) computed from their ice thickness reconstruction of the northern and central Antarctic Peninsula a maximum potential sea level rise contribution of 69 ± 5 mm.

Rott et al. (2014) estimated the total dynamic ice mass loss for the glaciers along the Nordenskjöld Coast and the Sjögren-Boydell glaciers after ice shelf disintegration to be 4.21 ± 0.37 Gt a^{-1} between 2011–2013. Seehaus et al. (2015; 2016) revealed similar values for tributary glaciers of the former Larsen-A and Prince-Gustav-Channel ice shelves. On the western Antarctic Peninsula south of -70° increased ice discharge and considerable thinning rates have been reported for various ice shelf tributaries (Wouters et al., 2015).

The main cause for the current increased ice discharge on the Antarctic Peninsula is the dynamic response of tributary glaciers to the disintegration and basal thinning of several ice shelves (e.g. Angelis and Skvarca, 2003; Pritchard et al., 2012; Rignot, 2006; Wouters et al., 2015; Wuite et al., 2015). With the reduction or loss of the buttressing effect of the ice shelves (Fürst et al., 2016; Mercer, 1978) due to thinning or disintegration, the tributary glaciers accelerate and show imbalance (Rignot et al., 2005; Rott et al., 2014; Scambos et al., 2004).

For the south-western Antarctic Peninsula Rignot et al. (2013) demonstrated that basal melt of George VI, Wilkins, Bach and Stange Ice Shelves exceeded the ablation induced by calving. For Wordie Ice Shelf high basal melt rates of 23.6 ± 10 m a^{-1} (2003–2008) and 14.79 ± 5.26 m a^{-1} (2009) have been reported by Rignot et al. (2013) and Depoorter et al. (2013) respectively. However, the presented melt ratios (i.e. the ratio between basal melt and the sum of calving flux and basal melt) differ between 46 % (Rignot et al., 2013) and 82 % (Depoorter et al., 2013).

Wilkins Ice Shelf experienced amplified basal thinning controlled by small-scale coastal atmospheric and oceanic processes that assist ventilation of the sub-ice-shelf cavity by upper-ocean water masses (e.g. variations in wind stress or reduced freshwater fluxes from runoff and ice-shelf basal melt) until ~8 years before break-up events took place in 2008 and 2009 (Braun and Humbert, 2009; Padman et al., 2012). Subsequent changes in ice dynamics and stresses leading to break-up have been observed (Rankl et al., 2016). On George VI Ice Shelf, surface lowering is linked to enhanced basal melt caused by an increased circulation of warmed Circumpolar Deep Water (CDW) (Holt et al., 2013) and a 13 % increase in ice flow was observed between 1992 and 2015 for its tributary glaciers (Hogg et al., 2017).

However, how the dynamic response after ice shelf loss progresses and how long this process lasts, is frequently unknown. Seehaus et al. (2016) showed that significant temporal differences in the adaptation of glacier dynamics in response to ice shelf decay can occur and that those can only be resolved, if dense time series of satellite-based measurements are available. Wendt et al. (2010) also concluded for Wordie Ice Shelf that its former tributaries were still far from reaching a new equilibrium after retreat and collapse of the ice shelf starting in the 1960's. However, given the limited data used in previous

studies, Wendt et al. (2010) pointed out that a much closer monitoring is required to verify this. A recent comparison of stacked surface velocities of Fleming Glacier derived from InSAR in 2008 with velocities obtained from Landsat 8 feature tracking in 2014and 2015 revealed that the glacier had sped up by ~400–500 m a^{-1}~~, which is the largest acceleration in ice flow recorded across all of Antarctica~~ (Walker and Gardner, 2017; Zhao et al., 2017). However, the question why the magnitude of change was much higher than recorded elsewhere at the western Antarctic Peninsula over a similar time period remained unanswered so far. In this study we investigate the glacier dynamics of Fleming Glacier after the disintegration of Wordie Ice Shelf on the south-western Antarctic Peninsula. Our study ties in with previous works in the region, but covers a much longer time period at a much higher temporal resolution. We provide a dense time series of ice velocity measurements from Synthetic Aperture Radar (SAR) satellite data for the time period 1994–2016 for Fleming Glacier. In order to investigate the observed changes in ice dynamics, we conducted an in-depth analysis of other geophysical and geodetic remote sensing data such as airborne Light Detection and Ranging (LiDAR) and satellite-borne laser altimetry, radio echo sounding for ice thickness, bistatic and monostatic SAR data as well as optical satellite images. We derive frontal retreat, surface velocity changes, ice elevation changes, grounding line positions and estimate the area of freely floating ice from hydrostatic equilibrium.

2 Study site

The former Wordie Ice Shelf was located in Marguerite Bay on the south-western Antarctic Peninsula. The ice shelf was originally fed by several major input units (Fig. 1). Among these, Fleming Glacier is the biggest. It has a current length of approx. 80 km and is up to 10 km wide at its tongue. With a speed of more than 8 m d^{-1} close to its calving front (Fig. 1), Fleming Glacier is also the fastest flowing glacier in Wordie Bay. Fleming Glacier merges with Seller and Airy Glacier ~8 km upstream of their joint calving front. Together with Rotz Glacier, which merges with Seller Glacier ~28 km upstream of the front, all four glaciers form the Airy-Rotz-Seller-Fleming glacier system, spanning a total catchment area of about 7000 km^2 (Cook et al., 2014).

Starting in the 1960s, Wordie Ice Shelf ran through a stepwise disintegration process (Fig. 1), which was controlled by pinning points (i.e. ice rises/rumples). Analyses of satellite imagery suggest that the ice shelf was temporarily grounded and stabilized at these pining points until one of the next rapid break-up events took place (Doake and Vaughan, 1991; Reynolds, 1988; Vaughan, 1993; Vaughan and Doake, 1996). However, during phases of ice front retreat, instead of protecting the ice shelf against decay, ice rises that were embedded in the ice shelf appeared to behave as indenting wedges, contributing to weakening the ice shelf and accelerating break-up (Doake and Vaughan, 1991; Vaughan, 1993). It is likely that the collapse of Wordie Ice Shelf was triggered by a combination of amplified ablation due to rising air temperatures (Doake and Vaughan, 1991), enhanced tidal action as a consequence of relaxed sea-ice conditions in Marguerite Bay (Reynolds, 1988) and increased basal melt rates on ice shelves in the Bellingshausen Sea due to rising ocean temperatures (Depoorter et al., 2013; Holland et al., 2010; Pritchard et al., 2012; Rignot et al., 2013).

After the last big disintegration event in 1989, the ice shelf was split into a northern and a southern part (Doake and Vaughan, 1991). In the early 1990s most of the remaining floating ice in Wordie Bay consisted only of the protruding, unconfined tongues of the disconnected tributary glaciers. These tongues disappeared between 1998 and 1999, so that in 1999 Fleming Glacier was already calving near its 1996 grounding line (Rignot et al., 2005). Wendt et al. (2010) found the remaining area of floating ice to be only 96 km^2 in 2009. At this time there was virtually no contiguous ice shelf left and only the glaciers of the Prospect unit and Hariot`s unnamed neighbouring glacier still possessed floating glacier tongues (Wendt et al., 2010). During the following years (2010–2015) the fronts of the glaciers in Wordie Bay remained quite stable, except at the Prospect system where the once interconnected floating ice tongues of the three glaciers disconnected and some floating ice was lost. This resulted in an total area of 84 km^2 of ice shelf in Wordie Bay in 2015, if taking the grounding line of 1996 as a baseline (Rignot et al., 2005; Rignot et al., 2011a) and ignoring any grounding line migration.

While in the early 1990's an acceleration was not yet observed from the visual inspection of optical satellite imagery (Doake and Vaughan, 1991; Vaughan, 1993), Rignot et al. (2005) found substantial dynamic thinning and an increase of surface velocities by 40–50 % in 1996 against 3 point measurements by Doake (1975) in 1974 on Fleming Glacier (Fig. 1). The higher velocities as well as further thinning were also confirmed through Global Navigation Satellite System (GNSS) measurements in 2008 and airborne LiDAR surveys in 2004 and 2008 respectively (Wendt et al., 2010). Then, further speed up of the order ~~an Antarctic-wide unprecedented acceleration~~ of ~ 400–500 m a^{-1} was recorded between 2008 and 2014/2015 (Walker and Gardner, 2017; Zhao et al., 2017).

3 Data

We used a broad remote sensing data set in order to investigate the changes in ice dynamics at Fleming Glacier between 1994 and 2016 after the disintegration of Wordie Ice Shelf. Tab. 1 gives an overview of the specifications and the time coverages of the sensors used. The Bedmap2 digital elevation model (DEM) of Antarctica (Fretwell et al., 2013), resampled to 100 m resolution, was taken as a topographic reference for orthorectification of the surface velocity fields and for the derivation of local incidence angles required for the conversion from slant to ground range displacement. Over the Antarctic Peninsula the Bedmap2 DEM provides a seamless compilation of data from the improved ASTER GDEM (from ASTER stereo images acquired between 2000 and 2009) (Cook et al., 2012), the SPIRIT DEM (from SPOT stereo images acquired in 2007 and 2008) and the NSIDC DEM (from ICESat data acquired between 2003 and 2005) (DiMarzio et al., 2007).

Calibrated and multi-looked SAR intensity images, Landsat 7 imagery and an existing dataset of ice shelf outlines (Ferrigno, 2008) were taken as a reference for the delineation of the ice shelf/glacier front (Tab. S1).

Calculations of elevation change rates were based on airborne LiDAR measurements, satellite-borne laser altimeter measurements and two DEMs derived from SAR interferometry (Tab. 1). The two DEMs covering the Airy-Rotz-Seller-Fleming glacier system were calculated from bistatic TerraSAR-X/TanDEM-X (TSX/TDX) Coregistered Single look Slant range Complex (CoSSC) strip map (SM) acquisitions on 2011-11-21 and monostatic TSX/TDX CoSSC SM acquisitions on

2014-11-03 (Fritz et al., 2012; Krieger et al., 2013). The TSX/TDX data were selected as close as possible to the dates of two NASA Operation IceBridge (OIB) Airborne Topographic Mapper (ATM) flights in 2011 and 2014, in order to be able to correct for radar penetration depth biases.

A simulated phase from a subset of the TanDEM-X global DEM with a spatial resolution of 12 m (Rizzoli et al., 2017) was used to facilitate phase unwrapping during the generation of the two TSX/TDX DEMs. The TanDEM-X global DEM was also used as a reference for the absolute height adjustment of the TSX/TDX DEMs.

For the determination of the floating area on the tongue of Fleming Glacier, we used information on ice thickness and surface elevation from several Pre-IceBridge (PIB) and OIB flight lines across the Airy-Rotz-Seller-Fleming glacier system between 2002-11-26 and 2014-11-16 (Tab. 1). Depending on the date of acquisition, ice thickness data was recorded by different versions of the Coherent Radar Depth Sounder (CoRDS) (Tab. 1).

Our estimation of the recent grounding line of Fleming Glacier was based on a combination of the information on hydrostatic equilibrium with bedrock topography data, profiles of surface velocities and elevation change rate patterns inferred from the 2011–2014 TSX/TDX data. Information on bedrock topography was taken from the modelled bedrock grid of Huss and Farinotti (2014), which represents the most detailed dataset on bedrock topography available for the Antarctic Peninsula. The dataset was generated by subtracting modelled ice thickness from the improved ASTER GDEM by Cook et al. (2012). Ice thickness was derived by constraining a simple model based on the shallow ice approximation for ice dynamics with observational data of ice thickness (OIB) and surface velocity (Rignot et al., 2011b). Where available the modelled ice thickness was corrected with OIB ice thickness data, leading to more precise ice thickness values in such areas. On average, the local uncertainty in ice thickness of the dataset is ~~±~~95 m, but uncertainties ~~values~~ can reach ~~±~~500 m for deep troughs without nearby OIB measurements. Since OIB coverage is fairly good across Fleming Glacier, uncertainties in modelled ice thickness are relatively low in this area. However, a comparison of bedrock elevations from Huss and Farinotti (2014) with bottom elevations calculated from OIB ATM and CoRDS measurements shows that although the modelled bedrock reflects the general subglacial topography well, the absolute difference in bottom elevation can be even more than 100 m (Fig. S5). One possible reason for this is a difference between ATM heights and the refined ASTER GDEM, which transfers to bedrock elevation.

4 Methods

4.1 Surface velocities

For each sensor consecutive pairs of coregistered single look complex SAR images were processed using an intensity offset tracking algorithm (Strozzi et al., 2002). A moving window was used to calculate surface displacements in azimuth and slant range direction between two SAR intensity images by localizing the peaks of an intensity-cross correlation function. The technique requires the definition of a tracking patch size and a step size (i.e. the distances in range and azimuth between the

centres of two consecutive moving windows, Tab. 1). The parameters were chosen according to the sensor specifications, the temporal baseline between the acquisitions and the expected displacement.

During the tracking procedure the implementation of a cross correlation threshold of 0.05 assured the removal of low quality offset estimates. Post-processing of the velocity fields comprises an additional filtering (Burgess et al., 2012) based on the comparison of the orientation and magnitude of the displacement vectors relative to their surrounding vectors. This algorithm discards over 99 % of unreasonable tracking results. The filtered displacement fields were then transferred from slant range geometry into ground range geometry, geocoded and orthorectified. The procedure to determine the error of the velocity measurements is described in the Supplemental material, Sect. S2. The errors for each velocity field and the proportion of velocity vectors removed by the filter are listed in Tab. S3.

4.2 Elevation change

We derived ice thinning rates on Fleming Glacier for 2004–2008 and 2011–2014 by comparing ellipsoid heights of the PIB (ATM L1B, 2004), the Centro de Estudios Científicos Airborne Mapping System (CAMS, 2008) and the OIB (ATM L1B, 2011, 2014) airborne LiDAR datasets. The vertical accuracy of the ATM L1B elevation data is estimated to be better than 0.1 m (Krabill et al., 2002; Martin et al., 2012). For the CAMS data, vertical accuracy is 0.2 m (Wendt et al. (2010). Before subtraction, overlapping data of the originally closely spaced measurements were condensed to a common set of median surface elevations with an equal spacing of 50 m in along and across track direction. The locations of the resulting points of differential elevation measurements are shown in Fig. 4. The uncertainty of the gridded measurements can be attributed to both physical topographical features and measurement error. We approximated the uncertainty of each gridded median surface elevation similar as recommended in the IceBridge ATM L2 user guide (https://nsidc.org/data/ILATM2/versions/2/) by calculating the normalized median absolute deviation (NMAD) of all measurements in a 50 m grid cell. For each LiDAR dataset the median NMAD value of all grid cells was taken as the total uncertainty in surface elevation. Total uncertainties in surface elevation were 0.46 m (2004), 0.39 m (2008), 0.38 m (2011) and 0.43 m (2014). For each pair of overlapping gridded median surface elevations we derived the uncertainty in elevation change rate by calculating the root of the sum squares (RSS) of the corresponding NMAD values and dividing the result by the difference in acquisition time (years). The total uncertainty in elevation change rate for a complete dataset was calculated as the median of the elevation change rate uncertainties of all grid cells. The total uncertainties in elevation change rate were 0.32 m a^{-1} for 2004–2008 and 0.24 m a^{-1} for 2011–2014.

Additionally to the airborne LiDAR measurements ice elevation change rates for the period 2004–2008 were calculated from ellipsoid heights measured by the Ice, Cloud and Land Elevation Satellite (ICESat). Saturation of the 1064 nm Geoscience Laser Altimeter System (GLAS) detector can occur over ice, leading to a distorted echo waveform (Schutz et al., 2005). Hence we applied a saturation elevation correction provided on the GLA12 product prior to subtracting both tracks and excluded elevation measurements with flagged invalid saturation correction values from our analyses. Since both repeat tracks are not overlapping but separated by ~150 m in across track direction, we linearly interpolated the elevation data of

the 2004 track onto the latitude values of the 2008 data prior to subtraction, as described in Fricker and Padman (2006). In order to keep the error induced by interpolation low, elevation values were only allowed to be interpolated between two footprint centre locations with an along track spacing of ~170 m. This assured that existing gaps in the real data were preserved. Shuman et al. (2006) report a relative accuracy of ~~±~~ 0.25 m for ICESat elevations measured on surface slopes between 1.5 and 2.0°. The mean surface slopes along the two ICESat elevation profiles were 1.9°. Hence, taking into account further possible inaccuracies of ~~±~~ 0.15 m due to interpolation, we estimated the accuracy of the ICESat ice elevations to be ± 0.4 m. By calculating the RSS of the ICESat elevation uncertainties and dividing the result by the time interval between the measurements (years), we estimated the uncertainty in ICESat elevation change rates to be 0.13 m a^{-1}.

A map of elevation change rates between 2011 and 2014 was calculated by differencing two TSX/TDX-DEMs. Both DEMs have a spatial resolution of 10 m. To generate the DEMs we applied a differential interferometric approach, which facilitates phase unwrapping by incorporating the topographic information of a reference DEM (Vijay and Braun, 2016). A subset of the TanDEM-X global DEM, covering the two TSX/TDX-DEMs, was chosen to be the reference DEM.

Before differencing, the TSX/TDX-DEMs must be vertically referenced. For this purpose the ~~median~~ vertical offset between the DEMs and the TanDEM-X global DEM was measured over stable areas (i.e. tops of nunataks and rock outcrops, which were not affected by image distortions) at altitudes between 150 m and 1000 m (Fig. S1). Both DEMs were adjusted according to the median values of all ground control measurements (n=35452), which were -5.1 m for the 2011 DEM and 0.48 m for the 2014 DEM.~~, before both DEMs were adjusted accordingly~~. After subtracting the vertically registered DEMs, the elevation differences were converted into yearly elevation change rates. We assessed the accuracy of the vertical registration over another set of stable areas at altitudes between 150 m and 1300 m (Fig. S1). The absolute median value of the extracted change rates was 0.37 m a^{-1} which primarily accounts for errors related to the vertical registration.

However, since radar signals can penetrate several meters into snow and ice, depending on the radar frequency and the dielectricity of the medium (Mätzler, 1987; Rignot et al., 2001), an additional bias is induced on glaciated areas when differencing interferometric DEMs from different times and/or frequencies (Berthier et al., 2016; Seehaus et al., 2015; Vijay and Braun, 2016). Since the TSX/TDX data was acquired only 4–7 days apart from the ATM data, differences in elevation change rates between the two datasets can be primarily attributed to differences in penetration depth at the TSX/TDX acquisitions in 2011 and 2014 and remaining vertical registration errors. In order to compare the TSX/TDX data with the ATM data, we extracted the TSX/TDX elevation change rates at the locations of the differential OIB ATM measurements using a buffer with a radius of 25 m and calculated the median for each point. Hypsometric reference values were taken from the resampled Bedmap2 DEM which we converted to ellipsoidal heights using the included geoid correction layer. The comparison between elevation change rates obtained from the 2011–2014 OIB ATM flights and the 2011–2014 TSX/TDX data after the vertical registration of the DEMs showed a maximum overestimation of ice thinning of 1.25 m a^{-1} for the TSX/TDX measurements (Fig. S4 a, b). However, the general trend of the elevation change rates fits well to those calculated from the LiDAR data and significant differences in elevation change were only measured in the lower areas of the glacier tongue. In the upper areas (above 600 m altitude) the difference between ATM and TSX/TDX elevation change rates was

close to 0 m. Here the snow volume was likely completely frozen on both dates of acquisition, so that the penetration bias cancelled out. A backscatter comparison showed lower values in 2014 than in 2011 in areas below 600 m altitude, whereas the backscatter in the upper areas above 600 m altitude was similar for both dates (Fig. S4 d). We corrected the TSX/TDX data with a local polynomial model based on the elevation change rate differences between the ATM and the TSX/TDX data (Fig. S4 b). We applied this correction to all glaciated areas below 1000 m and clipped the TSX/TDX elevation change rate map accordingly. The RMSE between the cubic fits of the ATM elevation change rates and the extracted values from the corrected TSX/TDX map was 0.02 m a^{-1} (Fig. S4 c). Nevertheless, penetration depths of the radar signal may be spatially variable at the same altitude e.g. due to local differences in surface melt or ice properties. Hence we checked the validity of the applied penetration depth correction by comparing the corrected TSX/TDX elevation change rates with an independent validation track of 2011–2014 ATM dh/dt rates (see Fig. 4 for location). Figure S4 e shows that the elevation change rates of both datasets are in good agreement. The RMSE between the cubic fits of the data was 0.24 m a^{-1}. Hence we estimate the uncertainty due to remaining penetration depth differences to be 0.3 m a^{-1}. ~~However, by taking into account unknown errors due to the extrapolation of the correction factors to the entire glacier area, we assumed a remaining error of ± 0.2 m a^{-1} related to penetration depth differences.~~ Together with the error of vertical registration, this resulted in a total error of ~~±~~ 0.67~~57~~ m a^{-1} for the TSX/TDX ice thinning rates.

For our analyses of elevation change we compared ice thinning rates from the PIB and the CAMS airborne laser altimeter data (2004–2008) with rates obtained from the OIB data (2011–2014) as well as elevation change rates from the TSX/TDX data (2011–2014) with those derived from ICESat in 2004 and 2008. For the comparison between the TSX/TDX and the ICESat data, ice thinning rates were extracted from the TSX/TDX map at the GLAS centre locations of the 2008-10-04 track. To take into account the 70 m footprint of the GLAS instrument, we applied a buffer with a radius of 35 m and calculated the median from the extracted values at each point.

4.3 Floating area (hydrostatic height anomalies) and estimation of recent grounding line

In order to determine the floating area on the tongue of the Airy-Rotz-Seller-Fleming glacier system at different points in time, we derived hydrostatic height anomalies Δe from the PIB and OIB elevation and ice thickness measurements between 2002 and 2014. For every measuring point of ice thickness, Δe was calculated similar to Fricker (2002) by subtracting a theoretical freeboard height in hydrostatic equilibrium e_{he} from a measured orthometric ATM ice surface elevation e:

$$\Delta e = e - e_{he} \quad (1)$$

Regions on the glacier tongue where $\Delta e \leq$ ~~$\approx$~~ 0 were considered as freely floating. Before deriving hydrostatic height anomalies, we merged simultaneously acquired ice thickness and ATM data by calculating the median elevation within a buffer of 50 m at each ice thickness measurement. As the ATM heights were originally measured relative to the WGS84 ellipsoid, we converted the ellipsoidal ATM values to orthometric heights prior to the buoyancy calculations. For the

conversion we used kriged geoid values calculated for a mean tide system with the EIGEN-6C4 global gravity field model (Förste et al., 2014). We calculated e_{he} by applying a modified formula after Griggs and Bamber (2011):

$$e_{he} = (H_i + \delta) - \frac{H_i \cdot \rho_i}{\rho_w} \quad (2)$$

where H_i is the measured PIB or OIB ice thickness, i.e. the ice thickness derived under the assumption that all ice is homogeneous and firn free, ρ_i is the ice density of pure ice, ρ_w is the density of sea water and δ is the firn density correction factor, i.e. the difference between the actual thickness of the firn layer above the glacier ice and the thickness that the firn would have if it were at the density of pure ice (Griggs and Bamber, 2011; van den Broeke, Michiel et al., 2008). Details on the uncertainties of all variables used for the calculations as well as the assessment of error propagation are provided in the Supplemental material, Sect. S3.

The buoyancy calculations provided information on the limit of hydrostatic equilibrium between 2002 and 2014 at several locations on the glacier system. As demonstrated in Seehaus et al. (2015), clear patterns of low or positive ice thinning rates in dh/dt maps reveal areas of floating ice, since buoyancy can cause originally grounded ice to bounce and/or decreases the effect of ice thinning on ice surface elevation to ~10 %.

Moreover, the grounding line marks the transition between two fundamentally different flow regimes of grounded and freely floating ice. Whereas the flow dynamics of grounded ice are dominated by vertical shear and controlled by basal drag, flow of floating ice is drag free and dominated by longitudinal stretching and lateral shear (Schoof, 2007). The difference in flow dynamics of grounded and floating ice can result in pronounced changes in surface velocity close to the grounding line (Stearns, 2007; Stearns, 2011). Furthermore, Rignot et al. (2002) demonstrated that if ungrounding occurs, the resulting flow acceleration usually affects both the floating and the grounded part of the glacier, but is largest near the grounding zone. Thus, velocity profiles can serve as additional information for locating the grounding line (Stearns, 2007; Stearns, 2011).

Bedrock elevation data can reveal subglacial topographic features which act as pinning points for the glacier. Hence, our estimations of recent and previous grounding line positions were based on information on hydrostatic equilibrium from the hydrostatic height anomaly calculations as well as maps and profiles of TDX/TSX 2011–2014 elevation change rates, modelled bedrock topography (Huss and Farinotti, 2014) and surface velocities. Wherever possible, we gave preference to information on hydrostatic equilibrium for the final decision of the recent grounding line location. For selected profiles across the glacier, recent and previous (2008) grounding line positions were estimated by combining evidence from elevation change, bedrock topography and surface velocity. In the remaining areas, the recent grounding line was interpolated ~~deduced by from~~ combining information on elevation change rate patterns in the TDX/TSX 2011–2014 dh/dt map with information on bedrock topography.

5 Results

5.1 Surface velocities

Figure 2 shows the multi sensor time series (1994–2016) of SAR intensity tracking derived velocities along a centreline profile on Fleming Glacier (Fig. 1). The profile extends from the grounding line location in 1996 to 16 km upstream. The relative distance of the glacier front to the 1996 grounding line is shown on the left side of the plot. Distances in the subsequent text are given in reference to the grounding line of 1996. Positive values relate to positions on the glacier upstream of (behind) the former grounding line, while negative values refer to locations seawards of the 1996 grounding line.

~~After 1999 the glacier front remained comparatively steady close to the grounding line location in 1996 for almost 10 years. Figure 2 shows that glacier velocities were rather stable between 1994 and 2007. The normalised median absolution deviation (NMAD) of the median velocities during this time was 0.06 m d^{-1}.~~ Figures 3a, b depict absolute and relative velocity changes for 1 km bins along the centreline profile for the periods 1997–January 2008, January 2008–April 2008, 2010–2011, April 2008–2011 and 2011–2015. In 2011 the location of the glacier front reached its most inland position. We excluded all measurements seaward of the 2011 glacier front from our analyses, since this is the section of the profile where frontal change took place and we did not want to compare velocities measured on sea ice or ice mélange.

Figure 2 shows that glacier velocities were rather stable between 1994 and January 2008 although almost all of the remaining floating tongue got lost between 1998 and 1999. After 1999 the glacier front remained comparatively steady close to the grounding line location in 1996 for almost 10 years. The NMAD of the median velocities between 1994 and January 2008 was 0.06 m d^{-1}(Fig. 2). Figure 3a reveals ~~A comparison of the velocities on 1995-10-27 and 2007-10-23 (Fig. 3a) along the centreline profile reveals~~ that the median velocity difference between 1997~~5~~ and January 2008~~7~~ along the centreline profile was just 0.07~~4~~ m d^{-1} with maximum velocity differences not exceeding 0.2 m d^{-1}.

Between January and April 2008 a rapid and almost constant acceleration ~~of Fleming Glacier~~of ~0.4 m d^{-1} was noticeable along the ~~-~~centreline until ~13 km upstream (Fig. 3a) and velocities >5 m d^{-1} propagated ~8 km inland (Fig. 2, orange and red colours). The median relative increase in surface velocity between 3 and 13 km upstream was ~8 %, with a maximum increase of ~10 % at ~13 km upstream (Fig. 3b). ~~, which propagated ~8 km inland.~~ Simultaneously, the front of Fleming Glacier retreated behind the 1996 grounding line for the first time. Since 2008 the glacier tongue has not advanced seaward of the 1996 grounding line position (Fig. 2).

The velocity pattern persisted until March 2010, when a second phase of acceleration began. Our velocity time series shows that velocities >5 m d^{-1} ~~the acceleration~~ gradually propagated further inland within one year, until they~~it~~ reached ~~its final extension~~ ~12 km upstream in early 2011. Velocity change during this time period increased towards the glacier front and reached a maximum value of ~~. Fig. 3a, b show absolute and relative velocity changes along the centreline profile for the periods 1995–2007, 2007–2011 and 2011–2015. In 2011 the location of the glacier front reached its most inland position.~~ ~0.9 m d^{-1} or ~16 % at ~6 km upstream. ~~Consequently velocities measured on sea ice or ice mélange in 2011 (seaward of the~~

2011 front) were excluded from our analyses. Large changes in surface velocity close to the 2011 front in the periods January 2008–2011, 2010–2011 and 2011–2016 were ignored, since they do not represent real dynamic change, but result from comparing the inherently higher frontal velocities in 2011 with lower velocities of the floating glacier tongue in 2008, 2010 and 2016. If looking at the complete period between January 2008 and 2011 Between 2007-10-23 and 2011-10-02 the increase in median surface velocity between ~4 and ~7 km upstream along the profile was ~1.3 m d^{-1} or ~32 % (Fig. 3a, b). If ignoring velocity change in the vicinity of the 2011 glacier front, the highest relative acceleration values of >1.4 m d^{-1} or ~28 % (~32–35 %) were recorded at ~ 6 km between ~7 and ~11 km upstream of the 1996 grounding line (Fig. 3ab). The amount of absolute and relative acceleration rises significantly at ~7 km and abruptly drops at ~12 km (Fig. 3 a, b). Peak absolute acceleration values of ~1.6 m d^{-1} were found at ~8 km. If excluding measurements at the 2011 front, no further marked changes in velocities were detected along our centreline profile after 2011. From 2011 to 2016 median velocity change was just 0.06 m d^{-1} between 4 and 16 km upstream and maximum values were smaller than 0.2 m d^{-1} (Fig. 3 a, b, Fig. 1). For the same time period the NMAD of the median centreline velocities was just 0.02 m d^{-1} (Fig. 2).

Surface velocities on 2013-12-24 at the three measuring sites of Doake (1975) ~50 km upstream (Fig. 1) were very similar to those measured in 1996 and 2008. Furthermore, the flow directions in 2013 were like those in 2008 and 1974. However, surface velocities derived from Landsat 8 feature tracking suggest that in 2015 velocities at the three measuring sites had increased by ~20% in comparison to 2008 (Walker and Gardner, 2017; Zhao et al., 2017) (Tab. 2).

5.2 Elevation change

Figure 4 shows elevation change rates on the Airy-Rotz-Seller-Fleming glacier system for the period between 2011 and 2014. The entire area undergoes a considerable drawdown. On Fleming Glacier the highest ice thinning rates with peak values of more than ~6 m a^{-1} were recorded in a zone extending from ~8 to ~14 km upstream. On Seller Glacier the ice loss exceeds ~6 m a^{-1} at about 7 km upstream. In general, ice thinning decreases towards higher altitudes. A tendency to lower negative or even positive elevation change rates was observed on the lower parts of the joint Fleming and Seller glacier tongue between 0 and up to ~9 km upstream. The pattern was not as clear as on Airy Glacier, where a distinct area of low ice thinning rates was detected between 0 and ~4 km upstream.

Figures 5 a) and b) show comparisons of elevation change rates for the times prior to (2004–2008) and after the glacier acceleration (2011–2014).The location of the data is shown in Fig. 4. In Fig. 5 a) elevation change rates from PIB ATM-CAMS measurements (2004–2008) are plotted together with rates from ATM measurements in 2011 and 2014. The large scattering of the data is due to the highly crevassed surface of the glacier tongue, where a purely horizontal displacement of crevasses can cause apparent positive and negative elevation differences. Therefore, a median filter was applied to the data before adjustment of a cubic function. Fig. 5 b) shows ice thinning rates from ICESat tracks in 2004 and 2008 together with rates calculated from 2011–2014 TSX/TDX data. Note that the ATM data in Fig. 5 a) and the ICESat data in Fig. 5 b) refer to different profiles.

Figure 5 shows that prior to the speedup in 2008, Fleming Glacier has already been affected by pronounced surface lowering. A clear trend of increasing ice thinning rates towards the glacier front is visible for 2004–2008 on both profiles. During this period the maximum negative elevation change rates were found close to the 1996 grounding line. Here the cubic regression functions imply that the ice surface lowered at a maximum of ~3.8 m a^{-1} for the CAMS-ATM measurements and at ~4.6 m a^{-1} for the ICESat data. For all median elevation change rates presented below, we calculated the NMAD in order to account for the statistical dispersion of the input data. The median ice thinning rates measured during 2004–2008 for the cubic fits were 1.5 ± 0.6 m a^{-1} on the CAMS-ATM flightpath and 1.9 ± 1 m a^{-1} on the ICESat track. The OIB ATM and the TSX/TDX elevation change rates between 2011 and 2014 reveal a significant change in pattern for the time after the glacier flow acceleration. A tendency to lower ice thinning rates is present towards the glacier front and high negative elevation change rates can be found in a zone 10–15 km upstream, with maximum ice losses of ~3.7 m a^{-1} for the ATM, and ~4.1 m a^{-1} for the TSX/TDX cubic regression functions. The median elevation change rates were -3.2 ± 0.8 m a^{-1} and -2.6 ± 1.2 m a^{-1} for the cubic fits of the 2011–2014 TSX/TDX data (Fig. 5 b) and the 2011–2014 ATM data (Fig. 5 a), respectively. Despite of lower ice thinning rates measured towards the ice front in 2011–2014, our data show an overall median increase of ice thinning rates along the profiles of ~1.1–1.3 m a^{-1} or ~70 % between the periods from 2004 to 2008 and from 2011 to 2014. However, in some areas 10–15 km upstream, ice thinning rates even doubled in the latter period.

5.3 Floating area (hydrostatic height anomalies) and estimation of recent grounding line

Figure 6 depicts the results of the hydrostatic height anomaly calculations from PIB and OIB elevation and ice thickness data acquired before (2002–2004) and after the speedup of Fleming Glacier (2011–2014). Detailed plots showing the results of the hydrostatic height anomaly calculations along PIB and OIB flight lines can be found in the Supplemental Material, Fig. S5 a–e.

The hydrostatic height anomaly data of 2002 and 2004 (Fig. 6, Track 1 and 2) clearly reveal that the ice inland of the 1996 grounding line was not floating at these times. However, the same calculations for data acquired in 2011 and 2014 (Fig. 6, Track 3–5) as well as patterns of low and positive elevation change rates in the TSX/TDX 2011–2014 dh/dt map (Fig. 4, S7) suggest that after the final stage of glacier acceleration in 2011 an area of about 56 km^2 (referring to the front in 2014) of the formerly grounded glacier tongue of the Airy Rotz Seller Fleming system had been afloat.

The bedrock elevation model of Huss and Farinotti (2014) exhibits, that the boundary of the area showing flotation follows bedrock ridges (Fig. 6). Those confine a subglacial trough underneath the Airy-Rotz-Seller-Fleming glacier system. The ridges reach up to ~9 km upstream of the 1996 grounding line. For most regions of the glacier tongue we estimate the current grounding line to coincide with these ridges at an elevation between ~-400 and -500 m. On Fleming and Seller Glacier our estimation of the recent grounding line also largely coincides with the extent of lower ice elevation change rates apparent in the TSX/TDX 2011–2014 dh/dt map (Fig. S7). However, on Airy Glacier a distinct area of low ice thinning rates on the lower part of the glacier tongue indicates floatation (Fig. 4, S7), whereas hydrostatic equilibrium in 2011 suggests that the glacier is grounded on a hump which reaches to the subglacial trough (Fig. 6).

We extracted data of surface velocities, TDX/TSX 2011–2014 elevation change rates and bedrock topography along four profiles on Airy and Fleming Glacier in order to estimate recent grounding line positions and those in 2008 after the first acceleration phase (Fig. S6 a–d). The locations of the profiles as well as the deduced grounding line locations are shown in Fig. 6. After the first acceleration phase in 2008 the front of Fleming Glacier had retreated behind the 1996 grounding line for the first time. Hence, on Fleming Glacier the grounding line must have been situated upstream of the 1996 position at this time. The profile plots in Fig. S6 b, c suggest that after the first acceleration phase in 2008 the grounding line was not located as far upstream as after the second acceleration phase between 2010 and 2011. However, since the estimation of the 2008 grounding line positions was based on surface velocities and modelled bedrock topography only, their precise locations remain unclear. Hence, the 2008 grounding line positions indicated in Fig. 6 are just a best guess based on the data we have in hand. A more detailed discussion on how the grounding line positions were finally decided from the profiles is provided in the Supplemental Material, Fig. S6 a–d. All in all, we estimated the current (2014) grounding line of Fleming Glacier to be located ~6–9 km upstream of its 1996 position. Its likely recent location is consistent with the maximum extent of upstream propagation of high velocities in 2008 on the centreline profile (Fig. 6).

6 Discussion

Our results confirm the previously detected acceleration of Fleming Glacier in response to the stepwise break-up and disintegration of Wordie Ice Shelf (Rignot et al. 2005). Median elevation change rates of -1.5 m a^{-1} and -1.9 m a^{-1} between 2004 and 2008 may suggest that Fleming Glacier had not reached a new equilibrium even almost 20 years after the partial disintegration of the ice shelf in 1989. Nevertheless, our dense velocity time series shows that surface velocities remained fairly stable between 1994 and 2007.

Between January and April 2008 the glacier had abruptly accelerated and high velocities had propagated upstream. Between March 2010 and early 2011 a second phase of acceleration was detected during which the speedup gradually propagated further upstream. This two-step acceleration of different characteristic has not been detected before and is important for the explanation of the strong recent dynamic changes on Fleming Glacier. Notwithstanding, t~~T~~he ~~remarkable~~ median speedup of ~1.3 m d^{-1} which we recorded between 2008~~7~~ and 2011 is in good agreement with an acceleration of ~ 400–500 m a^{-1} reported by Walker and Gardner (2017) and Zhao et al. (2017) for the period 2008–2014/2015. However, a comparison of our velocities in 2013 with their velocities in 2015 at the three measuring sites of Doake (1975) ~50 km upstream suggests that the recent speedup had not propagated up to these locations prior to 2015.

Abrupt speedups of tributary glaciers are often recorded as a direct consequence of loss of the buttressing force or major calving events (e.g. Seehaus et al., 2015). However, we did not observe any major calving event, which could have been responsible for the observed acceleration in 2008 or afterwards. In Greenland seasonal velocity fluctuations have been linked to both enhanced basal sliding due to the penetration of surface melt water to the ice-bedrock interface and inter-annual differences in drainage efficiency (Moon et al., 2014; Sundal et al., 2011; Zwally et al., 2002). However, the meltwater

production on Fleming Glacier is considered to be generally not sufficient to percolate to the glacier bed (Rignot et al., 2005). Furthermore, a trend of cooling air temperatures is reported for the Antarctic Peninsula since the end of the 1990s (e.g. Turner et al., 2016). Although decadal mean surface temperatures in the period 2006–2015 were 0.2 °C higher than in 1996–2005 at San Martin station (~120 km north of Wordie Ice Shelf), warming rates have decreased markedly since the decade 1996–2005 and show a cooling trend in 2006–2015 (Oliva et al., 2017). This may have further reduced surface melt during recent years. All in all, enhanced basal sliding due to percolating meltwater is likely not the explanation for the observed increase in flow velocities. However, we do not rule out that as a consequence of the acceleration, basal sliding increased in grounded areas by meltwater generated from greater basal frictional heat. Hydrostatic height anomalies calculated from OIB ice thickness and surface elevation data, TSX/TDX elevation change rates, surface velocities and modelled bedrock topography suggest that the current grounding line of Fleming Glacier is located ~6–~~–~~9 km upstream of its 1996 position, following the edges of a subglacial trough. By calculating hydrostatic equilibrium for a small subsection of OIB tracks at the outer glacier front close to the margins of Mount Balfour (Figure 6, Track 5 and Figure 4 grey dots), Walker and Gardner (2017) found that the grounding line had retreated by ~500 m between 2002 and 2014. However, they did not calculate hydrostatic equilibrium for the glacier`s centre and referred to the grounding line in 1996 instead. We now provide an estimate of the current grounding line on the central part of the glacier for the first time and show that it had substantially retreated. This is additional key information for the explanation of the recent glaciological changes on Fleming Glacier, since ~~When~~ ungrounding causes parts of the glacier tongue to go afloat, which reduces ~~,~~ buttressing and basal friction ~~is reduced~~. This in turn provokes the glacier to speed up and to dynamically thin. We hence propose that unpinning and grounding line retreat are the main causes of the observed strong acceleration of Fleming Glacier. This is an advance in the understanding of the recent processes at the glacier and updates the interpretation of Walker and Gardner (2017), who attributed the observed changes to increased frontal ablation and could not rule out that the acceleration is a delayed response to ice shelf disintegration in 1989. ~~We propose that unpinning and grounding line retreat are the main causes of the observed strong acceleration of Fleming Glacier.~~

Fairly stable velocities between 1994 and January 2008~~2007~~ as well as hydrostatic height anomalies in 2002 and 2004 do not indicate that ungrounding from the 1996 grounding line position had happened prior to January 2008. Although we were not able to give a precise estimate of the grounding line in 2008, the fact that during the acceleration phase in 2008 the glacier front had retreated behind the 1996 grounding line for the first time, shows that the 2008 grounding line must have been located upstream of the 1996 position. However, our data suggest that in 2008 the grounding line had not retreated to the edge of the subglacial trough at ~6–9 km upstream, yet. The rapidity of the acceleration in 2008 indicates that resistance to glacier flow must have abruptly been reduced. This is characteristic of a response to sudden unpinning rather than to gradual grounding line retreat. We hence propose that in 2008 the frontal part of the glacier abruptly detached from a pinning point (likely a sill) located at the 1996 grounding line. A cavity underneath the ice has probably already existed. Between 2008 and early 2010 Fleming Glacier was possibly grounded and stabilized on a gentle hill ~2.5~~–~~4 km upstream of the 1996 grounding line. The second phase of gradual acceleration and upstream propagation of high velocities between March 2010

and early 2011 is likely a response to further gradual grounding line retreat to the recent position ~6-9 km upstream. On our centerline profile highest changes in ice velocity were recorded ~6 km upstream, which is where the glacier now starts to be grounded.

Furthermore, 70 % higher median ice thinning rates in the period between 2011 and 2014 in comparison to the period 2004–2008 point to increased dynamic thinning and mass loss after grounding line retreat. The highest negative elevation change rates migrated upstream and can now be found in the vicinity of the estimated current grounding line. A tendency of lower ice thinning rates towards the glacier front, which was detected along the 2011–2014 OIB ATM profiles as well as ~~and~~ in the 2011–2014 TSX/TDX dh/dt map, indicates floatation of the glacier tongue. This has neither been observed by Zhao et al. (2017), who did not specifically analyse elevation change for this time period, nor by ~~is in contrast to~~ Walker and Gardner (2017), who calculated elevation change from the same OIB ATM dataset. The latter ~~do not see the positive trend of elevation change for the same OIB ATM dataset. Their approach of averaging~~ binned elevation change in 5 km intervals and excluded all data up to 5.5 km landward of the 1996 grounding line, which is the part of the profile where the trend towards lower ice thinning ~~probably filtered out the positive trend that~~ is most prominent. ~~on the lowest 3 km of the profile.~~

Rignot et al. (2013) and Depoorter et al. (2013) reported high basal melt rates of 23.6 ± 10 m a^{-1} (2003–2008) and 14.79 ± 5.26 m a^{-1} (2009) for the remaining parts of Wordie Ice Shelf, respectively. The magnitude of basal thinning is comparable to those found for ice shelves in the Amundsen Sea sector, where the influx of relatively warm CDW onto the continental shelf is thought to be the dominant driver for recent substantial grounding line retreat, acceleration and dynamic thinning of several glaciers (Turner et al., 2017). Periodical pulses of warm CDW are also known to flood onto the continental shelf of Marguerite Bay (Holland et al., 2010). Significant warming of Antarctic Continental Shelf Bottom Water (ASBW) of 0.1° to 0.3°C $decade^{-1}$ since the 1990s were recorded in the Bellingshausen Sea region and linked to increased warming and shoaling of CDW (Schmidtko et al., 2014). Cook et al. (2016) proposed that oceanic melt induced by an increased shoaling of relatively warm CDW is responsible for an accelerated frontal retreat of tidewater glaciers in the south-western Antarctic Peninsula since the 1990s. Other studies reported considerable thinning of the nearby George VI Ice Shelf (Hogg et al., 2017; Holt et al., 2013) and other ice shelves on the south-western Antarctic Peninsula (e.g. Rignot et al., 2013) due to increased basal melt. The onset of Fleming Glacier`s speedup between January and ~~–~~April 2008 corresponds well with observations of Wouters et al. (2015). They reported first signs of a near simultaneous increase of ice mass loss for glaciers all across the western Antarctic Peninsula south of -70° since 2008 and an unabated rapid ice loss since 2009. For the glaciers on Western Palmer Land Hogg et al. (2017) showed that ~35% of the ice loss after 2009 can be attributed to dynamic thinning triggered by ocean driven melt.

Walker and Gardner (2017) found that in 2008/2009 and 2010/2011exceptional warm water intrusions into Wordie Bay occurred due to upwelling CDW in response to phases of anomalously strong north-westerly winds during strong La Niña and positive SAM (Southern Annular Mode) events. Highest temperatures were not only recorded at depths between 100–200 m but also at ~~below~~ 400 m, which is close to where~~re~~ Fleming Glacier is grounded. The coincident timing with the two phases of glacier acceleration substantiates the link between ocean warming and our observed dynamic changes. It is very

likely that submarine ice melting was increased during phases of strong CDW upwelling and that this has triggered unpinning from the 1996 grounding line position in 2008 as well as further gradual grounding line retreat in 2010–2011.

The strong basal melt rates proposed by Rignot et al. (2013) for 2003–2008 ~~and~~ Depoorter et al. ~~(~~2013~~)~~ ~~further~~ suggest that basal melt ~~probably~~ has already occurred prior to 2008. This, together with increased dynamic thinning towards the ice front between 2004 and 2008 has likely weakened the ice at the pinning point, which may have fostered unpinning in 2008. Furthermore, the bed topography reveals that the trough underneath the joint Airy-Rotz-Seller-Fleming glacier tongue has a retrograde slope on its central part (Fig. S6 b, 0–6 km). Such a bed topography is known to be an unstable configuration for the glacier (e.g. DeConto and Pollard, 2016; Favier et al., 2014; Rignot et al., 2014; Schoof, 2012), which may have promoted gradual grounding line retreat between 2010 and 2011. ~~Figure S8 summarizes our interpretation of grounding line retreat at Fleming Glacier.~~

The bedrock topography of Fleming Glacier also shows a retrograde bed slope starting at ~3–4 km upstream of the current grounding line, which transitions into a pronounced deep trough (up to 1100 m below sea level) at about 10 km upstream. Hence, if grounding line retreat exceeds the edge of this trough, destabilisation like on Thwaites Glacier and in the Pine Island Bay region is possible, which would involve further rapid grounding line retreat and amplified mass loss in the future (Favier et al., 2014; Rignot et al., 2014).

7 Conclusions

We present a detailed history of the glacier dynamics of Fleming Glacier after the retreat and disintegration of Wordie Ice Shelf. ~~by analysing glacier extent, surfaces velocities, elevation change rates andhydrostatic equilibrium.~~ While previous studies analysed only rather limited amounts of velocity data (Rignot et al., 2005; Walker and Gardner, 2017; Wendt et al., 2010; Zhao et al., 2017), we now show a complete time series of SAR surface velocities of Fleming Glacier at high temporal resolution for the period 1994–2016. These data enable a much better temporal constraint and characterisation of glaciological changes in the region. By combining this unique dataset with recently published data on oceanic forcing (Walker and Gardner, 2017) and new data on surface elevation change from TSX/TDX interferometry, ICESat laser altimetry and airborne LiDAR, as well as modelled bedrock topography and hydrostatic equilibrium, we are able to relate precisely dated events of acceleration to increased dynamic ice thinning and ocean driven grounding line retreat. This complements previous studies in the region and provides new and more detailed information on the glaciological changes and their drivers. ~~Especially our dense SAR time series enables us to precisely date events of velocity change jointly with glacier retreat, elevation changes and grounding line retreat.~~

Our results show that until 2008 the dynamics of Fleming Glacier were primarily controlled by the impacts of break-up events of Wordie Ice Shelf before the early 1990s. The retreat of the ice shelf reduced glacier buttressing and led to an increase in surface velocities (Rignot et al., 2005), which in turn caused the glacier to dynamically thin. The last floating ice shelf parts were lost between 1998 and 1999, but this showed no detectable effects on glacier flow dynamics.

After two decades of rather stable velocities, the glacier abruptly accelerated between January and April 2008. Our interpretation is that this happened due to the detachment of the glacier tongue from a pinning point located at the 1996 grounding line position. The unpinning was likely fostered by weakening of the ice due to basal melt and dynamic thinning prior to 2008. Further gradual retreat of the grounding line between 2010 and 2011, an increase in surface velocities of ~2730 % as well as ~70 % higher ice thinning rates show that ungrounding in 2008 has initiated a new phase of dynamic imbalance. The unfavourable retrograde bed slope underneath Fleming Glacier probably amplified the grounding line retreat. The coincident timing of reported strong upwelling events of warm CDW with the two phases of acceleration and grounding line retreat shows that enhanced basal melt due to increased shoaling of warm CDW most likely played a major role for the recent changes at Fleming Glacier. The reduction in buttressing due to unpinning and grounding line retreat is able to explain why the magnitude of velocity change was much higher than in other places at the western Antarctic Peninsula during this time.

Today Fleming Glacier and the other glaciers of the Airy-Rotz-Seller-Fleming glacier system are far away from reaching a new equilibrium. The modelled subglacial topography of Fleming Glacier upstream of the recent grounding line is characterized by some smaller landward deepening troughs which are separated by chains of gentle hills. Pronounced oceanic forcing will presumably continue, since the SAM is forecasted to be shifted further poleward, which will foster conditions like those during the strong La Niña/+SAM events in 2008/2009 and 2010/2011 (Abram et al., 2014; Fogt et al., 2011; Walker and Gardner, 2017). Thus, further retreat of the grounding line and more dynamic thinning are possible expected on Fleming Glacier. If the ungrounding would reach upstream to the retrograde bed slope at about ~3–4 km from the current grounding line and further to the deep subglacial trough, this can trigger a positive feedback loop of rapid grounding line retreat, flow acceleration, dynamic thinning, increased calving and mass loss. However, on Airy and Seller glaciers the more favourable subglacial geometry of an overall landward steepening slope may slow down or prevent further grounding line retreat in the near future

Author contributions

Peter Friedl processed and analysed all SAR, optical, elevation and ground penetrating radar data. Thorsten C. Seehaus processed the ALOS PALSAR data and supported the interferometric DEM generation. Anja Wendt provided the CAMS LiDAR data and gave valuable comments. Matthias H. Braun coordinated the research and wrote the manuscript jointly with Peter Friedl. Kathrin Höppner initiated the project, co-coordinated the research in close cooperation with Matthias H. Braun and contributed to discussions of the results throughout. All authors revised the manuscript.

Competing interests

The authors declare no competing financial interests.

Acknowledgements

This project was mainly funded by the DLR VO-R Young Investigator Group “Antarctic Research”. Thorsten C. Seehaus was funded by Deutsche Forschungsgemeinschaft (DFG) in the framework of the priority program "Antarctic Research with comparative investigations in Arctic ice areas" by a grant to M.B. (BR 2105/9-1). Matthias H. Braun and Thorsten C. Seehaus would like to thank the HGF Alliance “Remote Sensing of Earth System Dynamics” (HA-310) and Marie-Curie-Network International Research Staff Exchange Scheme IMCONet (EU FP7-PEOPLE-2012-IRSES, Project Reference: 318718) for additional support. TerraSAR-X and TanDEM-X data were provided by DLR through the projects HYD3008 and XTI_GLAC7015. We would like to thank Rainer Lorenz (German Remote Sensing Data Centre, DLR) for his support retrieving the ERS-1/-2 SLC data from the ESA ERS-1/-2 Processing and Archiving Facility (D-PAF) at DLR and the ENVISAT ASAR SLC data from the ESA ENVISAT Processing and Archiving Centre (D-PAC) at DLR. All ERS, ENVISAT and TSX/TDX data were received at the ~~GARS (~~German Antarctic Receiving Station~~)~~ GARS O’Higgins of DLR. The CAMS data were acquired and made available by the Centro de Estudios Científicos, Chile. Furthermore, we are grateful to Christian Kienholz (University of Alaska Fairbanks) and Bill Hauer (Alaska Satellite Facility) for providing the Radarsat-1 SLC data. Other remote sensing data was kindly made available by ~~various institutions, e.g.~~ ESA, NASA, JAXA, USGS and CReSIS. Finally, we would like to thank Paul Wachter, Saurabh Vijay and the tree anonymous reviewers for their helpful comments on the manuscript.

References

Abram, N. J., Mulvaney, R., Vimeux, F., Phipps, S. J., Turner, J. and England, M. H.: Evolution of the Southern Annular Mode during the past millennium, Nature Climate change, 4, 564–569, doi: 10.1038/nclimate2235, 2014.

Angelis, H. de and Skvarca, P.: Glacier surge after ice shelf collapse, Science (New York, N.Y.), 299, 1560–1562, doi: 10.1126/science.1077987, 2003.

Berthier, E., Cabot, V., Vincent, C. and Six, D.: Decadal Region-Wide and Glacier-Wide Mass Balances Derived from Multi-Temporal ASTER Satellite Digital Elevation Models. Validation over the Mont-Blanc Area, Front. Earth Sci., 4, 1103, doi: 10.3389/feart.2016.00063, 2016.

Braun, M. and Humbert, A.: Recent Retreat of Wilkins Ice Shelf Reveals New Insights in Ice Shelf Breakup Mechanisms, IEEE Geosci. Remote Sensing Lett., 6, 263–267, doi: 10.1109/LGRS.2008.2011925, 2009.

Burgess, E. W., Forster, R. R., Larsen, C. F. and Braun, M.: Surge dynamics on Bering Glacier, Alaska, in 2008–2011, The Cryosphere, 6, 1251–1262, doi: 10.5194/tc-6-1251-2012, 2012.

Cook, A. J., Holland, P. R., Meredith, M. P., Murray, T., Luckman, A. and Vaughan, D. G.: Ocean forcing of glacier retreat in the western Antarctic Peninsula, Science (New York, N.Y.), 353, 283–286, doi: 10.1126/science.aae0017, 2016.

Cook, A. J., Murray, T., Luckman, A., Vaughan, D. G. and Barrand, N. E.: A new 100-m Digital Elevation Model of the Antarctic Peninsula derived from ASTER Global DEM: methods and accuracy assessment, Earth Syst. Sci. Data, 4, 129–142, doi: 10.5194/essd-4-129-2012, 2012.

Cook, A. J., Vaughan, D. G., Luckman, A. J. and Murray, T.: A new Antarctic Peninsula glacier basin inventory and observed area changes since the 1940s, Antarctic Science, 26, 614–624, doi: 10.1017/S0954102014000200, 2014.

DeConto, R. M. and Pollard, D.: Contribution of Antarctica to past and future sea-level rise, Nature, 531, 591–597, doi: 10.1038/nature17145, 2016.

Depoorter, M. A., Bamber, J. L., Griggs, J. A., Lenaerts, J T M, Ligtenberg, S R M, van den Broeke, M R and Moholdt, G.: Calving fluxes and basal melt rates of Antarctic ice shelves, Nature, 502, 89–92, doi: 10.1038/nature12567, 2013.

DiMarzio, J., Brenner, A., Schutz, R., Shuman, C. A. and Zwally, H. J.: GLAS/ICESat 500 m laser altimetry digital elevation model of Antarctica, Boulder, Colorado USA, 2007.

Doake, C. S. M.: Bottom sliding of a glacier measured from the surface, Nature, 257, 780–782, doi: 10.1038/257780a0, 1975.

Doake, C. S. M. and Vaughan, D. G.: Rapid disintegration of the Wordie Ice Shelf in response to atmospheric warming, Nature, 350, 328–330, doi: 10.1038/350328a0, 1991.

Favier, L., Durand, G., Cornford, S. L., Gudmundsson, G. H., Gagliardini, O., Gillet-Chaulet, F., Zwinger, T., Payne, A. J. and Le Brocq, A. M.: Retreat of Pine Island Glacier controlled by marine ice-sheet instability, Nature Climate change, 4, 117–121, doi: 10.1038/nclimate2094, 2014.

Ferrigno, J. G.: Coastal-change and glaciological map of the Larsen Ice Shelf area, Antarctica, 1940-2005, Reston, Va., 2008.

Fogt, R. L., Bromwich, D. H. and Hines, K. M.: Understanding the SAM influence on the South Pacific ENSO teleconnection, Clim Dyn, 36, 1555–1576, 2011.

Förste, C., Bruinsma, S.L., Abrikosov, O., Lemoine, J.-M., Marty, J. C., Flechtner, F., Balmino, G., Barthelmes, F. and Biancale, R.: EIGEN-6C4 The latest combined global gravity field model including GOCE data up to degree and order 2190 of GFZ Potsdam and GRGS Toulouse, GFZ Data Services, 2014.

Fretwell, P., Pritchard, H. D., Vaughan, D. G., Bamber, J. L., Barrand, N. E., Bell, R., Bianchi, C., Bingham, R. G., Blankenship, D. D., Casassa, G., Catania, G., Callens, D., Conway, H., Cook, A. J., Corr, H. F. J., Damaske, D., Damm, V., Ferraccioli, F., Forsberg, R., Fujita, S., Gim, Y., Gogineni, P., Griggs, J. A., Hindmarsh, R. C. A., Holmlund, P., Holt, J. W., Jacobel, R. W., Jenkins, A., Jokat, W., Jordan, T., King, E. C., Kohler, J., Krabill, W., Riger-Kusk, M., Langley, K. A., Leitchenkov, G., Leuschen, C., Luyendyk, B. P., Matsuoka, K., Mouginot, J., Nitsche, F. O., Nogi, Y., Nost, O. A., Popov, S. V., Rignot, E., Rippin, D. M., Rivera, A., Roberts, J., Ross, N., Siegert, M. J., Smith, A. M., Steinhage, D., Studinger, M., Sun, B., Tinto, B. K., Welch, B. C., Wilson, D., Young, D. A., Xiangbin, C. and Zirizzotti, A.: Bedmap2: improved ice bed, surface and thickness datasets for Antarctica, The Cryosphere, 7, 375–393, doi: 10.5194/tc-7-375-2013, 2013.

Fricker, H. Amanda: Redefinition of the Amery Ice Shelf, East Antarctica, grounding zone, J. Geophys. Res., 107, doi: 10.1029/2001JB000383, 2002.

Fricker, H. Amanda and Padman, L.: Ice shelf grounding zone structure from ICESat laser altimetry, Geophys. Res. Lett., 33, doi: 10.1029/2006GL026907, 2006.

Fritz, T., Breit, H., Rossi, C., Balss, U., Lachaise, M. and Duque, S.: Interferometric processing and products of the TanDEM-X mission, Munich, Germany, 2012.

Fürst, J. Jakob, Durand, G., Gillet-Chaulet, F., Tavard, L., Rankl, M., Braun, M. and Gagliardini, O.: The safety band of Antarctic ice shelves, Nature Climate change, doi: 10.1038/nclimate2912, 2016.

Griggs, J. A. and Bamber, J. L.: Antarctic ice-shelf thickness from satellite radar altimetry, Journal of Glaciology, 57, 485–498, doi: 10.3189/002214311796905659, 2011.

Hogg, A. E., Shepherd, A., Cornford, S. L., Briggs, K. H., Gourmelen, N., Graham, J. A., Joughin, I., Mouginot, J., Nagler, T., Payne, A. J., Rignot, E. and Wuite, J.: Increased ice flow in Western Palmer Land linked to ocean melting, Geophys. Res. Lett., 353, 283, doi: 10.1002/2016GL072110, 2017.

Holland, P. R., Jenkins, A. and Holland, D. M.: Ice and ocean processes in the Bellingshausen Sea, Antarctica, J. Geophys. Res., 115, doi: 10.1029/2008JC005219, 2010.

Holt, T. O., Glasser, N. F., Quincey, D. J. and Siegfried, M. R.: Speedup and fracturing of George VI Ice Shelf, Antarctic Peninsula, The Cryosphere, 7, 797–816, doi: 10.5194/tc-7-797-2013, 2013.

Huss, M. and Farinotti, D.: A high-resolution bedrock map for the Antarctic Peninsula, The Cryosphere, 8, 1261–1273, doi: 10.5194/tc-8-1261-2014, 2014.

Krabill, W. B.: IceBridge ATM L1B Elevation and Return Strength, Version 2. [2011-11-17 - 2014-11-16], NASA National Snow and Ice Data Center Distributed Active Archive Center, Boulder, Colorado USA, 2010, updated 2016.

Krabill, W. B.: Pre-IceBridge ATM L1B Qfit Elevation and Return Strength, Version 1. [2002-11-16, 2004-11-18], NASA National Snow and Ice Data Center Distributed Active Archive Center, 2012.

Krabill, W. B., Abdalati, W., Frederick, E. B., Manizade, S. S., Martin, C. F., Sonntag, J. G., Swift, R. N., Thomas, R. H. and Yungel, J. G.: Aircraft laser altimetry measurement of elevation changes of the greenland ice sheet. Technique and accuracy assessment, Journal of Geodynamics, 34, 357–376, doi: 10.1016/S0264-3707(02)00040-6, 2002.

Krieger, G., Zink, M., Bachmann, M., Bräutigam, B., Schulze, D., Martone, M., Rizzoli, P., Steinbrecher, U., Walter Antony, J., Zan, F. de, Hajnsek, I., Papathanassiou, K., Kugler, F., Rodriguez Cassola, M., Younis, M., Baumgartner, S., López-Dekker, P., Prats, P. and Moreira, A.: TanDEM-X: A radar interferometer with two formation-flying satellites, Acta Astronautica, 89, 83–98, doi: 10.1016/j.actaastro.2013.03.008, 2013.

Martin, C. F., Krabill, W. B., Manizade, S. S., Russell, R. L., Sonntag, J. G., Swift, R. N. and Yungel, J. K.: Airborne topographic mapper calibration procedures and accuracy assessment, Hanover, Tech. Rep. NASA/TM-2012-215891, 32 pp., 2012.

Mätzler, C.: Applications of the interaction of microwaves with the natural snow cover, Remote Sensing Reviews, 2, 259–387, doi: 10.1080/02757258709532086, 1987.

Mercer, J. H.: West Antarctic ice sheet and CO2 greenhouse effect: a threat of disaster, Nature, 271, 321–325, doi: 10.1038/271321a0, 1978.

Moon, T., Joughin, I., Smith, B., Broeke, M. R., Berg, W. Jan, Noël, B. and Usher, M.: Distinct patterns of seasonal Greenland glacier velocity, Geophysical Research Letters, 41, 7209–7216, doi: 10.1002/2014GL061836, 2014.

Oliva, M., Navarro, F., Hrbáček, F., Hernández, A., Nývlt, D., Pereira, P., Ruiz-Fernández, J. and Trigo, R.: Recent regional climate cooling on the Antarctic Peninsula and associated impacts on the cryosphere, The Science of the total environment, 580, 210–223, doi: 10.1016/j.scitotenv.2016.12.030, 2017.

Padman, L., Costa, D. P., Dinniman, M. S., Fricker, H. A., Goebel, M. E., Huckstadt, L. A., Humbert, A., Joughin, I., Lenaerts, Jan T. M., Ligtenberg, Stefan R. M., Scambos, T. and Van Den Broeke, Michiel R.: Oceanic controls on the mass balance of Wilkins Ice Shelf, Antarctica, J. Geophys. Res., 117, doi: 10.1029/2011JC007301, 2012.

Pritchard, H. D., Ligtenberg, S R M, Fricker, H. A., Vaughan, D. G., van den Broeke, M R and Padman, L.: Antarctic ice-sheet loss driven by basal melting of ice shelves, Nature, 484, 502–505, doi: 10.1038/nature10968, 2012.

Rankl, M., Fürst, J. Jakob, Humbert, A. and Braun, M. Holger: Dynamic changes on Wilkins Ice Shelf during the 2006-2009 retreat derived from satellite observations, The Cryosphere Discuss., 1–17, doi: 10.5194/tc-2016-218, 2016.

Reynolds, J. M.: The structure of Wordie ice shelf, Antarctic peninsula, Bulletin-British Antarctic Survey, 57–64, 1988.

Rignot, E.: Changes in ice dynamics and mass balance of the Antarctic ice sheet, Philosophical transactions. Series A, Mathematical, physical, and engineering sciences, 364, 1637–1655, doi: 10.1098/rsta.2006.1793, 2006.

Rignot, E., Casassa, G., Gogineni, P., Kanagaratnam, P., Krabill, W., Pritchard, H. D., Rivera, A., Thomas, R., Turner, J. and Vaughan, D. G.: Recent ice loss from the Fleming and other glaciers, Wordie Bay, West Antarctic Peninsula, Geophys. Res. Lett., 32, doi: 10.1029/2004GL021947, 2005.

Rignot, E., Echelmeyer, K. and Krabill, W.: Penetration depth of interferometric synthetic-aperture radar signals in snow and ice, Geophys. Res. Lett., 28, 3501–3504, doi: 10.1029/2000GL012484, 2001.

Rignot, E., Jacobs, S., Mouginot, J. and Scheuchl, B.: Ice-shelf melting around Antarctica, Science (New York, N.Y.), 341, 266–270, doi: 10.1126/science.1235798, 2013.

Rignot, E., Mouginot, J., Morlighem, M., Seroussi, H. and Scheuchl, B.: Widespread, rapid grounding line retreat of Pine Island, Thwaites, Smith, and Kohler glaciers, West Antarctica, from 1992 to 2011, Geophys. Res. Lett., 41, 3502–3509, doi: 10.1002/2014GL060140, 2014.

Rignot, E., Mouginot, J. and Scheuchl, B.: Antarctic grounding line mapping from differential satellite radar interferometry, Geophys. Res. Lett., 38, n/a, doi: 10.1029/2011GL047109, 2011a.

Rignot, E., Mouginot, J. and Scheuchl, B.: Ice flow of the Antarctic ice sheet, Science (New York, N.Y.), 333, 1427–1430, doi: 10.1126/science.1208336, 2011b.

Rignot, E., Vaughan, D. G., Schmeltz, M., Dupont, T. and MacAyeal, D.: Acceleration of Pine Island and Thwaites Glaciers, West Antarctica, Annals of Glaciology, 34, 189–194, doi: 10.3189/172756402781817950, 2002.

Rizzoli, P., Martone, M., Gonzalez, C., Wecklich, C., Borla Tridon, D., Bräutigam, B., Bachmann, M., Schulze, D., Fritz, T., Huber, M., Wessel, B., Krieger, G., Zink, M. and Moreira, A.: Generation and performance assessment of the global TanDEM-X digital elevation model, ISPRS Journal of Photogrammetry and Remote Sensing, 132, 119–139, doi: 10.1016/j.isprsjprs.2017.08.008, 2017.

Rott, H., Floricioiu, D., Wuite, J., Scheiblauer, S., Nagler, T. and Kern, M.: Mass changes of outlet glaciers along the Nordensjköld Coast, northern Antarctic Peninsula, based on TanDEM-X satellite measurements, Geophys. Res. Lett., 41, 8123–8129, doi: 10.1002/2014GL061613, 2014.

Scambos, T. A., Bohlander, J., Shuman, C. A. and Skvarca, P.: Glacier acceleration and thinning after ice shelf collapse in the Larsen B embayment, Antarctica, Geophys. Res. Lett., 31, doi: 10.1029/2004GL020670, 2004.

Schmidtko, S., Heywood, K. J., Thompson, A. F. and Aoki, S.: Multidecadal warming of Antarctic waters, Science, 346, 1227–1231, doi: 10.1126/science.1256117, 2014.

Schoof, C.: Ice sheet grounding line dynamics. Steady states, stability, and hysteresis, J. Geophys. Res., 112, 1720, doi: 10.1029/2006JF000664, 2007.

Schoof, C.: Marine ice sheet stability, J. Fluid Mech., 698, 62–72, doi: 10.1017/jfm.2012.43, 2012.

Schutz, B. E., Zwally, H. J., Shuman, C. A., Hancock, D. and DiMarzio, J. P.: Overview of the ICESat Mission, Geophys. Res. Lett., 32, doi: 10.1029/2005GL024009, 2005.

Seehaus, T., Marinsek, S., Helm, V., Skvarca, P. and Braun, M.: Changes in ice dynamics, elevation and mass discharge of Dinsmoor–Bombardier–Edgeworth glacier system, Antarctic Peninsula, Earth and Planetary Science Letters, 427, 125–135, doi: 10.1016/j.epsl.2015.06.047, 2015.

Seehaus, T., Marinsek, S., Skvarca, P., van Wessem, J. M., Reijmer, C. H., Seco, J. L. and Braun, M. H.: Dynamic Response of Sjögren Inlet Glaciers, Antarctic Peninsula, to Ice Shelf Breakup Derived from Multi-Mission Remote Sensing Time Series, Front. Earth Sci., 4, F01005, doi: 10.3389/feart.2016.00066, 2016.

Shepherd, A., Ivins, E. R., A, G., Barletta, V. R., Bentley, M. J., Bettadpur, S., Briggs, K. H., Bromwich, D. H., Forsberg, R., Galin, N., Horwath, M., Jacobs, S., Joughin, I., King, M. A., Lenaerts, Jan T M, Li, J., Ligtenberg, Stefan R M, Luckman, A., Luthcke, S. B., McMillan, M., Meister, R., Milne, G., Mouginot, J., Muir, A., Nicolas, J. P., Paden, J., Payne, A. J., Pritchard, H., Rignot, E., Rott, H., Sørensen, L. Sandberg, Scambos, T. A., Scheuchl, B., Schrama, Ernst J O, Smith, B., Sundal, A. V., van Angelen, Jan H, van de Berg, Willem J, van den Broeke, Michiel R, Vaughan, D. G., Velicogna, I., Wahr, J., Whitehouse, P. L., Wingham, D. J., Yi, D., Young, D. and Zwally, H. Jay: A reconciled estimate of ice-sheet mass balance, Science (New York, N.Y.), 338, 1183–1189, doi: 10.1126/science.1228102, 2012.

Shuman, C. A., Zwally, H. J., Schutz, B. E., Brenner, A. C., DiMarzio, J. P., Suchdeo, V. P. and Fricker, H. A.: ICESat Antarctic elevation data. Preliminary precision and accuracy assessment, Geophys. Res. Lett., 33, doi: 10.1029/2005GL025227, 2006.

Stearns, L. A.: Outlet glacier dynamics in East Greenland and East Antarctica, Ph.D. thesis, Univ. of Maine, Orono, 2007.

Stearns, L. A.: Dynamics and mass balance of four large East Antarctic outlet glaciers, Ann. Glaciol., 52, 116–126, doi: 10.3189/172756411799096187, 2011.

Strozzi, T., Luckman, A., Murray, T., Wegmuller, U. and Werner, C. L.: Glacier motion estimation using SAR offset-tracking procedures, IEEE Trans. Geosci. Remote Sensing, 40, 2384–2391, doi: 10.1109/TGRS.2002.805079, 2002.

Sundal, A. Venke, Shepherd, A., NIENOW, P., Hanna, E., Palmer, S. and Huybrechts, P.: Melt-induced speed-up of Greenland ice sheet offset by efficient subglacial drainage, Nature, 469, 521–524, doi: 10.1038/nature09740, 2011.

Turner, J., Lu, H., White, I., King, J. C., Phillips, T., Hosking, J. Scott, Bracegirdle, T. J., Marshall, G. J., Mulvaney, R. and Deb, P.: Absence of 21st century warming on Antarctic Peninsula consistent with natural variability, Nature, 535, 411–415, doi: 10.1038/nature18645, 2016.

Turner, J., Orr, A., Gudmundsson, G. Hilmar, Jenkins, A., Bingham, R. G., Hillenbrand, C.-D. and Bracegirdle, T. J.: Atmosphere-Ocean-Ice Interactions in the Amundsen Sea Embayment, West Antarctica, Rev. Geophys., doi: 10.1002/2016RG000532, 2017.

van den Broeke, Michiel, van de Berg, Willem Jan and van Meijgaard, E.: Firn depth correction along the Antarctic grounding line, Antarctic Science, 20, 513–517, doi: 10.1017/S095410200800148X, 2008.

Vaughan, D. G.: Implications of the break-up of Wordie Ice Shelf, Antarctica for sea level, Antarctic Science, 5, doi: 10.1017/S0954102093000537, 1993.

Vaughan, D. G. and Doake, C. S. M.: Recent atmospheric warming and retreat of ice shelves on the Antarctic Peninsula, Nature, 379, 328–331, doi: 10.1038/379328a0, 1996.

Vijay, S. and Braun, M.: Elevation Change Rates of Glaciers in the Lahaul-Spiti (Western Himalaya, India) during 2000–2012 and 2012–2013, Remote Sensing, 8, 1038, doi: 10.3390/rs8121038, 2016.

Walker, C. C. and Gardner, A. S.: Rapid drawdown of Antarctica's Wordie Ice Shelf glaciers in response to ENSO/Southern Annular Mode-driven warming in the Southern Ocean, Earth and Planetary Science Letters, 476, 100–110, doi: 10.1016/j.epsl.2017.08.005, 2017.

Wendt, J., Rivera, A., Wendt, A., Bown, F., Zamora, R., Casassa, G. and Bravo, C.: Recent ice-surface-elevation changes of Fleming Glacier in response to the removal of the Wordie Ice Shelf, Antarctic Peninsula, Annals of Glaciology, 51, 97–102, doi: 10.3189/172756410791392727, 2010.

Wouters, B., Martin-Español, A., Helm, V., Flament, T., van Wessem, J M, Ligtenberg, S R M, van den Broeke, M R and Bamber, J. L.: Glacier mass loss. Dynamic thinning of glaciers on the Southern Antarctic Peninsula, Science (New York, N.Y.), 348, 899–903, doi: 10.1126/science.aaa5727, 2015.

Wuite, J., Rott, H., Hetzenecker, M., Floricioiu, D., Rydt, J. de, Gudmundsson, G. H., Nagler, T. and Kern, M.: Evolution of surface velocities and ice discharge of Larsen B outlet glaciers from 1995 to 2013, The Cryosphere, 9, 957–969, doi: 10.5194/tc-9-957-2015, 2015.

Zhao, C., King, M. A., Watson, C. S., Barletta, V. R., Bordoni, A., Dell, M. and Whitehouse, P. L.: Rapid ice unloading in the Fleming Glacier region, southern Antarctic Peninsula, and its effect on bedrock uplift rates, Earth and Planetary Science Letters, 473, 164–176, doi: 10.1016/j.epsl.2017.06.002, 2017.

Zwally, H. J., Schutz, R., Bentley, C., Bufton, J., Herring, T., Minster, J., Spinhirne, J. and Thomas, R.: GLAS/ICESat L2 Antarctic and Greenland Ice Sheet Altimetry Data, Version 34, NASA National Snow and Ice Data Center Distributed Active Archive Center, Boulder, Colorado USA, 2014.

Zwally, H. Jay, Abdalati, W., Herring, T., Larson, K., Saba, J. and Steffen, K.: Surface melt-induced acceleration of Greenland ice-sheet flow, Science (New York, N.Y.), 297, 218–222, doi: 10.1126/science.1072708, 2002.

Figures

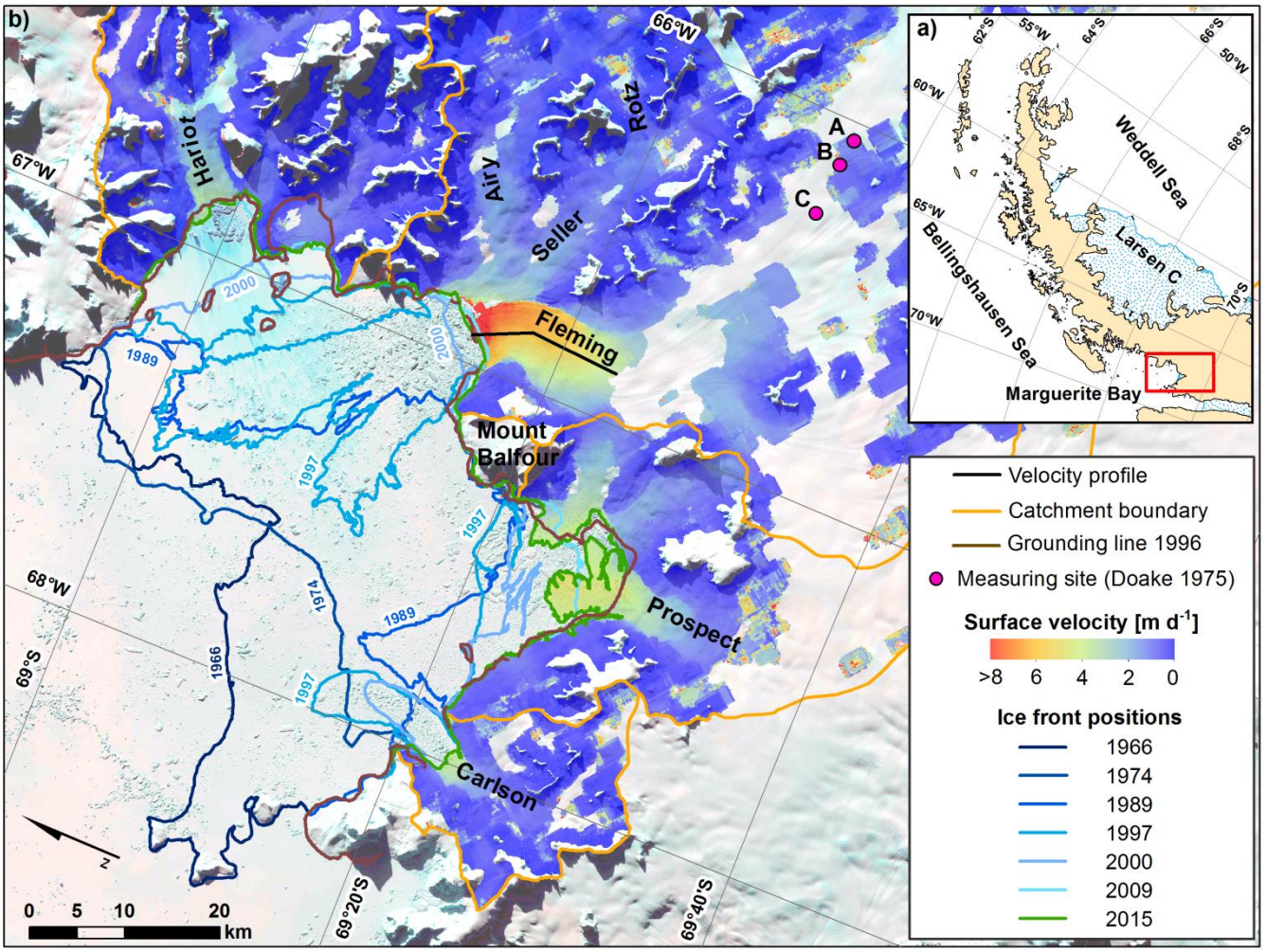

Figure 1: (a) Location of Wordie Bay at the Antarctic Peninsula. Map base: SCAR Antarctic Digital Database, version 6.0. **(b)** Surface velocity field and frontal positions of Wordie Ice Shelf between 1966 and 2015. Surface velocities were derived from Sentinel-1 acquisitions acquired on 28-08-2015 and 09-09-2015. Front positions (blue and green lines) were taken from existing datasets or manually mapped from calibrated and multi-looked SAR intensity images. For detailed information on the data sources used for the frontal delineation see Supplemental material Tab. S1. The grounding line in 1996 (brown line) was derived from ERS-1/2 double difference interferometry (Rignot et al., 2005; Rignot et al., 2011a). Black line: Extraction profile for the velocity time series presented in Sect. 5. Orange Line: Glacier system catchment boundaries from the SCAR Antarctic Digital Database, version 6.0. Pink dots: Sites of the velocity measurements undertaken by Doake, 1975 in 1974. Background: Mosaic of two Landsat-8 „Natural Colour“ images, acquired on 2015-09-16 ©USGS.

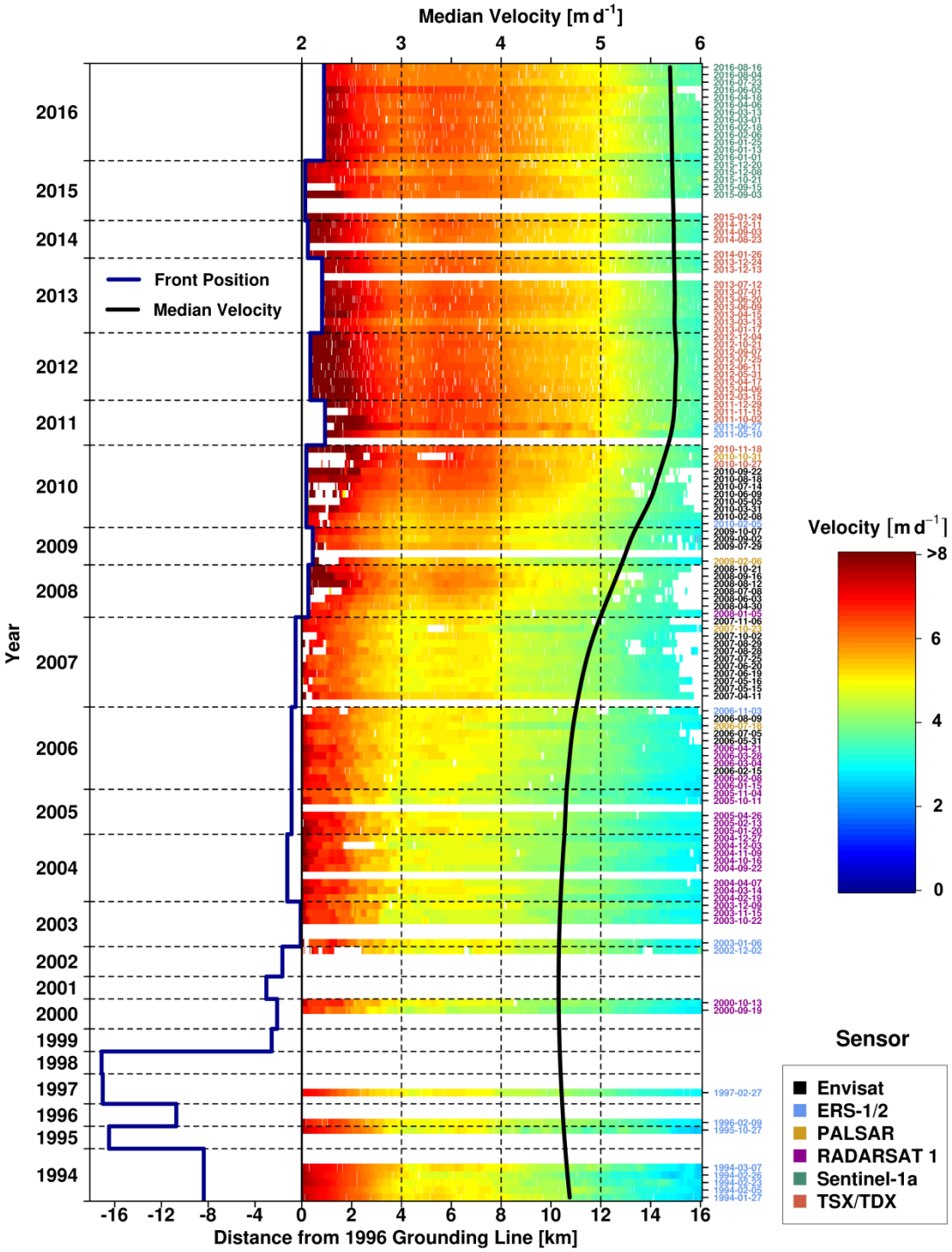

Figure 2: Left side (blue line): relative distance of the glacier front to the grounding line position in 1996. See Tab. S1 for data used for front mapping. Right side: velocity time series and smoothed median velocities (black line) derived from multi sensor SAR intensity tracking along a centreline profile on Fleming Glacier starting at the 1996 grounding line (Fig. 1).

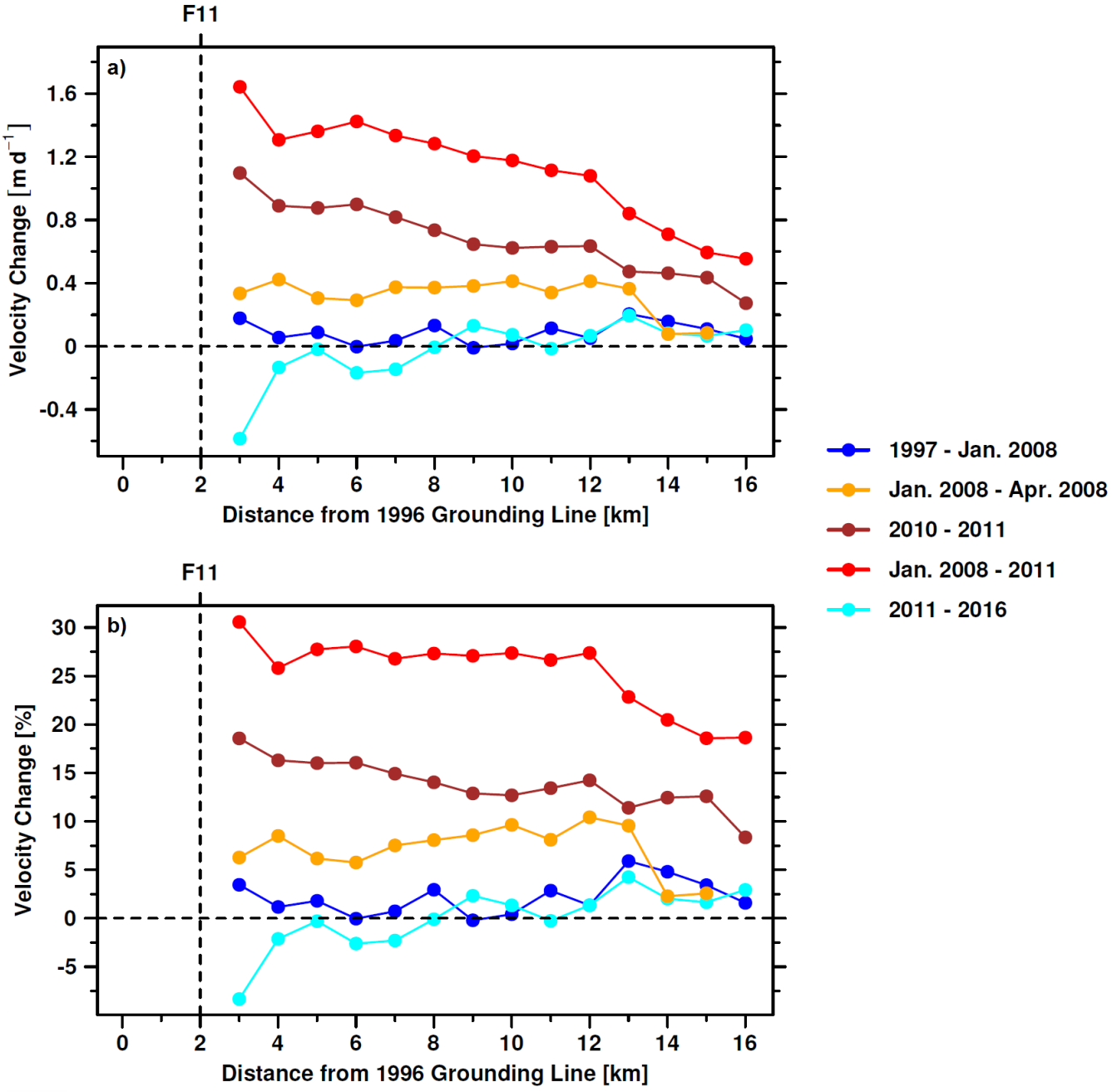
F11
a)
Velocity Change [m d^{-1}]
1.6
1.2
0.8
0.4
0
-0.4
0
2
4
6
8
10
12
14
16
Distance from 1996 Grounding Line [km]
F11
b)
Velocity Change [%]
30
25
20
15
10
5
0
-5
0
2
4
6
8
10
12
14
16
Distance from 1996 Grounding Line [km]
1997 - Jan. 2008
Jan. 2008 - Apr. 2008
2010 - 2011
Jan. 2008 - 2011
2011 - 2016

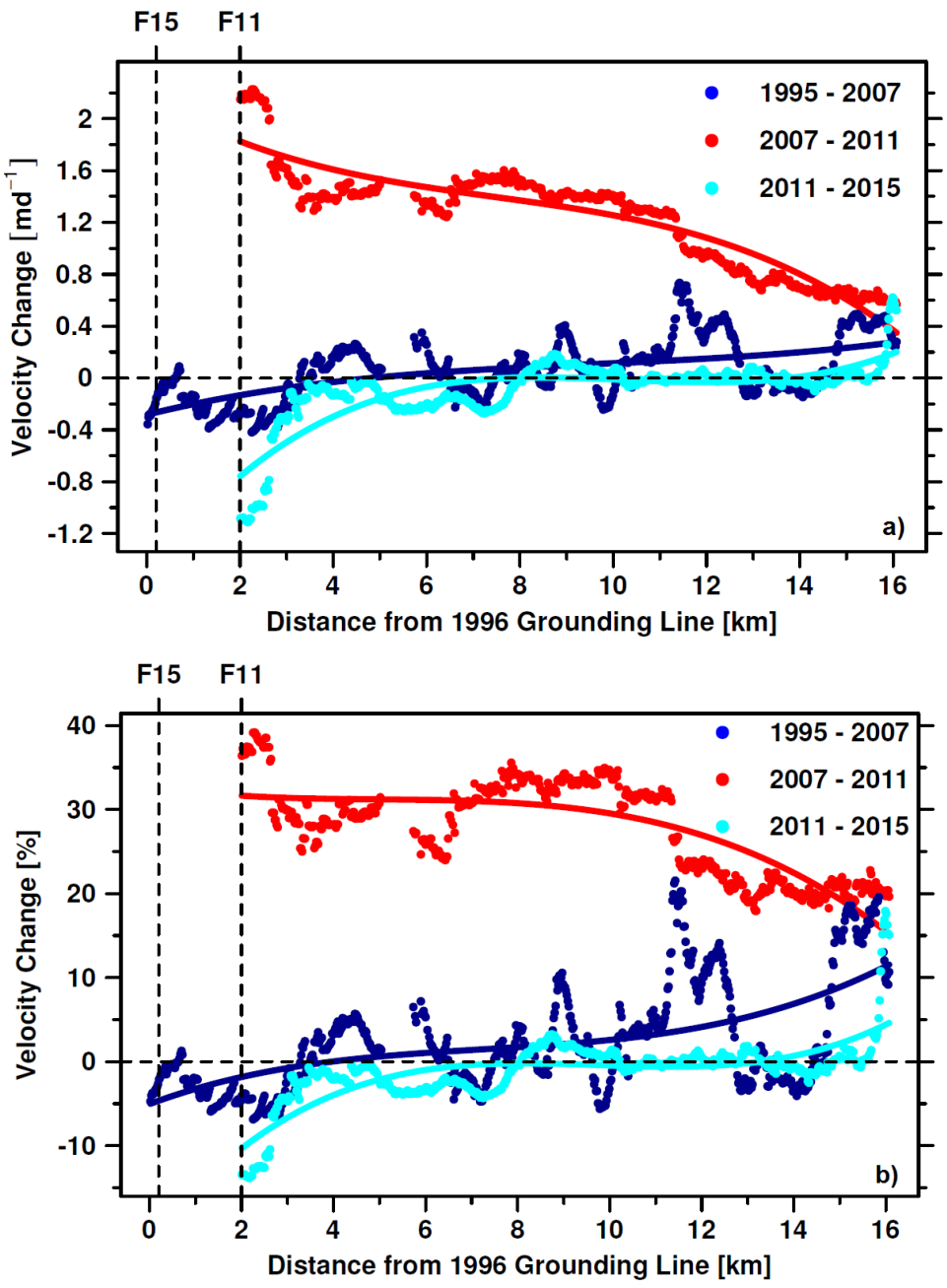

Figure 3: Absolute **(a)** and relative **(b)** velocity change along the centreline profile on Fleming Glacier (Fig. 1) for 199~~7~~5-02~~1~~0-27 to 200~~8~~7-01~~1~~0-05~~2~~3, 200~~8~~7-01~~1~~0-05~~2~~3 to 20081~~1~~-04~~1~~0-30, 2010-02-08 to ~~02 and~~ 2011-10-02, 2008-01-05 to 2011-10-02 and 2011-10-02 to 201~~6~~5-03~~1~~0-~~3~~21. ~~Coloured lines show cubic functions fitted to the data.~~ F11: front position in 2011. ~~F15: Front position in 2015.~~ See Tab. S1 for data used for front mapping.

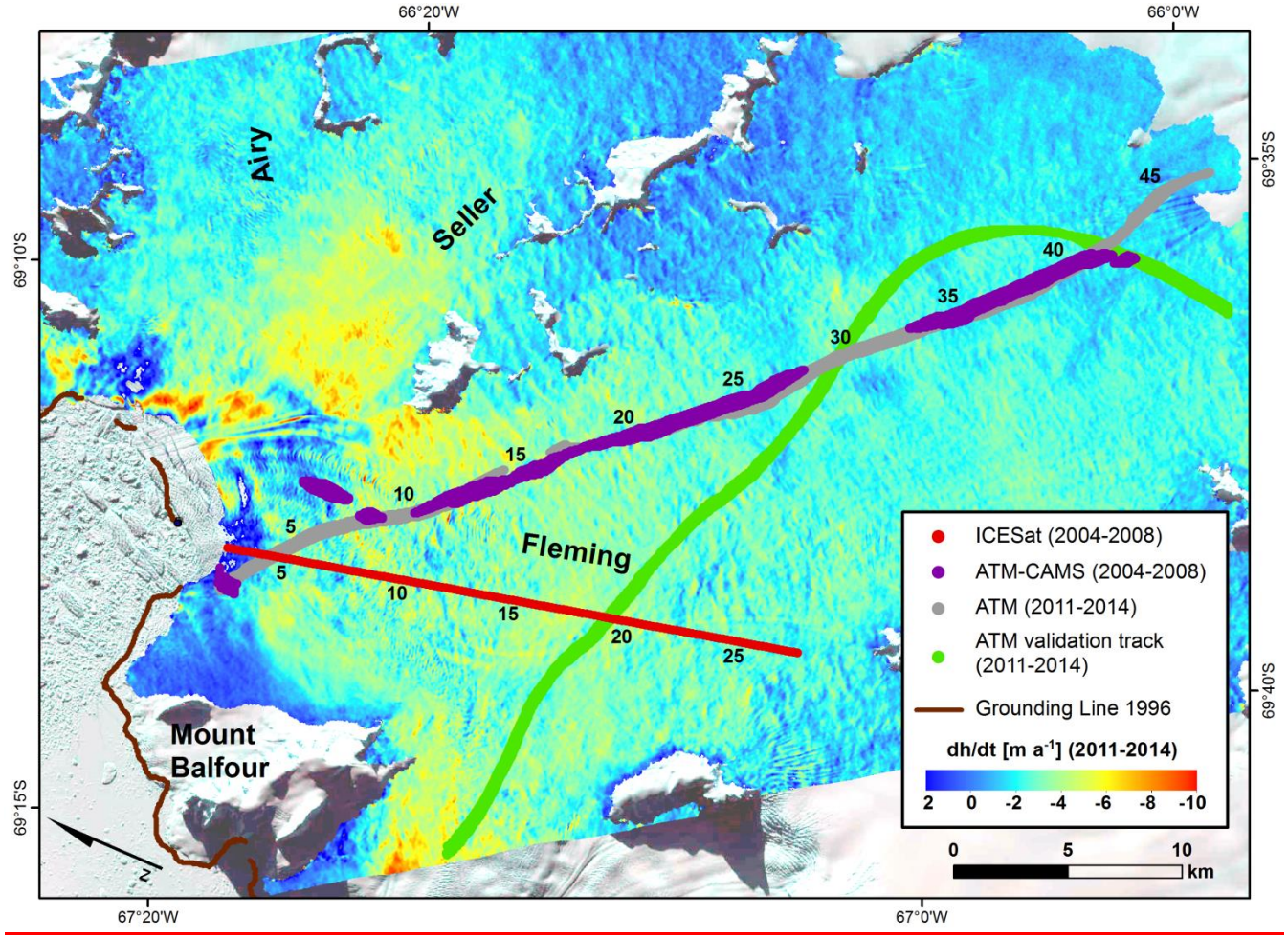

Figure 4: Glacier surface elevation change on Fleming Glacier between 2011 and 2014 derived from TSX/TDX bistatic and monostatic acquisitions. Red dots: ICESat track on 2008-10-04 taken as reference for ICESat 2004–2008 dh/dt calculations. Purple dots: common locations of PIB ATM and CAMS LiDAR measurements in 2004 and 2008. Grey dots: common locations of OIB ATM LiDAR measurements in 2011 and 2014. Green dots: common locations of OIB ATM LiDAR measurements in 2011 and 2014 taken for validation of the 2011–2014 TSX/TDX dh/dt measurements. Brown line: grounding line in 1996 from Rignot et al. (2005) and Rignot et al. (2011a). Numbers indicate distances to the 1996 grounding line. Background: Mosaic of two Landsat-8 "Natural Color" images, acquired on 2015-09-16 ©USGS.

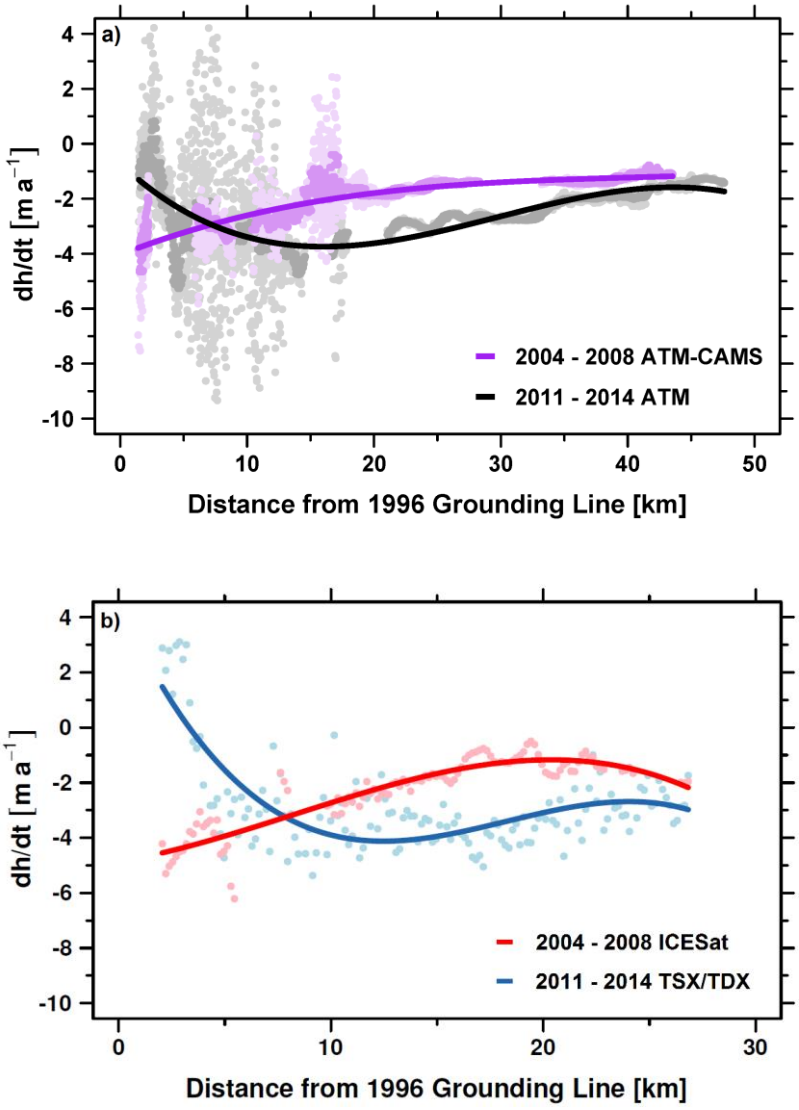

Figure 5: (a) Elevation change rates on Fleming Glacier 2004–2008 and 2011–2014 plotted against distance from the 1996 grounding line. Light purple dots: change rates from PIB ATM and CAMS LiDAR measurements in 2004 and 2008. Purple dots: median filtered elevation change rates 2004–2008. Light grey dots: change rates from OIB ATM LiDAR measurements in 2011 and 2014. Dark grey dots: median filtered elevation change rates 2004–2008. See Fig. 4 for flight path locations. Purple and black lines: Cubic functions fitted to the median filtered elevation change rates. **(b)** Elevation change rates on Fleming Glacier 2004–2008 and 2011–2014 plotted against distance from the 1996 grounding line. Light red dots: change rates from ICESat measurements in 2004 and 2008. Light blue dots: change rates between 2011 and 2014, extracted from the TSX/TDX dh/dt map along the 2008 ICESat track (see Fig. 4 for location). Red and blue lines: Cubic functions fitted to both datasets.

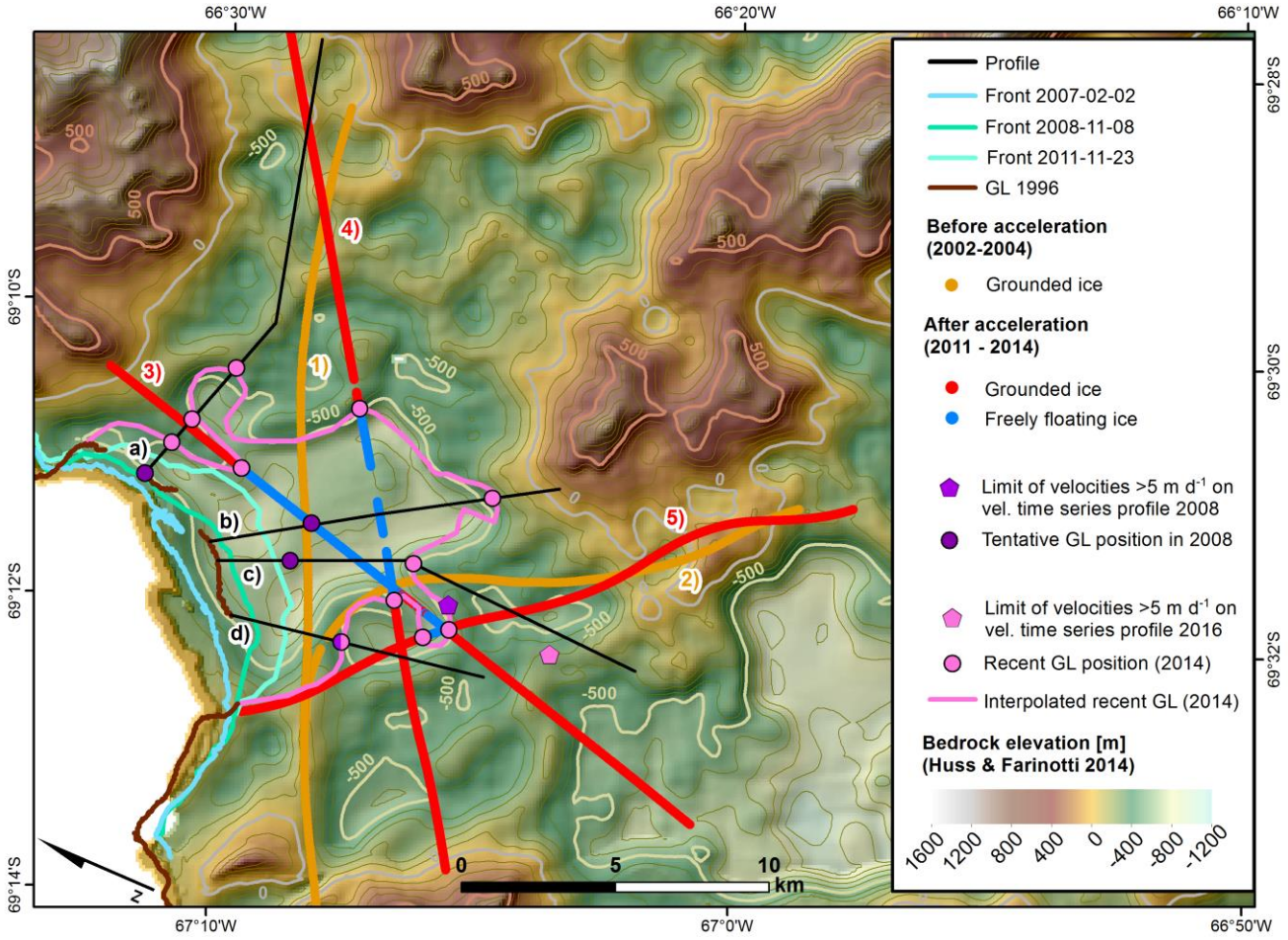

Figure 6: Floating area of Fleming Glacier and estimation of the recent grounding line. Black lines 1–4: Profiles for extraction of modeled bedrock elevations, surface velocities and elevation change rates (see Fig. S6 a–d). Elevation contours are shown at an interval of 100 m. Light blue and cyan lines: glacier fronts on 2007-02-02 and 2011-11-23. Brown line: grounding line in 1996 (Rignot et al., 2005; Rignot et al., 2011a).Orange dots: Grounded ice before acceleration as derived from PIB LiDAR and ice thickness data.. Dates of PIB flights: 1) 2002-11-26, 2) 2004-11-18. Background: bedrock elevation from Huss and Farinotti (2014). Blue and red dots: Freely floating and grounded ice after acceleration as derived from OIB laser altimeter and ice thickness data. Dates of OIB flights: 3) 2011-11-17, 4) 2014-11-16, 5) 2014-11-10. Purple pentagon: Location of the limit of velocities >5 m d^{-1}~~high acceleration~~ on the velocity time series profile in 2008 (Fig. 1 and 2). Purple circle: likely grounding line location in 2008. Purple circles with cross: possible grounding line locations in 2008. Pink pentagon: Location of the limit of acceleration on the velocity time series profile in 2015 (Fig. 1 and 2). Pink circles: Estimated positions of the recent grounding line (2014) obtained from buoyancy calculations, surface velocities, elevation change rate patterns and/or modeled bedrock elevations on profiles a–d. Pink line: Final solution of the ~~likely~~ interpolated recent (2014) grounding line ~~location~~.

Tables

Table 1: Sensors and data used in this study and their main specifications. Intensity tracking parameters are provided in pixels [p] in slant range geometry.

SAR sensors

Platform	Sensor	Mode	SAR band	Repetition cycle [d]	Time interval [yyyy-mm-dd] – [yyyy-mm-dd]	Tracking patch sizes [p x p]	Tracking step size [p x p]
ERS-1/2	AMI SAR	IM	C band	35/3/1	1994-01-26 – 2011-06-29	64x320	5x25
RADARSAT 1	SAR	ST	C band	24	2000-09-07 – 2008-01-17	128x512	5x20
Envisat	ASAR	IM	C band	35	2006-02-15 – 2010-10-10	64x320	5x25
ALOS	PALSAR	FBS	L band	46	2006-06-25 – 2010-11-23	128x384	10x30
TerraSAR-X/ TanDEM-X	SAR	SM	X band	11	2008-10-14 – 2015-01-30	512x512	25x25
Sentinel-1a	SAR	IW	C band	12	2015-08-28 – 2016-08-22	640x128	50x10

LiDAR/Laser Altimeter

Mission	Sensor	Type	Wavelength [nm]	Footprint [m]	Dates [yyyy-mm-dd]	Estimated accuracy	Reference
Pre-IceBridge (PIB)	ATM (L1B)	LIDAR	532	1	2002-11-26 2004-11-18	0.120 m	Krabill (2012)
ICESat	GLAS	Laser Altimeter	1064	70	2004-05-18 2008-10-04	0.420 m	Zwally et al. (2014)
CECS/FACH	CAMS	LiDAR	900	1	2008-12-07	0.205 m	Wendt et al. (2010)
Operation IceBridge (OIB)	ATM (L1B)	LiDAR	532	1	2011-11-17 2014-11-10 2014-11-16	0.120 m	Krabill (2010, updated 2016)

Ice Thickness

Mission	Sensor	Type	Bandwidth [MHz]	Sample spacing [m]	Dates [yyyy-mm-dd]
Pre-IceBridge (PIB)	ICoRDS-2	Radar	141.5-158.5	~130	2002-11-26
Pre-IceBridge (PIB)	ACoRDS	Radar	140-160	~30	2004-11-18
Operation IceBridge (OIB)	MCoRDS	Radar	180-210	~15	2011-11-17
Operation IceBridge (OIB)	MCoRDS 2	Radar	165-215	~15	2014-11-10 2014-11-16

Table 2: Comparison of surface velocities and flow directions at Fleming Glacier obtained by an optical survey in 1974 (Doake, 1975), SAR interferometry in 1996 (Rignot et al., 2005),GPS measurements in 2008 (Wendt et al., 2010) and SAR intensity tracking in 2013. Velocities and flow directions in 2013 were derived from intensity tracking applied on two TSX/TDX acquisitions on 2013-12-19 and 2013-12-30. Velocities in 2015 are from (Zhao et al., 2017). For the locations of the measuring sites see Fig. 1.

Location	1974		1996		2008		2013		2015	
	Magnitude m a^{-1}	Direction °	Magnitude m a^{-1}	Direction °	Magnitude m a^{-1}	Direction °	Magnitude m a^{-1}	Direction °	Magnitude m a^{-1}	Direction °
A (69.505° S, 66.049° W)	146 ± 4	277 ± 5	244 ± 10	285	205.5 ± 0.02	275.8 ± 0.1	205 ± 22	272	271 ± 20	NA
B (69.502° S, 66.123° W)	175 ± 4	272 ± 5	271 ± 10	287	NA	NA	244 ± 22	271	299 ± 20	NA
C (69.500° S, 66.267° W)	201 ± 4	283 ± 5	306 ± 10	300	312.8 ± 0.04	286.3 ± 0.1	323 ± 22	284	356 ± 20	NA

Supplement

S1 Data used for front line delineation

Table S1: Data used for mapping the front positions in Fig. 1, 2, 3, 6 and S6.

Year	Platform	Reference	Date
1966	Aerial photography	Ferrigno, 2008	11/12 1966
1974	Landsat-1	Ferrigno, 2008	1974-01-06
1989	Landsat-3	Ferrigno, 2008	1989-02-20
1994	ERS-1/2		1994-02-01
1995	ERS-1/2		1995-10-27
1996	ERS-1/2		1996-02-10
1997	ERS-1/2		1997-01-29
1998	ERS-1/2		1998-01-30
1999	ERS-1/2		1999-11-10
2000	ERS-1/2		2000-02-20
2001	Landsat-7		2001-01-04
2002	ERS-1/2		2002-02-23
2003	ERS-1/2		2003-01-24
2004	ERS-1/2		2004-03-03
2005	ERS-1/2		2005-01-28
2007	ERS-1/2		2007-02-02
2008*	Envisat	Wendt et al., 2010	2008-04-13
2008*	Envisat		2008-11-08
2009	ASTER	Wendt et al., 2010	2009-02-02
2010	ERS-1/2		2010-02-26
2011	TSX/TDX		2011-11-23
2012	TSX/TDX		2012-10-16
2013	TSX/TDX		2013-12-08
2014	TSX/TDX		2014-11-03
2015	Sentinel 1a		2015-09-09
2016	Sentinel 1a		2016-01-31

*****The 2008-04-13 front position is shown in Fig. 1 and the 2008-11-08 front position is shown in Fig. 6 and S6.

S2 Error estimation of surface velocity measurements

The corresponding errors of the velocity measurements were estimated as described in detail in Seehaus et al. (2015). It is assumed that the resulting uncertainties for each velocity field are induced by two major sources: the coregistration process and the tracking algorithm itself. The error caused by residual inaccuracies of the coregistration (σ_V^C) was determined by calculating the median velocity for 19 to 64 points on stable non-moving surfaces (e.g. rock outcrops) (Fig. S1). The error induced by the tracking algorithm (σ_V^T) was estimated according to the following formula, modified from McNabb et al. (2012):

$$\sigma_V^T = \frac{C\Delta x}{z\Delta t} \quad (1)$$

where C is the uncertainty of the tracking algorithm (assumed to be 0.4 pixels), Δx is the image resolution (mean values for each sensor are listed in Tab. S2), z is the oversampling factor (we applied a factor of two) and Δt is the temporal baseline between the SAR images. The total error (σ_V) of the velocity measurement is the sum of σ_V^C and σ_V^T. Table S3 lists the values Δt, σ_V^C, σ_V^T and σ_V for each velocity field. As in Seehaus et al. (2015) the quite large σ_V^T values for ERS-1/2 measurements during one of the sensor`s "Tandem" or "Ice Phases", where the satellites orbited in 1- or 3-day repeat passes, were excluded from our estimation of σ_V.

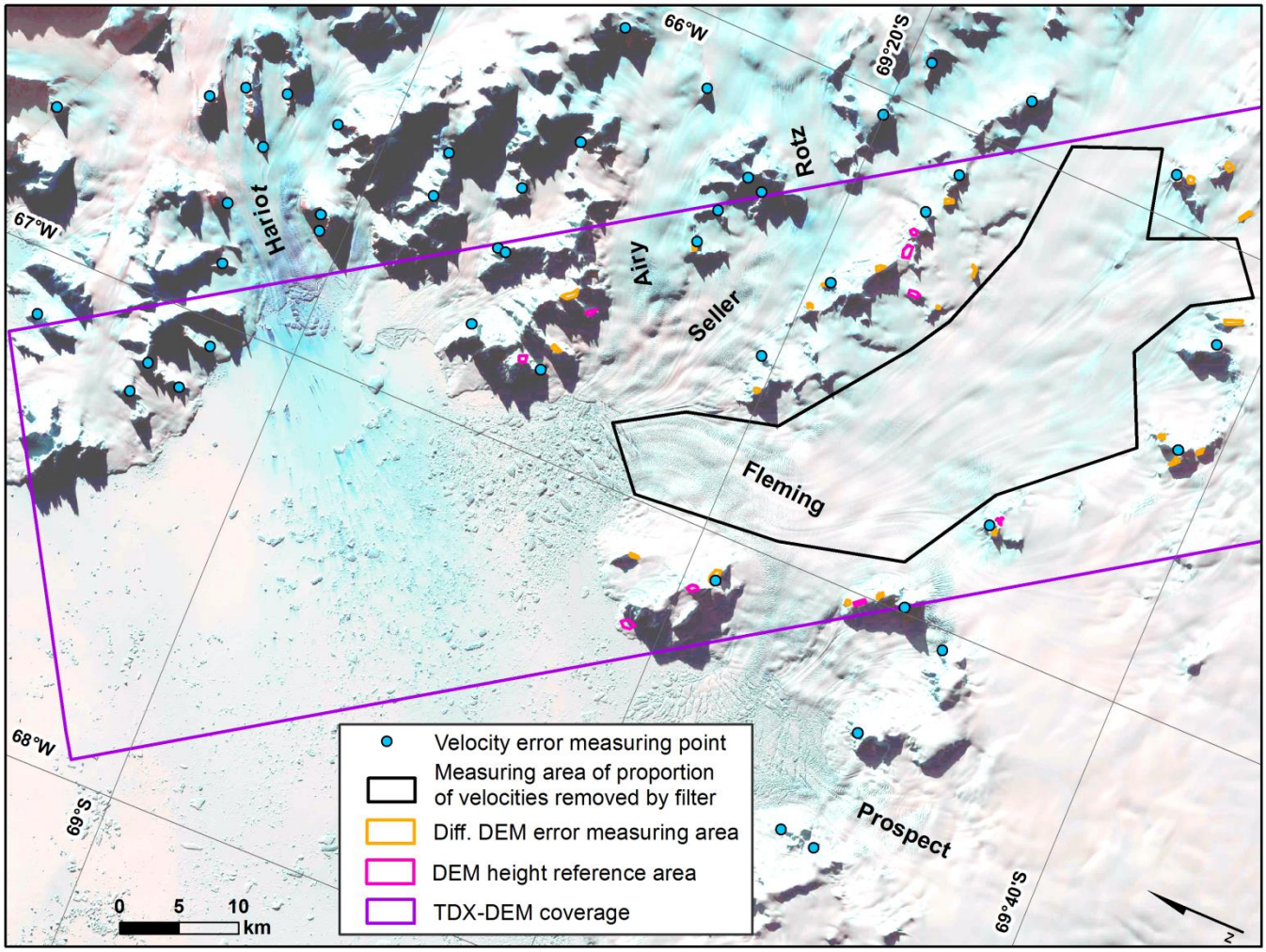

Figure S1: Blue dots: Stable points used for the coregistration error estimation of the intensity tracking results; Black polygon: reference area for the calculation of the proportion of velocity measurements removed by the filter of Burgess et al. (2012) (values of each velocity field are listed in Tab. S.3). Orange polygons: stable areas on nunataks and hills for accuracy assessment of elevation change measurements. Pink polygons: stable areas on nunataks and hills for vertical height referencing of the TanDEM-X DEMs. Purple polygon: spatial coverage of the TanDEM-X DEMs. Background: Mosaic of two Landsat-8 „Natural Color“ images, acquired on September 16, 2015 ©USGS.

Table S2: Ground range resolution Δx_{GR}, azimuth resolution Δx_{AZ} and image resolution Δx used in Formula 1 (S2) for calculating velocity errors. For most of the sensors Δx_{GR} is coarser than Δx_{AZ}, except for Sentinel-1a that has a coarser resolution in azimuth direction and TSX/TDX which have fairly equal resolutions in both directions. In order to make a conservative estimate of velocity errors, always the coarser resolution value was chosen to be Δx.

Sensor	Δx_{GR} [m]	Δx_{AZ} [m]	Δx [m]
AMI SAR (ERS-1/2)	20	4	20
R1 (Radarsat 1)	20	4	20
ASAR (Envisat)	17	4	17
PALSAR (ALOS)	7	3	7
TSX/TDX(TerraSAR-X/TanDEM-X)	2	2	2
S1 (Sentinel-1a)	3	14	14

Table S3: Uncertainty σ_V of processed velocity fields and proportion of removed velocity measurements by the filter of Burgess et al. (2012) ~~(reference area is shown in Fig. S.1)~~. Date: Mean date of SAR acquisitions; Δt: Time interval in days between repeat SAR acquisitions; σ_V^C: Uncertainty of image coregistration; σ_V^T: Uncertainty of intensity tracking processing; ERS velocity fields with $\Delta t \leq 3$d: $\sigma_V = \sigma_V^C$. The percentage of filtered velocities is listed for a reference area on the tongue of Fleming Glacier (Fig. S.1) and each complete velocity field. The table is continued on the next pages.

Date [yyyy-mm-dd]	Sensor	Δt [d]	σ_V^C [m d^{-1}]	σ_V^T [m d^{-1}]	σ_V [m d^{-1}]	Removed by filter (area) [%]	Removed by filter (total) [%]
1994-01-27	AMI SAR	3	0.13	1.33	0.13	1.47	20.58
1994-02-05	AMI SAR	3	0.19	1.33	0.19	1.01	22.36
1994-02-23	AMI SAR	3	0.14	1.33	0.14	3.85	22.04
1994-02-26	AMI SAR	3	0.34	1.33	0.34	4.41	19.4
1994-03-07	AMI SAR	3	0.2	1.33	0.2	1.93	23.96
1995-10-27	AMI SAR	1	0.25	4	0.25	1.34	14.48
1996-02-09	AMI SAR	35	0.12	0.11	0.23	3.88	11.19
1997-02-27	AMI SAR	35	0.12	0.11	0.23	4.91	22.04
2000-09-19	R1	24	0.11	0.14	0.25	7.1	27.19
2000-10-13	R1	24	0.11	0.14	0.25	4.58	27.32
2002-12-02	AMI SAR	35	0.19	0.11	0.3	1.64	15.37
2003-01-06	AMI SAR	35	0.13	0.11	0.24	1.83	14.78
2003-10-22	R1	24	0.12	0.14	0.26	2.98	30.17
2003-11-15	R1	24	0.19	0.14	0.33	4.21	28.82
2003-12-09	R1	24	0.09	0.14	0.23	4.38	28.71
2004-02-19	R1	24	0.08	0.14	0.22	2.63	29.25
2004-03-14	R1	24	0.12	0.14	0.26	3.19	28.85
2004-04-07	R1	24	0.17	0.14	0.31	3.36	28.55
2004-09-22	R1	24	0.1	0.14	0.24	3.61	30.05
2004-10-16	R1	24	0.21	0.14	0.35	3.91	29.8
2004-11-09	R1	24	0.09	0.14	0.23	2.63	31.13
2004-12-03	R1	24	0.14	0.14	0.28	3.49	30.63
2004-12-27	R1	24	0.15	0.14	0.29	13.79	19.03
2005-01-20	R1	24	0.26	0.14	0.4	11.63	17.7
2005-02-13	R1	24	0.07	0.14	0.21	14.86	18.07
2005-04-26	R1	24	0.19	0.14	0.33	2.59	30.13
2005-10-11	R1	24	0.13	0.14	0.27	18.38	17.42
2005-11-04	R1	24	0.17	0.14	0.31	1.75	30.48
2006-01-15	R1	24	0.12	0.14	0.26	10.81	15.89
2006-02-08	R1	24	0.16	0.14	0.3	1.7	29.42
2006-02-15	ASAR	35	0.15	0.11	0.26	3.29	11.15

Date [yyyy-mm-dd]	Sensor	Δt [d]	σ_V^C [m d^{-1}]	σ_V^T [m d^{-1}]	σ_V [m d^{-1}]	Removed by filter (area) [%]	Removed by filter (total) [%]
2006-03-04	R1	24	0.06	0.14	0.2	1.23	30.23
2006-03-28	R1	24	0.23	0.14	0.37	1.27	30.25
2006-04-21	R1	24	0.17	0.14	0.31	1.25	30.13
2006-05-31	ASAR	35	0.09	0.11	0.2	3.35	8.81
2006-07-05	ASAR	35	0.11	0.11	0.22	3.2	8.74
2006-07-18	PALSAR	46	0.06	0.03	0.09	27.76	12.77
2006-08-09	ASAR	35	0.14	0.11	0.25	3.82	8.82
2006-11-03	AMI SAR	35	0.18	0.11	0.29	3.1	9.16
2007-04-10	ASAR	35	0.17	0.11	0.28	11.26	8.89
2007-05-15	ASAR	35	0.06	0.11	0.17	1.29	13.54
2007-05-16	ASAR	35	0.09	0.11	0.2	3.44	9.7
2007-06-19	ASAR	35	0.05	0.11	0.16	3.44	12.76
2007-06-20	ASAR	35	0.08	0.11	0.19	1.33	11.22
2007-07-25	ASAR	35	0.05	0.11	0.16	3.92	11.41
2007-08-28	ASAR	35	0.1	0.11	0.21	1.41	13.03
2007-08-29	ASAR	35	0.13	0.11	0.24	4.08	10.76
2007-10-02	ASAR	35	0.08	0.11	0.19	1.45	11.25
2007-10-03	ASAR	35	0.11	0.11	0.22	4.25	10.71
2007-10-23	PALSAR	46	0.05	0.03	0.08	20.19	12.04
2007-11-06	ASAR	35	0.06	0.11	0.17	1.63	13.35
2008-01-05	R1	24	0.2	0.14	0.34	1.95	29.79
2008-04-30	ASAR	35	0.11	0.11	0.22	5.52	11.36
2008-06-03	ASAR	35	0.08	0.11	0.19	1.97	14.19
2008-07-08	ASAR	35	0.06	0.11	0.17	2.05	14.17
2008-08-12	ASAR	35	0.08	0.11	0.19	2.37	13.69
2008-09-16	ASAR	35	0.08	0.11	0.19	2.22	14.31
2008-10-21	ASAR	35	0.07	0.11	0.18	2.45	14.51
2009-02-06	PALSAR	46	0.15	0.03	0.18	26.83	14.54
2009-04-14	ASAR	35	0.22	0.11	0.33	6.95	7.04
2009-07-29	ASAR	35	0.09	0.11	0.2	6.57	11.92
2009-09-02	ASAR	35	0.09	0.11	0.2	6.44	10.57
2009-10-07	ASAR	35	0.09	0.11	0.2	6.63	10.48
2010-02-08	ASAR	35	0.08	0.11	0.19	4.69	11.03
2010-02-11	ASAR	35	0.19	0.11	0.3	0.02	5.38
2010-03-31	ASAR	35	0.09	0.11	0.2	5.16	9.52

Date [yyyy-mm-dd]	Sensor	Δt [d]	σ_V^C [m d^{-1}]	σ_V^T [m d^{-1}]	σ_V [m d^{-1}]	Removed by filter (area) [%]	Removed by filter (total) [%]
2010-05-05	ASAR	35	0.1	0.11	0.21	5.49	11.38
2010-06-09	ASAR	35	0.08	0.11	0.19	5.29	11.08
2010-07-14	ASAR	35	0.09	0.11	0.2	5.39	11.51
2010-08-18	ASAR	35	0.1	0.11	0.21	5.87	11.49
2010-09-22	ASAR	35	0.09	0.11	0.2	6.04	11.49
2010-10-27	TSX/TDX	33	0.01	0.01	0.02	3.7	12.01
2010-10-31	PALSAR	46	0.33	0.03	0.36	28.43	10.62
2010-11-18	TSX/TDX	11	0.02	0.04	0.06	4.06	11.68
2011-05-10	AMI SAR	3	0.25	1.33	0.25	2.52	19.79
2011-06-27	AMI SAR	3	0.36	1.33	0.36	6.46	20.24
2011-10-02	TSX/TDX	11	0.02	0.04	0.06	2.94	8.23
2011-11-15	TSX/TDX	11	0.03	0.04	0.07	5.02	10.86
2011-12-29	TSX/TDX	11	0.01	0.04	0.05	6.47	10.21
2012-03-15	TSX/TDX	11	0.02	0.04	0.06	3.55	9.64
2012-04-06	TSX/TDX	11	0.02	0.04	0.06	4.56	10.76
2012-04-17	TSX/TDX	11	0.02	0.04	0.06	3.66	9.34
2012-05-31	TSX/TDX	11	0.03	0.04	0.07	4.14	10.34
2012-06-11	TSX/TDX	11	0.01	0.04	0.05	4.01	10.41
2012-07-25	TSX/TDX	11	0.02	0.04	0.06	1.69	10.52
2012-09-07	TSX/TDX	11	0.02	0.04	0.06	4.53	10.29
2012-10-21	TSX/TDX	11	0.02	0.04	0.06	4.34	10.33
2012-12-04	TSX/TDX	11	0.02	0.04	0.06	3.37	9.84
2013-01-17	TSX/TDX	11	0.01	0.04	0.05	3.94	8.18
2013-03-13	TSX/TDX	11	0.03	0.04	0.07	3.8	9.63
2013-03-23	TSX/TDX	11	0.08	0.04	0.12	2.19	6.64
2013-04-15	TSX/TDX	11	0.03	0.04	0.07	3.47	10.15
2013-06-09	TSX/TDX	11	0.02	0.04	0.06	2.56	8.79
2013-06-20	TSX/TDX	11	0.02	0.04	0.06	3.94	8.76
2013-07-01	TSX/TDX	11	0.02	0.04	0.06	2.37	8.48
2013-07-12	TSX/TDX	11	0.02	0.04	0.06	2.2	8.48
2013-11-20	TSX/TDX	11	0.04	0.04	0.08	0.71	5.77
2013-12-13	TSX/TDX	11	0.03	0.04	0.07	4.25	8.29
2013-12-24	TSX/TDX	11	0.02	0.04	0.06	3.57	8.02
2014-01-26	TSX/TDX	11	0.01	0.04	0.05	3.2	7.72
2014-08-23	TSX/TDX	11	0.02	0.04	0.06	4.67	10.98

Date [yyyy-mm-dd]	Sensor	Δt [d]	σ_V^C [m d^{-1}]	σ_V^T [m d^{-1}]	σ_V [m d^{-1}]	Removed by filter (area) [%]	Removed by filter (total) [%]
2014-09-03	TSX/TDX	11	0.03	0.04	0.07	4.52	10.36
2014-12-11	TSX/TDX	11	0.01	0.04	0.05	4.05	6.79
2015-01-24	TSX/TDX	11	0.03	0.04	0.07	2.2	9.04
2015-09-03	S1	12	0.06	0.23	0.29	2.47	19.85
2015-09-15	S1	12	0.05	0.23	0.28	2.51	20.36
2015-10-21	S1	12	0.15	0.23	0.38	2.51	19.74
2015-12-08	S1	12	0.11	0.23	0.34	2.03	12.42
2015-12-20	S1	12	0.07	0.23	0.3	2.13	13.99
2016-01-01	S1	12	0.09	0.23	0.32	2.21	13.15
2016-01-13	S1	12	0.05	0.23	0.28	2.08	13.79
2016-01-25	S1	12	0.08	0.23	0.31	2.18	13.59
2016-02-06	S1	12	0.08	0.23	0.31	2.15	12.85
2016-02-18	S1	12	0.08	0.23	0.31	2.1	13.56
2016-03-01	S1	12	0.09	0.23	0.32	2.15	12.63
2016-03-13	S1	12	0.08	0.23	0.31	2.11	13.58
2016-04-06	S1	12	0.09	0.23	0.32	2.01	12.64
2016-04-18	S1	12	0.07	0.23	0.3	2.12	13.43
2016-06-05	S1	12	0.12	0.23	0.35	1.97	13.02
2016-07-23	S1	12	0.1	0.23	0.33	2.09	12.36
2016-08-04	S1	12	0.08	0.23	0.31	2.07	12.51
2016-08-16	S1	12	0.06	0.23	0.29	2.17	14.7

S3 Uncertainty estimation of variables for the hydrostatic height anomaly calculations and assessment of error propagation

In order to assess the propagation of uncertainties for the calculation of hydrostatic height anomalies, we estimated the error of each variable of Formula 2. The accuracy of the ATM elevations was estimated to be ± 0.2 m. The overall uncertainty of the EIGEN-6C4 geoid is 0.24 m (http://icgem.gfz-potsdam.de/ICGEM/). Accounting for an unknown additional error induced by kriging of the geoid values, we assumed a total accuracy of ± 0.5 m for e. Following the recommendation of the CReSIS Radar Depth Sounders (RDS) user guide (ftp://data.cresis.ku.edu/data/rds/rds_readme.pdf) we defined the error of H_i as the sum of the RMS error of the sensor`s range resolution and the RMS error of the dielectric. Depending on the sensor, the uncertainty of H_i varies between ~6 and ~14 m for an ice thickness of 750 m, which is the approx. mean ice thickness in the vicinity of the current grounding line measured on our OIB profiles. For ρ_i we used a value of 917 kg m^{-3}, which is the standard density of pure ice (Benn and Evans, 2013). However, since impurities in the ice can cause this value to vary by around ± 5 kg m^{-3} (Griggs and Bamber, 2011), we chose this rate to be the uncertainty of ρ_i. The global mean density of sea water is 1027 kg m^{-3}, but this value can vary locally. According to Griggs and Bamber (2011) we therefore assumed an error of ± 5 kg m^{-3} for ρ_w. The firn density correction factor for pure glacier ice is 0. In situ values of about 10 m have been measured for δ on Larsen C Ice Shelf (Griggs and Bamber, 2009) and firn density correction factors > 20 m have been reported for areas of convergent flow on the Ross Ice Shelf (Bamber and Bentley, 1994). Modelled firn densities (van den Broeke, Michiel et al., 2008) indicate a firn correction factor of ~17 ± 4 m for the glacier tongue of the Airy-Rotz-Seller-Fleming glacier system. ~~Since δ can vary spatially and we had no information on firn densities on the Airy Rotz-Seller Fleming glacier system, we used a mean firn density correction factor of 10 m throughout our calculations and noted an uncertainty of ± 10 m~~. In order to quantify the total error of Δe and to consider the propagation of uncertainties, we run a Monte Carlo simulation based on Formula 1 and 2 with 100.000 runs. For all possible sensor-depending errors of H_i=750 m the Monte Carlo simulation yielded a standard deviation of ~~<~~ 6~~12~~ m for Δe. Thus we assumed the total uncertainty of Δe to be ~6~~12~~ m. Consequently, we assigned locations on our OIB and PIB profiles to be freely floating ice, if the calculated values of Δe lay within this range. In the vicinity of the grounding zone the TDX global DEM has a minimum slope of 1°, and therefore we estimate the uncertainty in the horizontal position of the transition from grounded to freely floating ice to be ~350~~700~~ m.

S4 Penetration bias correction of TSX/TDX 2011–2014 elevation change rates

Figure S4 a–c: Penetration bias correction of TSX/TDX 2011–2014 elevation change rates

(a) Comparison of yearly elevation change rates obtained from OIB ATM LiDAR measurements (2011-11-17/2014-11-10) and TSX/TDX DEMs (2011-11-21/2014-11-03) after vertical registration of the TSX/TDX DEMs. Data is plotted against absolute ellipsoidal elevations from the resampled Bedmap 2 DEM (Fretwell et al., 2013). Grey dots: elevation change rates between 2011 and 2014 from OIB ATM. Black line: cubic function fitted to the OIB ATM measurements. Light blue dots: elevation change rates between 2011 and 2014 from TSX/TDX. Blue line: cubic function fitted to the TSX/TDX measurements

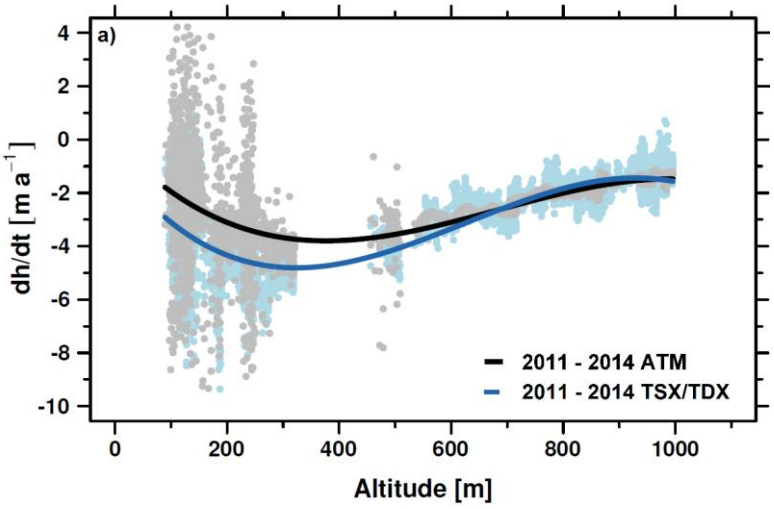

(b) Penetration bias correction model for TSX/TDX change rates. Data is plotted against absolute ellipsoidal elevations from the resampled Bedmap 2 DEM (Fretwell et al., 2013). Black dots: differences between TSX/TDX elevation change rates (r_{DEM}) and OIB ATM rates (r_{ATM}). Green line: local polynomial model fitted to the measurements.

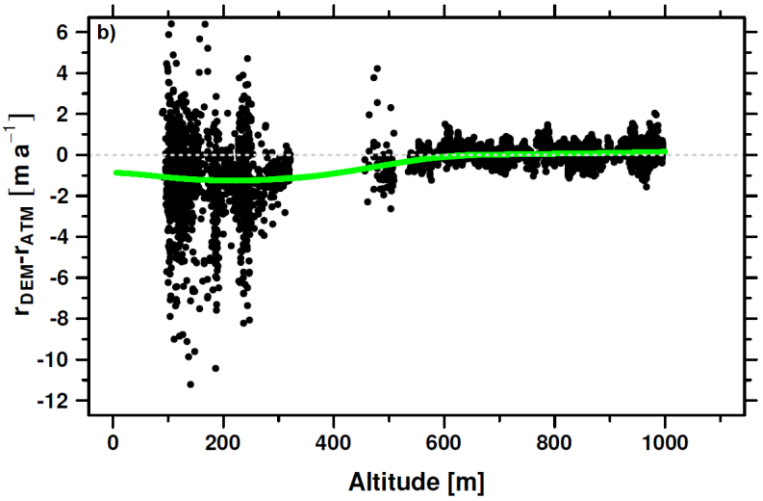

(c) Comparison of yearly elevation change rates obtained from OIB ATM LiDAR measurements (2011-11-17/2014-11-10) and TSX/TDX DEMs (2011-11-21/2014-11-03) after vertical registration and penetration depth bias correction of the TSX/TDX elevation change map. Data is plotted against absolute ellipsoidal elevations from the resampled Bedmap 2 DEM (Fretwell et al., 2013). Grey dots: elevation change rates between 2011 and 2014 from OIB ATM. Black line: cubic function fitted to the OIB ATM measurements. Light blue dots: elevation change rates between 2011 and 2014 from TSX/TDX. Blue line: cubic function fitted to the TSX/TDX measurements

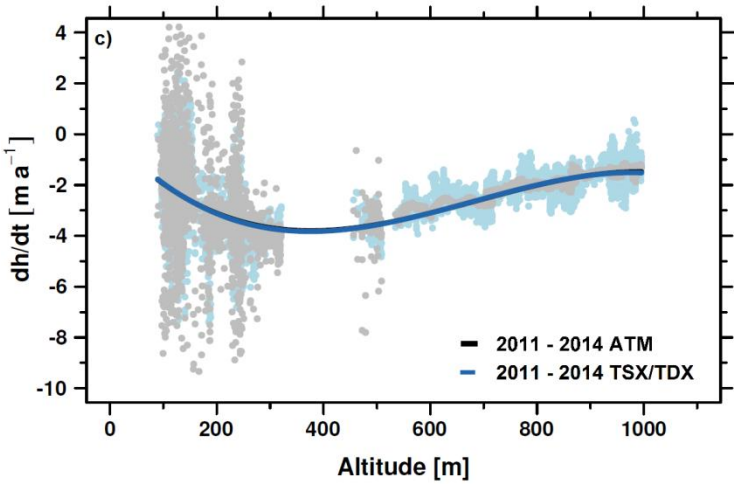

(d) Comparison of median filtered backscatter values of TSX/TDX acquisitions on 2011-11-21 and 2014-11-03. Data is plotted against absolute ellipsoidal elevations from the resampled Bedmap 2 DEM (Fretwell et al., 2013). Light pink dots: backscatter of the master image on 2011-11-21. Brown line: cubic function fitted to the 2011-11-21 backscatter values. Light blue dots: backscatter of the master image on 2014-11-03. Dark blue line: cubic function fitted to the 2014-11-03 backscatter values.

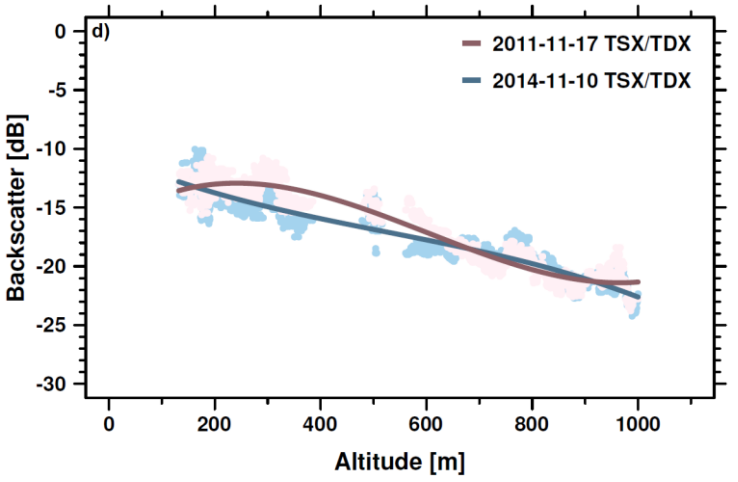

(e) Comparison of yearly elevation change rates along a validation track of OIB ATM LiDAR measurements (2011-11-17/2014-11-10) (Figure 4) and elevation change rates from the penetration depth corrected differential TSX/TDX DEM (2011-11-21/2014-11-03). Data is plotted against absolute ellipsoidal elevations from the resampled Bedmap 2 DEM (Fretwell et al., 2013). Grey dots: elevation change rates between 2011 and 2014 from OIB ATM. Black line: cubic function fitted to the OIB ATM measurements. Light blue dots: elevation change rates between 2011 and 2014 from TSX/TDX. Blue line: cubic function fitted to the TSX/TDX measurements

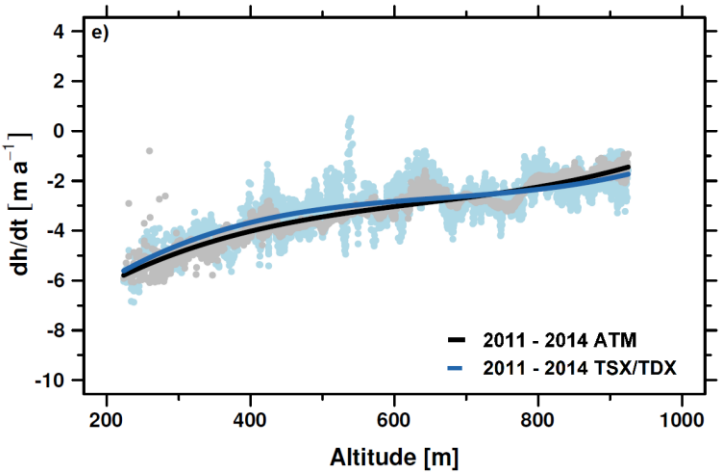

S5 Results of the hydrostatic height anomaly calculations

Figure S5 a–e: Fulfillment of the hydrostatic equilibrium assumption from hydrostatic height anomaly calculations along PIB and OIB profiles. Profiles are to read from left to right (in upstream direction). Dates of PIB and OIB flights: a) 2002-11-26, b) 2004-11-18, c) 2011-11-17, d) 2014-11-16, e) 2014-11-10. Purple dots: PIB/OIB ice surface/bottom elevations. Ice surface elevation is taken from PIB/OIB ATM measurements and ice bottom elevation is calculated by subtracting OIB/PIB ice thickness from ice surface elevation. Brown line: Bedrock elevation from Huss and Farinotti, 2014. Yellow line: Bedrock elevation from Bedmap 2 (Fretwell et al., 2013). Red and blue dots: calculated ice surface elevation in hydrostatic equilibrium e_{he} and information on hydrostatic equilibrium (blue: freely floating ice, red: grounded ice)

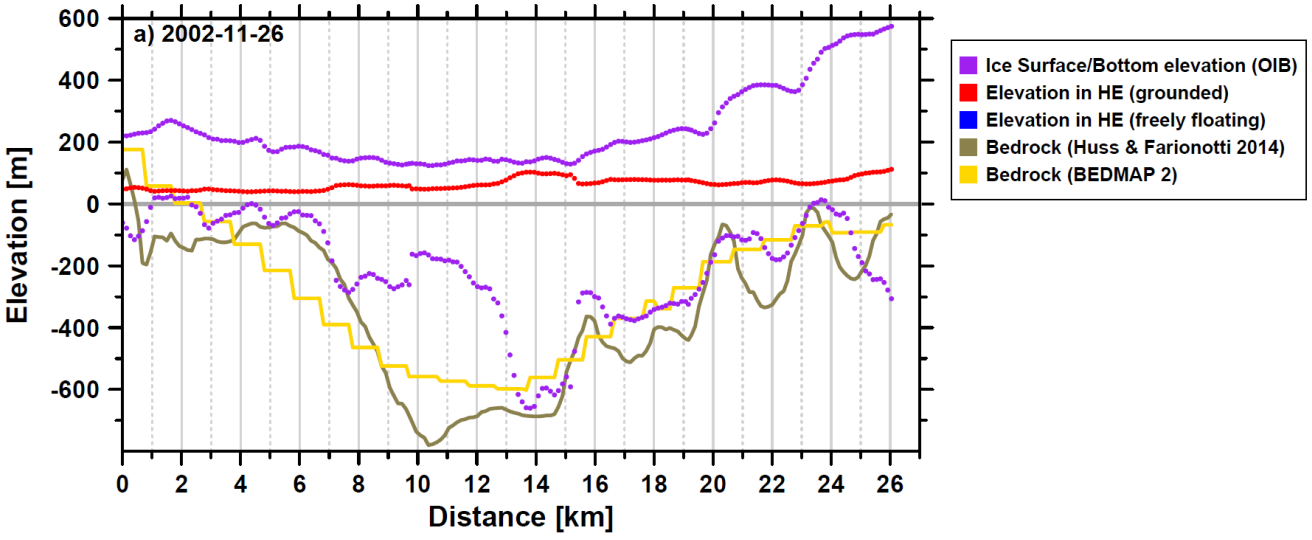

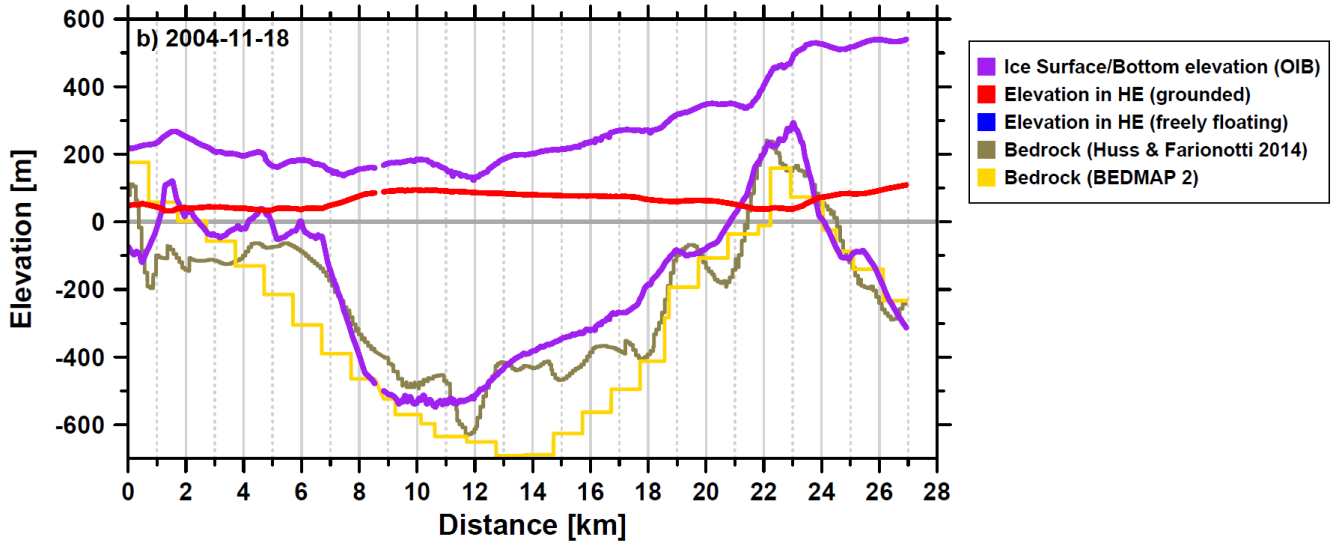

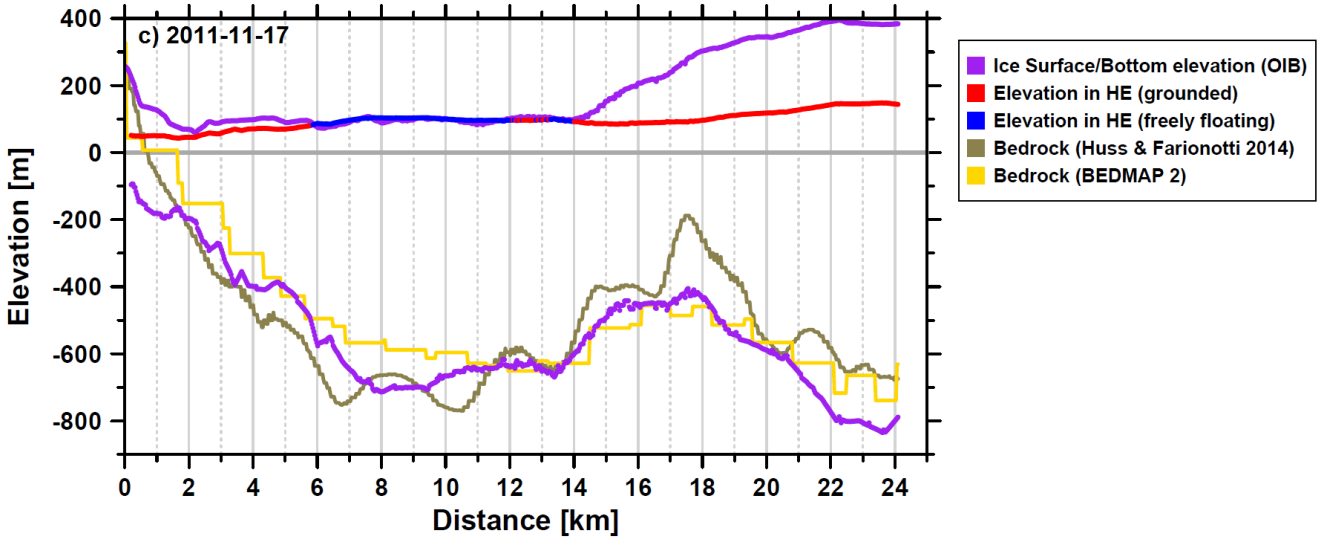
c) 2011-11-17
Elevation [m]
Distance [km]
Ice Surface/Bottom elevation (OIB)
Elevation in HE (grounded)
Elevation in HE (freely floating)
Bedrock (Huss & Farionotti 2014)
Bedrock (BEDMAP 2)

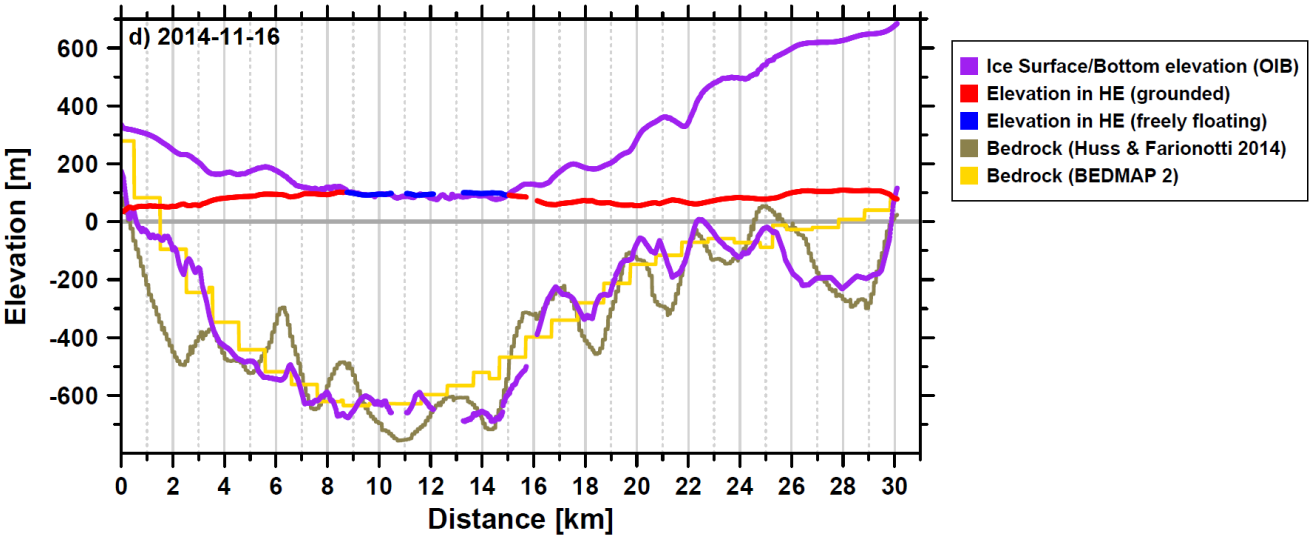
d) 2014-11-16
Elevation [m]
Distance [km]
Ice Surface/Bottom elevation (OIB)
Elevation in HE (grounded)
Elevation in HE (freely floating)
Bedrock (Huss & Farionotti 2014)
Bedrock (BEDMAP 2)

5

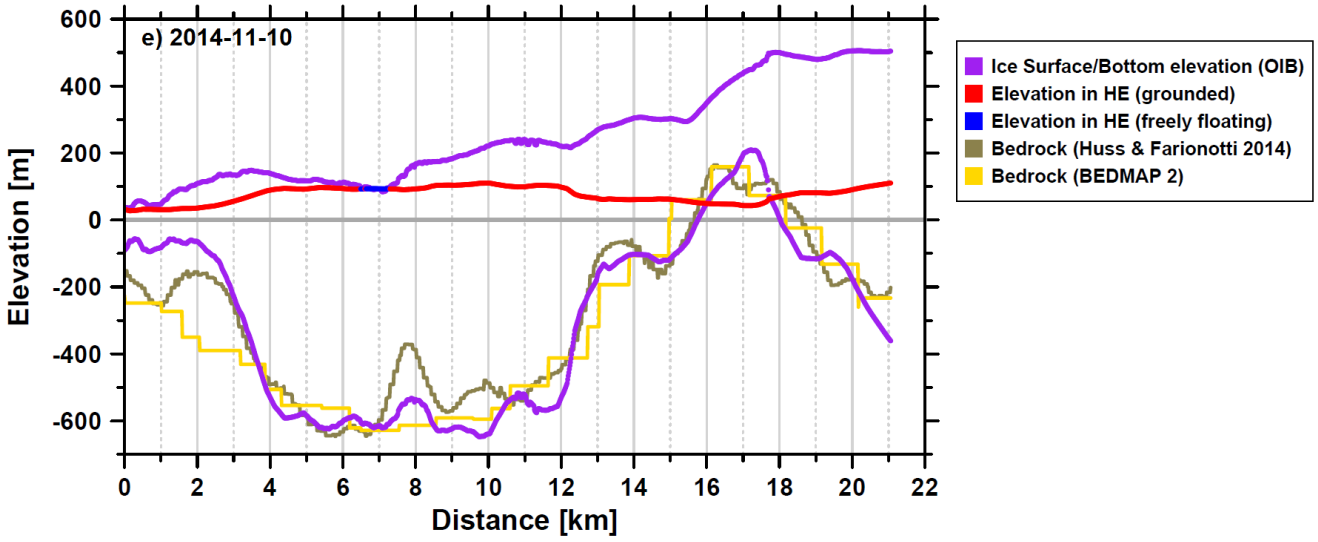
e) 2014-11-10
Elevation [m]
Distance [km]
600
400
200
0
-200
-400
-600
0
2
4
6
8
10
12
14
16
18
20
22
Ice Surface/Bottom elevation (OIB)
Elevation in HE (grounded)
Elevation in HE (freely floating)
Bedrock (Huss & Farionotti 2014)
Bedrock (BEDMAP 2)

5

S6 Estimation of grounding line positions along profiles of surface velocity, bedrock topography, ice elevations and hydrostatic height anomalies

Figure S6 a–d: Estimated grounding line positions on profiles a–d (for location see Fig. 6) based on surface velocities and elevation change rates from TDX (black line). Distances for Fig. S6 a–d are relative to the 1996 grounding line. F: Front, GL: Grounding Line. Brown line: Bedrock elevation from Huss and Farinotti (2014). Yellow line: Bedrock elevation from Bedmap 2 (Fretwell et al. 2013).

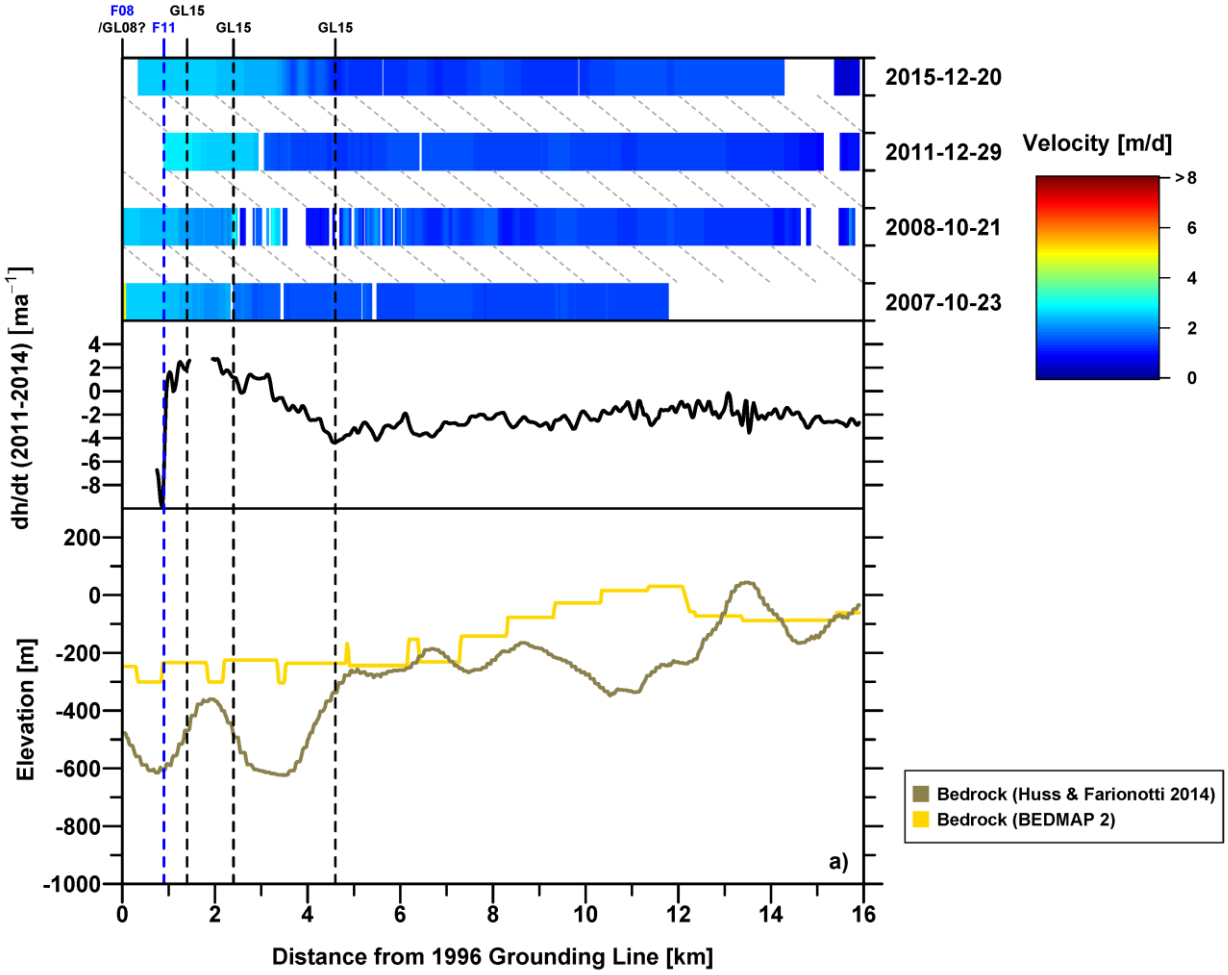

Figure S6 a exhibits that in contrast to Fleming Glacier, on Airy Glacier velocity data extracted along Profile a (Fig. 6) does not show signs of acceleration between 2007 and 2008. Furthermore in 2008 the front was still located at the 1996 grounding line. Hence, we assume that in 2008 Airy Glacier was still grounded at the 1996grounding line position. However, in 2011 the front had retreated behind the 1996 grounding line. This shows that the grounding line must have had retreated from its 1996 position by this time. An abrupt change in the 2011–2014 TSX/TDX elevation change rates is visible at 4–5 km upstream, which coincides with the edge of the subglacial trough in the bedrock data. A similar extent of accelerated surface

velocities is visible on the velocity profiles in 2011 and 2015. Hence, this location is likely the recent location of the grounding line. A distinct area of low elevation change rates which is visible on the TSX/TDX dh/dt map (Fig. S7) suggests that the entire Airy Glacier tongue may be currently floating up to ~4 km upstream of the 1996 grounding line. However, this is in contrast to the buoyancy calculations (Fig. 6, Track 3) which indicate that in 2011 the ice was grounded on a hill ~2 km upstream, which reaches to the subglacial trough. Since we assume that the hydrostatic height anomalies from 2011 are the most reliable source of information for grounding line detection we have, we delineated the recent grounding line accordingly. However, we cannot rule out that the ice which rested on the hill in 2011 is afloat today.

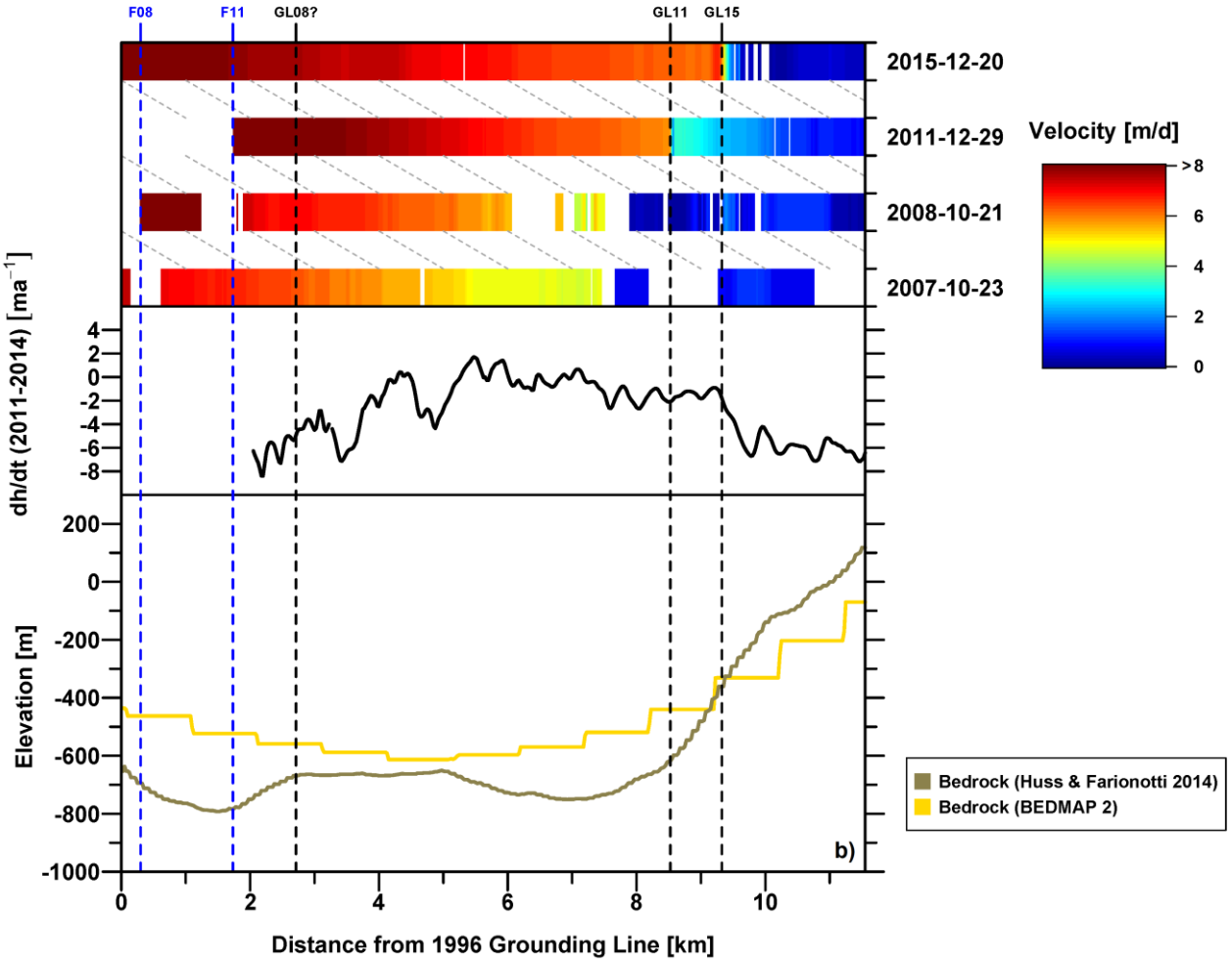

Figure S6 b depicts data extracted along Profile b (Fig. 6), close to the confluence of Fleming and Seller Glacier. Here velocities show acceleration between 2007 and 2008. While the glacier had accelerated, the glacier front had retreated behind the 1996 grounding line. Hence, in 2008 the grounding line must have been located upstream of the 1996 position. The

upstream extent of acceleration visible on the velocity profile suggests that in 2008 the grounding line had not retreated as far as in 2011 and 2015, yet. A reasonable estimate would be that the grounding line in 2008 was located on a gentle hill apparent in the bedrock data close to the 2011 front, ~4 km upstream. However, given the limitations of the modelled bedrock topography (Sect. 3) and the lack of further information, the exact grounding line position in 2008 remains vague.

In 2011 the glacier had substantially accelerated and in 2015 high velocities had further propagated inland by ~1 km up to the edge of the subglacial trough at ~9 km upstream. The limit of high velocities in 2015 coincides with a marked change of the TSX/TDX 2011–2014 elevation change rates, indicating that at this position the ice starts to float. Based on these evidences, we estimate that the grounding line position in 2011 was likely already located at the edge of the subglacial trough and had probably further retreated by ~1 km in 2015.

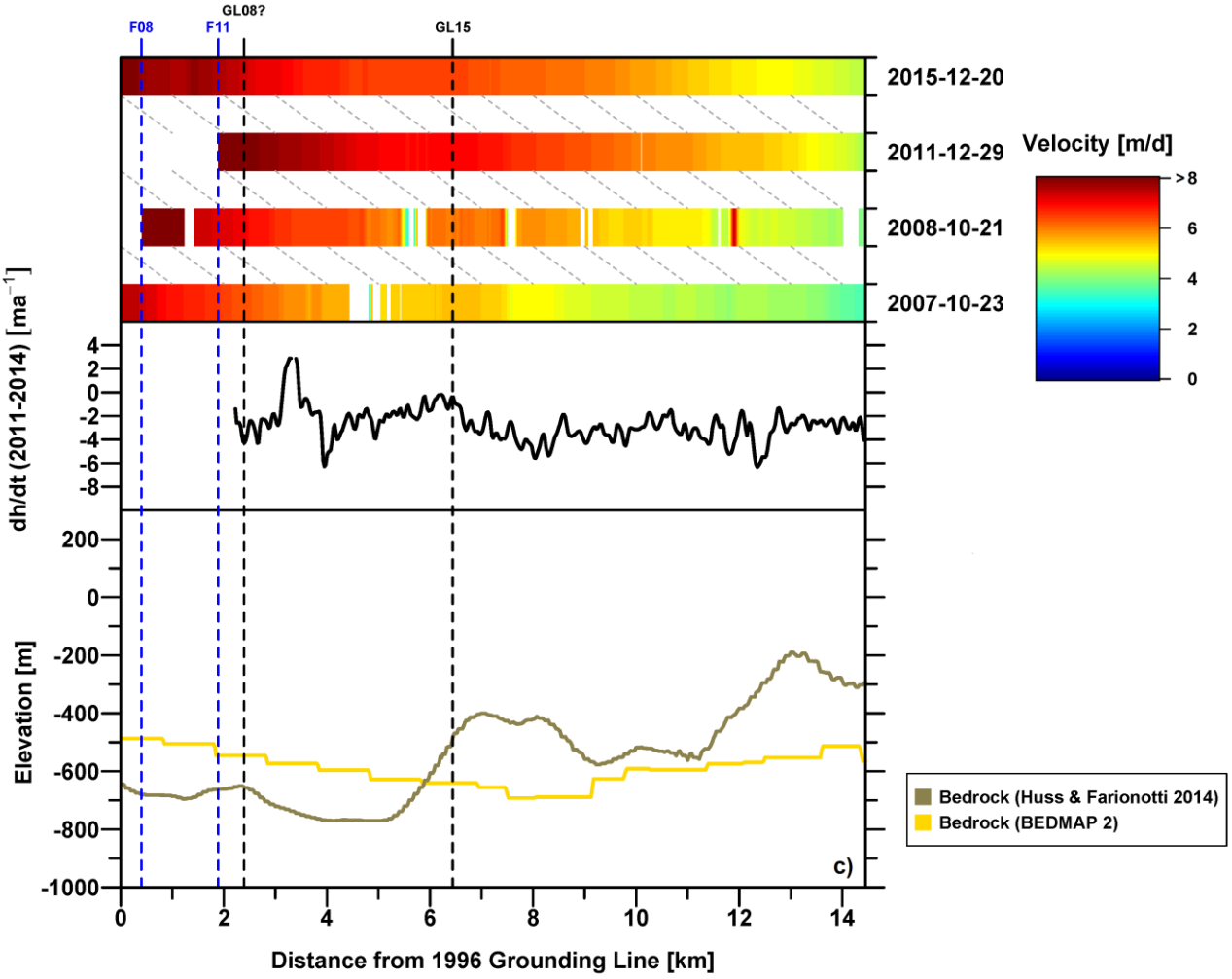

Figure S6 c reveals that velocities extracted along Profile 3 (Fig. 6) show an upstream propagation of high velocities between 2007 and 2008 of up to 11 km. In 2008, the glacier front had retreated behind the 1996 grounding line. This indicates that in 2008 the grounding line must have been located upstream from its 1996 position. Since the acceleration had not yet propagated as far upstream as in 2011 and 2015, we assume that the 2008 grounding line was located more seawards than in 2011 and 2015 respectively. A possible grounding line location in 2008 is a smaller hill visible in the bedrock data close to the front in 2011 at ~2, 5 km upstream. However, due to the limitations of the bedrock data (Sect. 3) and the lack of further evidence, the precise 2008 position remains unclear.

In 2011 and 2015 the glacier had markedly accelerated, indicating that the grounding line had further retreated. The 2011/2014 TSX/TDX dh/dt profile shows a slight drop in ice thinning rates at ~6 km upstream of the 1996 grounding line which coincides with the edge of the subglacial trough in the bedrock data. Although the change of elevation change rates is not as pronounced as on the other profiles, hydrostatic height anomalies along an OIB-flight path running close to this position (Fig. 6, Track 4) show that in 2014 the glacier was freely floating downstream. OIB data acquired in 2011 and 2014 (Fig. 6, Track 3 and 5) indicate that the ice is currently grounded upstream of the hill chain. We hence estimate the recent grounding line position to be located at the edge of the subglacial trough ~6 km upstream.

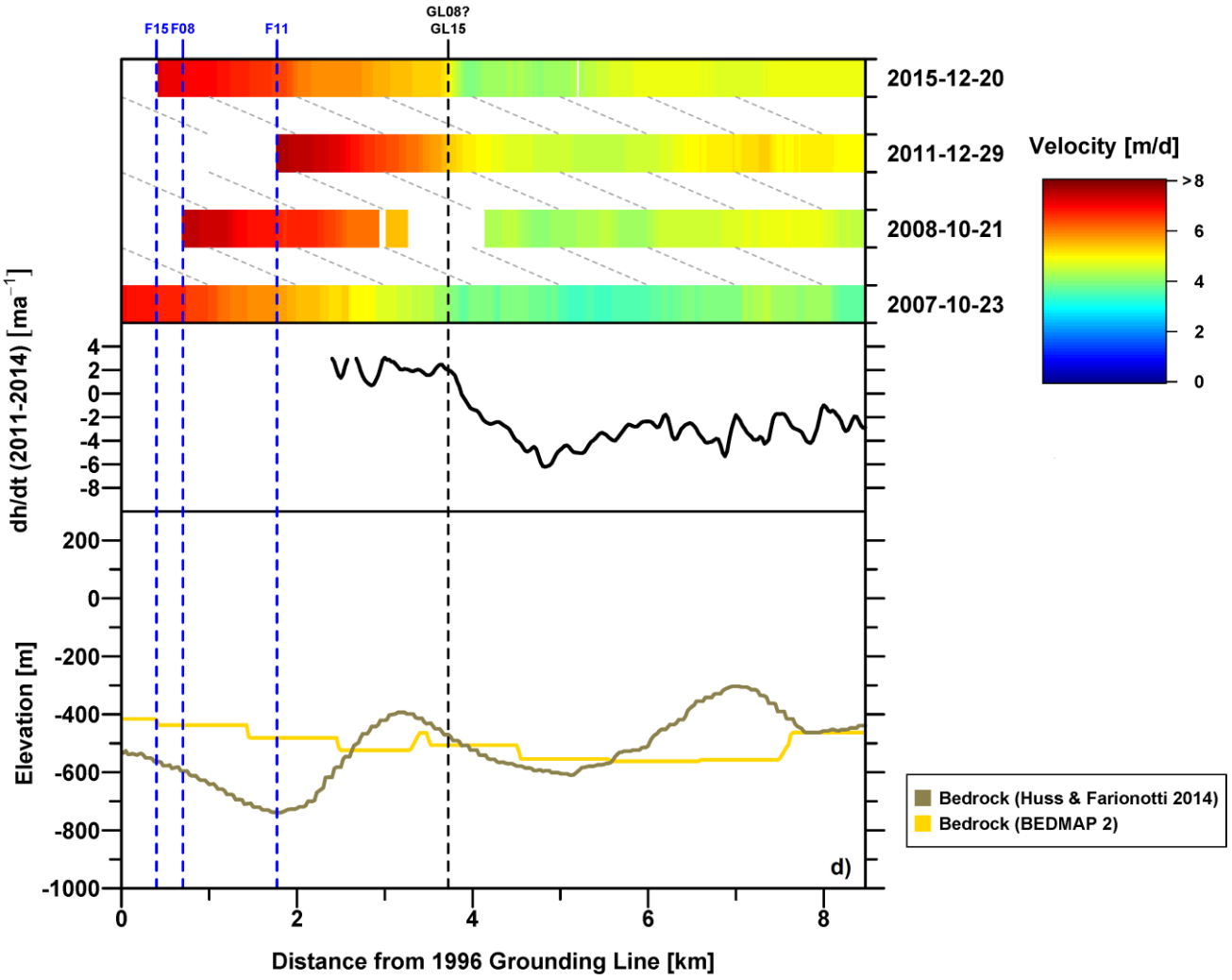

Figure S6 d shows that between 2007 and 2008 a pronounced acceleration is detected along Profile d (Fig. 6). In 2008 the glacier front had retreated behind the 1996 grounding line for the first time. Thus, the grounding line in 2008 must have been located upstream of the 1996 position in 2008. The velocity patterns look similar in 2008, 2011 and 2015, suggesting that no further grounding line retreat occurred after 2008. We hence assume that the 2008 grounding line position is more or less identical with the recent location. However, given the lack of further evidence the precise grounding line position of 2008 remains vague.

A sharp increase in surface velocities is visible at 3–4 km upstream in 2011 and 2015. This location is consistent with a pronounced change in ice thinning rates visible on the TSX/TDX 2011–2014 dh/dt profile and on the map (Fig. S7), which indicates that the ice is currently floating downstream. On the other hand, hydrostatic height anomalies along OIB tracks 4

and 5 in Figure 6 reveal that the ice is grounded further upstream. Additionally the 2011 front was located ~ 2 km upstream of the grounding line. Combining all of the information, we estimate the recent grounding line to be located at a position ~3–4 km upstream. However, the modeled bedrock data suggests that the grounding line is not situated on the upslope but on the downslope side of a subglacial hill. We hence cannot rule out that the hill may be shifted to the north in the modelled bedrock data, or that – if the modelled bedrock topography is correct - the recent grounding line is located ~ 1 km further to the south.

S7 Recent grounding line and TSX/TDX 2011–2014 elevation change

Figure S7: Glacier surface elevation change on Fleming Glacier between 2011 and 2014 derived from TSX/TDX bistatic and monostatic acquisitions with final solution of the interpolated ~~likely~~ recent (2014) grounding line ~~location~~ (pink line). Brown line: grounding line in 1996 from Rignot et al. (2005) and Rignot et al. (2011). Background: Mosaic of two Landsat-8 „Natural Color" images, acquired on 2015-09-16 ©USGS.

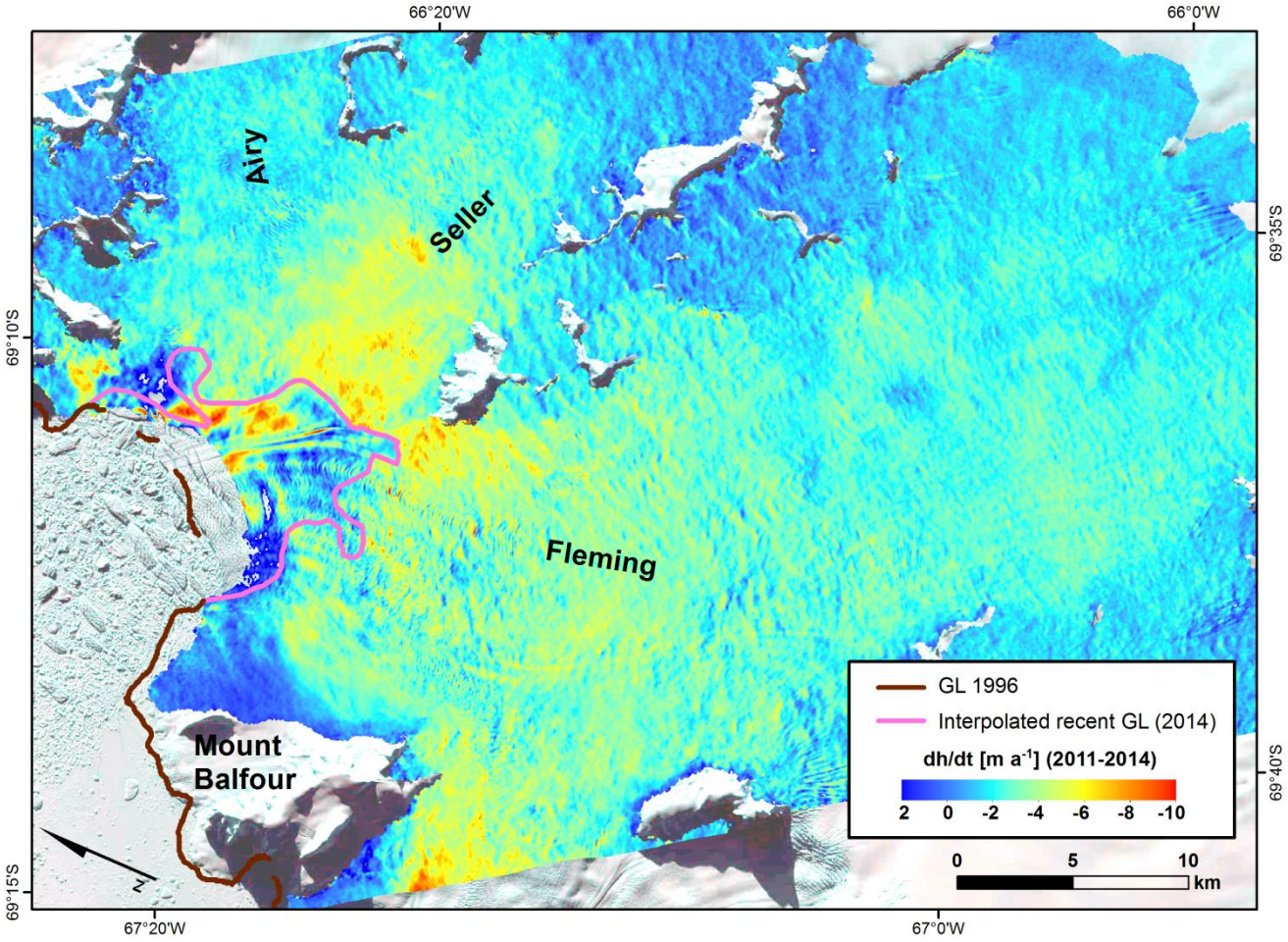

~~S8 Evolution of the grounding line before 2008–today~~

~~Figure S8: **Schematic drawing of the ungrounding history of Fleming Glacier from before 2008 to today. Interpretation is based on the data presented in this study and in the literature. Figures are not drawn to scale.**~~

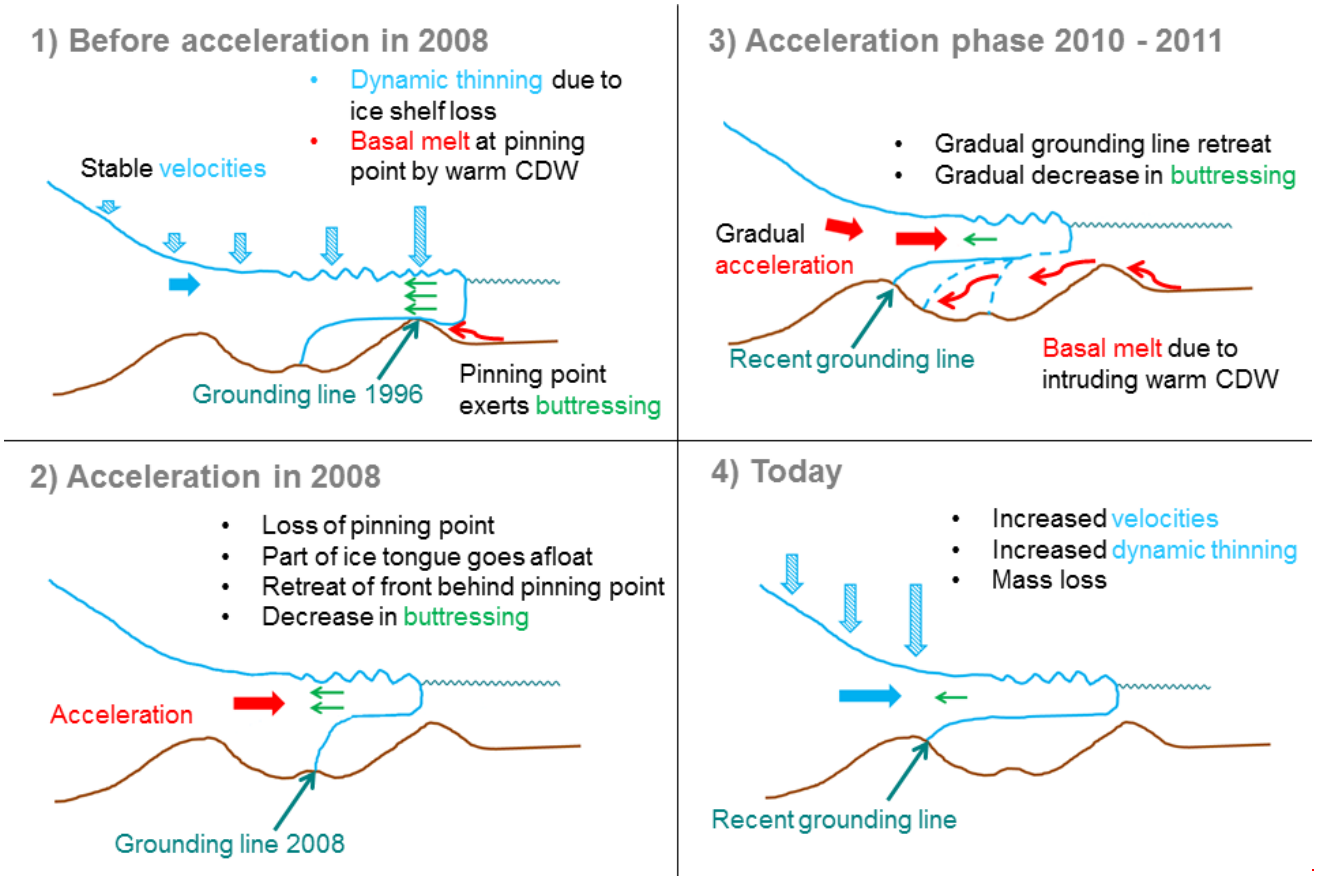

References

Bamber, J. and Bentley, C.: A comparison of satellite-altimetry and ice-thickness measurements of the Ross Ice Shelf, Antarctica, Annals of Glaciology, 20, 357–364, 1994.

Benn, D. I. and Evans, D. J. A.: Glaciers & glaciation, Routledge, London, 2013.

Burgess, E. W., Forster, R. R., Larsen, C. F. and Braun, M.: Surge dynamics on Bering Glacier, Alaska, in 2008–2011, The Cryosphere, 6, 1251–1262, doi: 10.5194/tc-6-1251-2012, 2012.

Ferrigno, J. G.: Coastal-change and glaciological map of the Larsen Ice Shelf area, Antarctica, 1940-2005, Reston, Va., 2008.

Fretwell, P., Pritchard, H. D., Vaughan, D. G., Bamber, J. L., Barrand, N. E., Bell, R., Bianchi, C., Bingham, R. G., Blankenship, D. D., Casassa, G., Catania, G., Callens, D., Conway, H., Cook, A. J., Corr, H. F. J., Damaske, D., Damm, V., Ferraccioli, F., Forsberg, R., Fujita, S., Gim, Y., Gogineni, P., Griggs, J. A., Hindmarsh, R. C. A., Holmlund, P., Holt, J. W., Jacobel, R. W., Jenkins, A., Jokat, W., Jordan, T., King, E. C., Kohler, J., Krabill, W., Riger-Kusk, M., Langley, K. A., Leitchenkov, G., Leuschen, C., Luyendyk, B. P., Matsuoka, K., Mouginot, J., Nitsche, F. O., Nogi, Y., Nost, O. A., Popov, S. V., Rignot, E., Rippin, D. M., Rivera, A., Roberts, J., Ross, N., Siegert, M. J., Smith, A. M., Steinhage, D., Studinger, M., Sun, B., Tinto, B. K., Welch, B. C., Wilson, D., Young, D. A., Xiangbin, C. and Zirizzotti, A.: Bedmap2: improved ice bed, surface and thickness datasets for Antarctica, The Cryosphere, 7, 375–393, doi: 10.5194/tc-7-375-2013, 2013.

Griggs, J. A. and Bamber, J. L.: Ice shelf thickness over Larsen C, Antarctica, derived from satellite altimetry, Geophys. Res. Lett., 36, doi: 10.1029/2009GL039527, 2009.

Griggs, J. A. and Bamber, J. L.: Antarctic ice-shelf thickness from satellite radar altimetry, Journal of Glaciology, 57, 485–498, doi: 10.3189/002214311796905659, 2011.

Huss, M. and Farinotti, D.: A high-resolution bedrock map for the Antarctic Peninsula, The Cryosphere, 8, 1261–1273, doi: 10.5194/tc-8-1261-2014, 2014.

McNabb, R. W., Hock, R., O'Neel, S., Rasmussen, L. A., Ahn, Y., Braun, M., Conway, H., Herreid, S., Joughin, I., Pfeffer, W. T., Smith, B. E. and Truffer, M.: Using surface velocities to calculate ice thickness and bed topography. A case study at Columbia Glacier, Alaska, USA, Journal of Glaciology, 58, 1151–1164, doi: 10.3189/2012JoG11J249, 2012.

Rignot, E., Casassa, G., Gogineni, P., Kanagaratnam, P., Krabill, W., Pritchard, H. D., Rivera, A., Thomas, R., Turner, J. and Vaughan, D. G.: Recent ice loss from the Fleming and other glaciers, Wordie Bay, West Antarctic Peninsula, Geophys. Res. Lett., 32, doi: 10.1029/2004GL021947, 2005.

Rignot, E., Mouginot, J. and Scheuchl, B.: Antarctic grounding line mapping from differential satellite radar interferometry, Geophys. Res. Lett., 38, n/a, doi: 10.1029/2011GL047109, 2011.

Seehaus, T., Marinsek, S., Helm, V., Skvarca, P. and Braun, M.: Changes in ice dynamics, elevation and mass discharge of Dinsmoor–Bombardier–Edgeworth glacier system, Antarctic Peninsula, Earth and Planetary Science Letters, 427, 125–135, doi: 10.1016/j.epsl.2015.06.047, 2015.

van den Broeke, Michiel, van de Berg, Willem Jan and van Meijgaard, E.: Firn depth correction along the Antarctic grounding line, Antarctic Science, 20, 513-517, doi: 10.1017/S095410200800148X, 2008.

Wendt, J., Rivera, A., Wendt, A., Bown, F., Zamora, R., Casassa, G. and Bravo, C.: Recent ice-surface-elevation changes of Fleming Glacier in response to the removal of the Wordie Ice Shelf, Antarctic Peninsula, Annals of Glaciology, 51, 97–102, doi: 10.3189/172756410791392727, 2010.